

A Survey on Over-the-Air Computation

Alphan Şahin*, *Member, IEEE* and Rui Yang†, *Member, IEEE*

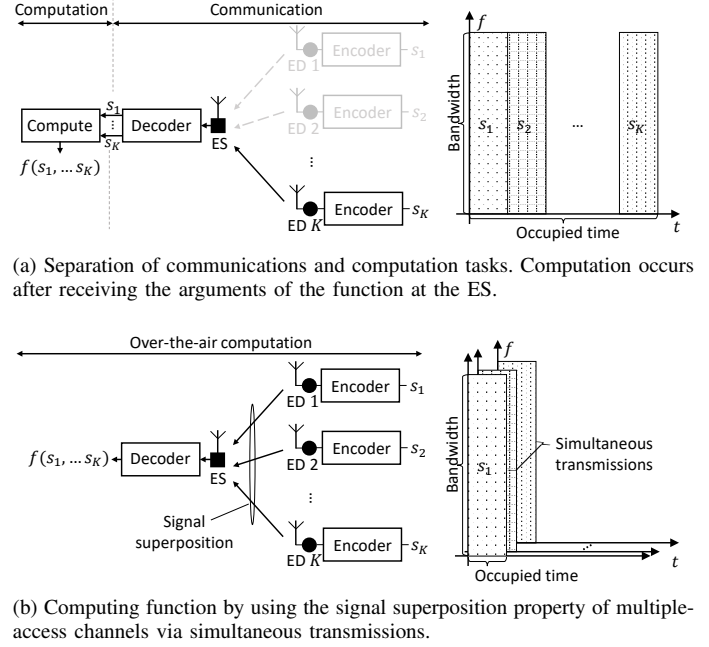
Abstract—Communication and computation are often viewed as separate tasks. This approach is very effective from the perspective of engineering as isolated optimizations can be performed. On the other hand, there are many cases where the main interest is a function of the local information at the devices instead of the local information itself. For such scenarios, information theoretical results show that harnessing the interference in a multiple-access channel for computation, i.e., over-the-air computation (OAC), can provide a significantly higher achievable computation rate than the one with the separation of communication and computation tasks. Besides, the gap between OAC and separation in terms of computation rate increases with more participating nodes. Given this motivation, in this study, we provide a comprehensive survey on practical OAC methods. After outlining fundamentals related to OAC, we discuss the available OAC schemes with their pros and cons. We provide an overview of the enabling mechanisms for achieving reliable computation in the wireless channel. Finally, we summarize the potential applications of OAC and point out some future directions.

Index Terms—Over-the-air computation

I. INTRODUCTION

Over-the-air computation (OAC) refers to the computation of mathematical functions by exploiting the signal superposition property of wireless multiple-access channels. The distinct feature of OAC is that the local data at the edge devices (EDs) such as smartphones, laptops, tablets, vehicles, or sensors, are not acquired over *orthogonal* channels to perform a computation task at a fusion node, e.g., an edge server (ES) at a base station or an access point. Instead, the computation is handled by harnessing the interference via *simultaneous transmissions*. For example, suppose that the goal is to evaluate a function $f(s_1, \dots, s_K)$ at an ES, where s_k is the symbol at the k th ED. With the separation of communication and computation tasks, the function is computed at the fusion node after each symbol is received via orthogonal or non-orthogonal channels (i.e., orthogonal multiple access (OMA) and non-orthogonal multiple access (NOMA)), as illustrated for time-domain multiple access (TDMA) in Fig. 1(a). On the other hand, with OAC, the function is intended to be computed through signal superposition in the channel as shown in Fig. 1(b). Since radio resources are consumed only once, a larger computation rate is achieved. In this example, the key observation is that if the ES is not interested in the local information but only in a function of them, OAC paves the way for reducing the resource usage, which otherwise scales with the number of EDs. Hence, it is a fundamental and disruptive concept to the traditional way of handling computation and communication tasks independently.

The idea of function computation over a multiple-access channel was first thoroughly analyzed in Bobak's pioneering



(a) Separation of communications and computation tasks. Computation occurs after receiving the arguments of the function at the ES.

(b) Computing function by using the signal superposition property of multiple-access channels via simultaneous transmissions.

Fig. 1. Separation of communications and computation versus OAC.

work in [1] and the theoretical limits of computation over multiple-access channels were investigated for a fixed many-to-one function. In [2], Goldenbaum made the first connection between nomographic functions and OAC. In [3] and [4], it was shown that OAC can provide a significantly higher achievable computation rate than the one with the separation of communications and computation tasks.

Given the promising information theoretical results, OAC has been drawing more and more attention in the literature. Initially, it has been applied to communication problems in the interference channel, e.g., physical layer network coding [5], [6], compute-and-forward relaying strategy [7], and wireless sensor networks (WSNs) to address the issues like acceleration in gossip networks [8] and several computation tasks [9], [10]. With the increased interest in applications that require heavy computation, it has recently been utilized in multi-disciplinary fields such as machine learning over wireless networks [11], wireless control systems [12], and computing frameworks like wireless data centers [13] and wireless intra-chip computations [14].

The exciting applications have led to the investigation of OAC from various perspectives and resulted in a wide-variety of computation strategies. This paper aims to discuss these OAC schemes without losing the mathematical rigor and how these methods address the challenges such as the detrimental impact of wireless channels on the computation, synchronization errors, maintaining accurate and fresh channel

Alphan Şahin and Rui Yang are affiliated with University of South Carolina, Columbia, SC and InterDigital, New York, NY, USA, respectively. E-mails: asahin@mailbox.sc.edu*, rui.yang@interdigital.com†.

state information (CSI) at the radios, security, and hardware impairments such as power amplifier non-linearity.

A. Relation to other surveys and our contributions

The reader can find the relevant discussions where the big umbrella is the distributed inference over sensor networks in [15]. The methods along with compute-and-forward relaying scheme and uncoded strategies for physical layer network coding are comprehensively discussed and compared in [16], [17]. To reduce the per-round communication latency for the implementation of distributed learning over a wireless network, OAC has been used in many recent work as an enabler. We refer the readers interested in wireless systems for machine learning in general to the excellent survey papers in [18]–[25] and the references therein. In [24], federated edge learning (FEEL), i.e., implementation of federated learning (FL) [26] over a wireless network, and its implications on the resource management are surveyed. In [11], several exciting applications of OAC and research directions in this area are discussed without mathematical details. In [27], semantic communication is thoroughly surveyed and OAC is mentioned as a one of the task-oriented semantic communication paradigms. In [28], [29], OAC is particularly analyzed from the perspective of integrated sensing, communication, and computation. In [30], over-the-air distributed computing for artificial intelligence applications is envisioned for 6G wireless networks. In [31], the particular interest is in the applications that enjoy signal superposition in general. Besides OAC, the topics such as NOMA, interference alignment, multiple antenna systems, security, and spectrum sensing are investigated. In [32], the design of aeronautical networks with computation paradigms such as edge computing and off-loading are surveyed. We also acknowledge the reference [33] which discusses the OAC from the perspective of various network architectures and provide an excellent survey on the OAC based on multiple antennas at the devices.¹

The main focus of this study is to investigate *how to compute a function over a wireless network reliably and efficiently*. Our priority is to form a composition that can provide a relative comparison of the state-of-the-art OAC techniques with pros and cons, particularly from the perspective of the physical layer of communication systems, to guide the readers who are interested in this topic. Since a wide variety of applications can benefit from the OAC, in this study, we focus on the computation itself, rather than a particular application. We seek answers to three main questions:

- 1) What functions can potentially be calculated with OAC? To answer this question, we review the nomographic functions that appear in both mathematics and communication literature.
- 2) What are the OAC schemes in the state-of-the-art and their trade-offs to deal with wireless channels? To address this question, we first give a general system model

along with fundamental metrics on OAC. Under this framework, we evaluate the methods based on how they achieve computation under fading channel and the encoding strategies.

- 3) What are the mechanisms that play a role in achieving a reliable OAC? To answer this question, we review the impacts of synchronization impairments, power management, and channel estimation on OAC and elaborate security aspects and computation architectures for OAC.

Finally, we provide an overview of the applications of OAC in the literature and point out the potential areas that can be improved for OAC.

Organization: The rest of study is organized as follows. In Section II, we provide an overview of the fundamentals and discuss the functions that can potentially be computed via OAC. In Section III, we discuss the state-of-the-art OAC schemes, comprehensively. In Section IV, we discuss the enabling mechanisms to achieve a reliable computation. We summarize the potential applications of OAC in various fields in Section V. We finalize our discussions with various topics that need to be investigated further in Section VI.

Notation: The complex and real numbers are denoted by \mathbb{C} and \mathbb{R} , respectively. The K -times Cartesian product of a space \mathbb{A} is shown as \mathbb{A}^K . $\mathcal{F}(\mathbb{A})$ represents the space of every function that maps \mathbb{A} to \mathbb{R} . \mathbb{E} denotes the unit interval $[0, 1]$. $\mathbb{E}\{\cdot\}$ denotes the expectation over all random variables. The function $\text{sign}(\cdot)$ results in 1, -1 , or 0 for a positive, a negative, or a zero-valued argument, respectively. The symbol \otimes denotes linear convolution. The function $\mathbb{I}[\cdot]$ results in 1 if its argument holds, otherwise it is 0. $\Pr(\cdot)$ is the probability of an event. The zero-mean multivariate complex Gaussian distribution with the covariance matrix \mathbf{C}_M of an M -dimensional random column vector $\mathbf{x} \in \mathbb{C}^M$ is denoted by $\mathbf{x} \sim \mathcal{CN}(\mathbf{0}_M, \mathbf{C}_M)$. $\mathcal{N}(\mu, \sigma^2)$ is the normal distribution with the mean μ and the variance σ^2 . The trace of a matrix is denoted by $\text{tr}\{\cdot\}$. The continuous uniform distribution is denoted by $\mathcal{U}_{[a,b]}$, where a and b are the minimum and the maximum values, respectively. The function $\log_2^+(x)$ is defined as $\max(\log_2(x), 0)$. Kronecker delta is expressed as δ_{ij} .

II. WHAT CAN BE CALCULATED WITH OAC?

OAC aims to compute a multi-variate function by relying on its representation that can structurally match with the underlying operation that multiple-access channel naturally performs. In wireless communications, multiple access channels are modeled with additive property, i.e., realizes the signal superposition. With this property, the OAC problem boils down to the representation of a target function with a special function, called *nomographic* function, or a set of nomographic functions over multiple wireless resources. These functions are called nomographic because they are inline with the nomographs that solve certain equations through some graphs, i.e., analog computing. A well-known example of a nomograph is Smith chart which assists in solving problems related to transmission lines. While the nomographs allows quick and accurate computations, the use cases of nomograph diminished historically due to the effectiveness of digital com-

¹Our paper and [33] are independently developed and compensate each other from the perspective of classifications of available OAC approaches. The corresponding pre-prints were listed on arXiv.org one day apart (October 19, 2022).

puters. Nevertheless, the fundamental theories about nomography are intricate, arguably connected to the neural networks, and pave the way for addressing the scenarios where digital computation suffers from latency, power consumption, and limited-communication bandwidth. In this section, we discuss the preliminaries on nomographic functions to reveal what functions can potentially be calculated with OAC.

A. Preliminaries

Definition 1 (Nomographic function [2], [34]–[36]). Let \mathbb{S}^K , $K \geq 2$, be a compact metric space. A function $f: \mathbb{S}^K \rightarrow \mathbb{R}$ for which there exist functions $\psi_k \in \mathcal{F}(\mathbb{S})$, $k \in \{1, \dots, K\}$, and $\varphi \in \mathcal{F}(\mathbb{R})$ such that f can be represented as

$$f(s_1, s_2, \dots, s_K) = \varphi\left(\sum_{k=1}^K \psi_k(s_k)\right), \quad (1)$$

is called nomographic function and $\mathcal{N}(\mathbb{S}^K)$ is the space of nomographic functions with the domain \mathbb{S}^K .

The functions ψ_k , $\forall k$, and the function φ are further called pre-processing functions (or inner functions) and post-processing function (or outer function), respectively. Equation (1) reveals why a nomographic function is relevant to OAC: Equation (1) can be interpreted as an evaluation of the function f in an ideal uplink (UL) channel (i.e., no noise, no multi-path channel distortion), where s_k and ψ_k are the symbols and the pre-processing functions at k th data-generating node, respectively, the sum of the signals from K nodes corresponds to the superposition that naturally occurs in the channel, and φ is the post-processing function at the fusion center. To the best of our knowledge, this connection is first made in Goldenbaum's work in [2], [34]–[36] while the non-linear function examples in the form of (1) appears in [37]–[39] without discussing the family of nomographic functions.

It is worth noting that the compactness mentioned in Definition 1 is an important assumption, especially in the analysis of continuous functions. For example, the range of a continuous function $f(s_1, s_2, \dots, s_K)$ on a compact space \mathbb{S}^K is compact. Since the function is bounded, one can ensure that the limits exist, or that suprema and infima are taken by the function. If the space is not compact, it can be harder to analyze the behavior of a given function and more structural properties related to the function need to be known. From the perspective of OAC, the compactness is inherited due to the practical limitations. For instance, the sensor spaces are typically compact because a sensor can quantify values in a finite closed interval, e.g., $0^\circ\text{C} \leq s_k \leq 100^\circ\text{C}$, $\forall k$. Hence, to make general statements about entire function spaces and not only about specific examples, the space \mathbb{S}^K in Definition 1 is considered to be compact.

Now, let us denote the space of nomographic functions, the space of nomographic functions with the restriction of continuous pre- and post-processing functions, and the space of continuous functions with the domain \mathbb{E}^K as $\mathcal{N}(\mathbb{E}^K)$, $\mathcal{N}^0(\mathbb{E}^K)$, and $\mathcal{C}^0(\mathbb{E}^K)$, respectively.² Sprecher and Buck pro-

vide insights into the representation of a function $f \in \mathcal{C}^0(\mathbb{E}^K)$ as a nomographic function as follows:

Theorem 1 (Sprecher'65 [40]). Every function $f \in \mathcal{C}^0(\mathbb{E}^K)$ can be represented with real, monotonic increasing pre-processing functions and possibly a discontinuous post-processing function.

Theorem 2 (Buck'79 [41]). Every function $f \in \mathcal{F}(\mathbb{E}^K)$ is nomographic (i.e. $\mathcal{N}(\mathbb{E}^K) = \mathcal{F}(\mathbb{E}^K)$).

The key idea for the proof of Theorem 2 is to show there exists a one-to-one mapping from \mathbb{E}^K to a space $\Gamma \subset \mathbb{R}$ in the form of $g(s_1, \dots, s_K) = \sum_{k=1}^K \psi_k(s_k)$. Given the existence of such g (therefore, the pre-processing functions exist), the post-processing function can then be expressed as $\varphi(x) = f(g^{-1}(x))$, where g^{-1} is the inverse function that maps $x \in \Gamma$ to (s_1, \dots, s_K) . Without any restriction on the pre-functions and the post-processing function, such a map can be obtained by choosing $\Gamma = \mathbb{E}$ and constructing the binary representation of $x \in \Gamma$ by uniformly interleaving the digits of the binary representations of the symbol s_k , $\forall k$ (see [41, p. 287] and [42, p. 2]). For this specific constructive proof, ψ_k relies on reading the binary representation of s_k in base 2^K , which implicitly causes discontinuity in its range. The proof also shows the existence of special nomographic functions with an interesting property:

Definition 2 (Universality). The pre-processing functions are *universal* if they are fixed and can be used to calculate every function in $\mathcal{F}(\mathbb{E}^K)$.

The universality is a desirable property for OAC because the pre-processing functions do not need to be re-designed (i.e., less communication overhead) if the target function changes over time. This property is exploited in [2], [34] for multi-cluster computation as discussed in Section IV-C. It is also mentioned that universality provides robustness against changes in network topology (via dropping and joining devices) in the sense that transmitting nodes do not need to adapt their pre-processing functions.

If one desires the pre- and post-processing functions to be continuous for an arbitrary continuous function f , Theorem 2 is unfortunately not valid:

Theorem 3 (Buck'82 [43]). $\mathcal{N}^0(\mathbb{E}^K)$ is nowhere dense in $\mathcal{C}^0(\mathbb{E}^K)$.

A canonical example of Theorem 3 is geometric mean, i.e., $f(s_1, s_2, \dots, s_K) = (\prod_{k=1}^K s_k)^{\frac{1}{K}}$. This function cannot be represented as $\varphi(\sum_{k=1}^K \psi_k(s_k))$ with the continuous functions $\psi_1, \dots, \psi_K, \varphi$ on \mathbb{E} as demonstrated for $K = 2$ by Arnold [44] and for an arbitrary K by Goldenbaum [2]. Theorem 3 unfortunately implies that there exist infinite number of continuous functions in $\mathcal{C}^0(\mathbb{E}^K)$ that cannot be approximated with a nomographic function in $\mathcal{N}^0(\mathbb{E}^K)$ for a given arbitrary precision. Kolmogorov remarkably addresses the issue of representing a continuous function with a set of nomographic functions in $\mathcal{N}^0(\mathbb{E}^K)$:

Theorem 4 (Kolmogorov'57 [45]). Every function $f \in \mathcal{C}^0(\mathbb{E}^K)$ can be represented as the superposition of at most

²Nomographic functions in mathematics are often investigated by defining the compact space \mathbb{S} as \mathbb{E} .

$2K + 1$ nomographic functions in $\mathcal{N}^0(\mathbb{E}^K)$, i.e.,

$$f(s_1, s_2, \dots, s_K) = \sum_{\ell=1}^{2K+1} \varphi_{\ell} \left(\sum_{k=1}^K \psi_{k\ell}(s_k) \right), \quad (2)$$

where the post-processing functions φ_{ℓ} depend on f and the functions $\psi_{k\ell}$ are independent of f .

Geometrically, the $2K + 1$ inner sums in (2) ensures the existence of a continuous and bijective correspondence between $(s_1, \dots, s_K) \in \mathbb{E}^K$ and $(\varphi_1(\sum_{k=1}^K \psi_{k1}(s_k)), \dots, \varphi_{2K+1}(\sum_{k=1}^K \psi_{k,2K+1}(s_k))) \in \mathbb{R}^{2K+1}$. Hence, the inner sums describe a homeomorphism that continuously embeds \mathbb{E}^K into \mathbb{R}^{2K+1} . In [46], Sternfeld enhances the statement of Theorem 4 by showing that the $2K + 1$ nomographic functions in (2) cannot be reduced to represent every $f \in \mathcal{C}^0(\mathbb{E}^K)$. Hence, from the perspective of OAC, Theorem 4 implies that at least $2K + 1$ wireless resources need to be allocated where each resource is dedicated to a nomographic function in $\mathcal{N}^0(\mathbb{E}^K)$ to calculate every function in $\mathcal{C}^0(\mathbb{E}^K)$.

In mathematics, Theorem 4, also known as Kolmogorov's superposition or Kolmogorov-Arnold representation theorem, is notable because it solves a more constrained (i.e., the function f needs to be continuous), but a more general form (i.e., the superposition of only one variable functions) of Hilbert's thirteenth problem in [47]. There are also other variants of Kolmogorov's superposition and constructive proofs that show how to obtain the pre- and post-processing functions. For a comprehensive discussion on the variants and constructions, we refer the reader to [48, Chapter 2]. A variant that is mentioned in the OAC literature [2] is as follows:

Theorem 5 (Braun'09 [49]). For every function $f \in \mathcal{C}^0(\mathbb{E}^K)$, there exist $2K + 1$ nomographic functions in $\mathcal{N}^0(\mathbb{E}^K)$ such that

$$f(s_1, s_2, \dots, s_K) = \sum_{\ell=1}^{2K+1} \varphi_{\ell} \left(\sum_{k=1}^K \alpha_k \psi(s_k + (\ell - 1)\beta) \right), \quad (3)$$

where the pre-processing function ψ is a well-defined, continuous, monotone, and independent of f , the coefficients α_k , $\forall k$, and β are appropriate non-negative real constants.

The key observation made in [2] based on Theorem 5 is that to calculate every function in $\mathcal{C}^0(\mathbb{E}^K)$ with continuous nomographic functions over $2K + 1$ resources, the pre-processing functions can be designed to be universal. Note that the superposition in (3) involves $2K + 1$ post-processing function and one single pre-processing function. In the literature, it is shown that the superposition can also be expressed with a single pre-processing function and a single post-processing function as discussed in [48, Theorem 1] and [50, Theorem 2.14] by introducing a shift to the arguments of the post-processing functions in (3). Also, Kolmogorov's superposition can be also be interpreted as a special feed-forward neural network, which can be useful to predict the complexity of a neural network (see the discussions in [51]–[53]).

In some cases, it may be desirable not to consume $2K + 1$ wireless resources to calculate a specific continuous function

with $2K + 1$ continuous nomographic functions. In this case, one may follow one of two different directions: Manipulating the domain of the target function or constructing an nomographic function that approximates to the target function. In the first approach, some part of the domain is cut out so that the nomographic function can be calculated with continuous pre- and post-processing functions. For instance, if \mathbb{S} is chosen as $[\alpha, 1]$ for $\alpha > 0$, the geometric mean can be calculated with a nomographic function with the continuous $\psi_k(x) = \ln(x)$, $\forall k$, and $\varphi(x) = e^{x/K}$ on \mathbb{S} . In the second approach, for a given compact space, the target function is approximated by a nomographic function. In [2], nomographic approximation is defined as follows:

Definition 3 (Nomographic approximation). Let $\epsilon > 0$ be an arbitrary constant. The space of approximable nomographic functions with respect to the precision ϵ is defined by

$$\mathcal{N}_{\epsilon}^0(\mathbb{E}^K) \triangleq \left\{ f \in \mathcal{F}(\mathbb{E}^K) \mid \exists (\psi_1, \dots, \psi_K, \varphi) \in \mathcal{C}^0(\mathbb{E}) \times \dots \dots \mathcal{C}^0(\mathbb{E}) \times \mathcal{C}^0(\mathbb{R}) : \left\| f - \varphi \left(\sum_{k=1}^K \psi_k(s_k) \right) \right\|_{\infty} \leq \epsilon \right\}. \quad (4)$$

If $f \in \mathcal{N}_{\epsilon}^0(\mathbb{E}^K)$, we write $f(s_1, \dots, s_K) \approx \varphi(\sum_{k=1}^K \psi_k(s_k))$.

For example, under Definition 3, the geometric mean on \mathbb{E}^K is a function in $\mathcal{N}_{\epsilon}^0(\mathbb{E}^K)$ because it can be approximated with $\psi_k(x) = \ln(x + 1/p_0(\epsilon))$ and $\varphi(x) = e^{x/K}$ for $p_0(\epsilon) > 0$. Nevertheless, a complete characterization of the approximate nomographic functions is still an area that requires more investigation as it is possible to define the space of approximable nomographic functions in different ways. For instance, in [54, Eq. (5)], an approximate nomographic function is defined in stochastic manner. For further theoretical investigations on approximate nomography, the reader is also referred to [54]–[57].

Another interesting function space is the class of symmetric functions elaborated in [58]:

Definition 4 (Symmetric function). Let $\sigma : \mathbb{S}^K \rightarrow \mathbb{S}^K$ denotes a permutation. A function $f : \mathbb{S}^K \rightarrow \mathbb{R}$ that is invariant with respect to permutations of its arguments, i.e.,

$$f(s_1, \dots, s_K) = f(\sigma(s_1, \dots, s_K)), \quad \forall \sigma \quad (5)$$

is called symmetric function.

A distinct feature of the space of symmetric function is that only the data itself is important, rather than its origin. From an application standpoint, many functions such as mean, maximum, minimum, median, and majority vote (MV) that have either exact or approximate nomographic function belong to this class. The second important feature is that the functions in this space can be calculated through the type function, i.e., frequency histogram [9], [10], [58], [59]. Type function can be defined as multiple weighted arithmetic sums of indicator functions, i.e., counting the number of devices based on a certain set, which is also investigated under type-based multiple access (TBMA) in [9], [10].

B. Common nomographic functions

In TABLE I, we list several exact and approximate nomographic functions discussed in the literature. While arithmetic mean, weighted sum, and MV are used in distributed learning applications, modulo-2 sum often appears in physical layer network coding. The product operation is used for key generation in [60]. The maximum, minimum, and counting functions are used in WSN (e.g. generating an alert if the temperature rises) or to calculate histogram (e.g., calculating measurement statistics with TBMA [9], [10]). Geometric mean, p -norm, and polynomial functions are often mentioned to provide nomographic function examples that can be calculated over a wireless network.

An interesting direction is to calculate an approximate nomographic function with a continuous and monotone post-processing function and continuous pre-processing functions for a given a continuous function. In [56], an approximation is obtained by using a combination of a dimensionwise function decomposition and optimization over a class of monotone polynomials. In this approach, the target function is skewed with a bijective function such that the resulting function can be approximated well with a first-order analysis of variance (ANOVA) decomposition. To calculate the skew function, Bernstein polynomials are used. It is worth nothing that Bernstein polynomials can be utilized to constructively prove Weierstrass approximation theorem that states every continuous function can be approximated with an arbitrary precision over any finite interval by a polynomial of a sufficient order.

Another interesting direction is to calculate the target function by expressing it as a solution of an optimization problem and solving the problem through iterations that can be expressed with some elementary nomographic functions. For example, as discussed in Section IV-E1, geometric median can be calculated through iterations over-the-air by using the Weiszfeld algorithm in [61]. In [62], [63] and [64], by using the binary representations of the parameters, several non-linear functions, e.g., maximum or minimum, are proposed to be calculated through the communication rounds. For instance, to calculate the maximum of the parameters, in the first round, the ES inquires to the EDs with bit 1 in the most significant bit position of the binary representation of the parameter. If there is any response to the inquiry, the ES detects that the most significant bit of the maximum of the parameters is 1, otherwise it is 0. In the second step, if the most significant bit is detected as 1, the ES inquires to the EDs with bit 1 in both most and second significant bits. Otherwise, the ES inquires to all EDs with bit 1 in the second significant bit position. From the responses to the second inquiry, the ES determines the second significant bit. The procedure continues until the least significant bit is detected. The same procedure can be used for computing minimum function by using the reciprocal of the parameters. The reader is also referred to [59] for successive partitions to compute functions.

III. WHAT ARE THE OAC SCHEMES?

An OAC scheme aims to realize (1) (or (2)) over a wireless multiple-access channel (MAC) with a fidelity criterion. For a rigorous classification and a generalization of

TABLE I
EXAMPLE NOMOGRAPHIC FUNCTIONS.

Description	$f(s_1, s_2, \dots, s_K)$	$\psi_k(x)$	$\varphi(x)$
Arithmetic mean	$\frac{1}{K} \sum_{k=1}^K s_k$	x	$\frac{x}{K}$
Weighted sum	$\sum_{k=1}^K w_k s_k, w_k \in \mathbb{R}$	$w_k x$	x
Polynomial function	$\sum_{k=1}^K c_k s_k^{k-1}, c_k \in \mathbb{R}$	$c_{k-1} x^{k-1}$	x
Majority vote	$\text{sign} \left(\sum_{k=1}^K \text{sign}(s_k) \right)$	$\text{sign}(x)$	$\text{sign}(x)$
Counting number of EDs with the class \mathcal{C}	$\sum_{k=1}^K \mathbb{I}[s_k \in \mathcal{C}]$	x	$\mathbb{I}[x \in \mathcal{C}]$
p -norm	$\left(\sum_{k=1}^K s_k ^p \right)^{1/p}$	$ x ^p$	$x^{\frac{1}{p}}$
Modulo-2 sum	$s_1 \oplus s_2 \dots \oplus s_K, s_k \in \mathbb{Z}_2$	x	$x \bmod 2$
Approximation of the product	$\prod_k s_k$	$\ln \left(x + \frac{1}{p_0(\epsilon)} \right)$	e^x
Approximation of the geometric mean	$\left(\prod_k s_k \right)^{1/K}$	$\ln \left(x + \frac{1}{p_0(\epsilon)} \right)$	$e^{\frac{x}{K}}$
Approximation of the cosine of the product	$\cos \left(\prod_k s_k \right)$	$\ln \left(x + \frac{1}{p_0(\epsilon)} \right)$	$\cos(e^x)$
Approximation of the maximum	$\max_k \{s_k\}$	$x^{p_0(\epsilon)}$	$\frac{1}{x^{p_0(\epsilon)}}$
Approximation of the minimum	$\min_k \{s_k\}$	$x^{-p_0(\epsilon)}$	$x^{-\frac{1}{p_0(\epsilon)}}$

the OAC schemes in the state-of-the-art, consider an OAC scheme that targets to calculate the nomographic function $z[n] = f(\mathbf{s}[n]) \triangleq f(s_1[n], \dots, s_K[n])$ for the symbol vector $\mathbf{s}[n] = [s_1[n], \dots, s_K[n]]^T, \forall n \in \{1, \dots, N_f\}, N_f \geq 1$. Let $\mathbf{s}_k = [s_k[1], \dots, s_k[N_f]]^T$ and $\mathbf{p}_k = [p_k[1], \dots, p_k[N_f]]^T$ denote the symbol vector and the pre-processed symbol vector at the k th ED for $p_k[n] = \varphi_k(s_k[n]) \in \mathbb{R}, \forall n$. The k th ED calculates the encoded vector $\mathbf{c}_k \in \mathbb{C}^B$ as

$$\mathbf{c}_k = [c_1, \dots, c_B]^T = \epsilon_k \{\mathbf{p}_k\}, \quad (6)$$

where $\epsilon_k : \mathbb{R}^{N_f} \rightarrow \mathbb{C}^B$ is the encoder (e.g., source encoder, channel encoder, constellation mapping, or a combination of these operations) and B is the number of modulation symbols in a complex-valued codeword.

Let \mathcal{M} be a resource mapper that maps B modulation symbols to the B available resources. Now, consider L modulation symbols among B symbols, denoted by $\mathbf{m}_k = [m_{k,1}, \dots, m_{k,L}]^T$, that are processed with a linear precoder $\mathbf{B}_k \in \mathbb{C}^{N_t \times L}$ as

$$\mathbf{x}_k = [x_{k,1}, \dots, x_{k,N_t}]^T = \mathbf{B}_k \mathbf{m}_k, \quad (7)$$

where $\mathbf{x}_k \in \mathbb{C}^{N_t}$ is the transmitted symbols from the k th ED over N_t dimensions. Hence, each ED applies $N_{\text{access}} \triangleq \lceil B/L \rceil$ linear precoders to the modulation symbols in total.

The received vector at the ES, denoted by $\mathbf{y} \in \mathbb{C}^{N_r}$, can be written as

$$\begin{aligned} \mathbf{y} = [y_1, \dots, y_{N_r}]^T &= \sum_{k=1}^K \sqrt{P_k} \mathbf{H}_k \mathbf{x}_k + \mathbf{n} \\ &= \sum_{k=1}^K \sqrt{P_k} \mathbf{H}_k \mathbf{B}_k \mathbf{m}_k + \mathbf{n}, \end{aligned} \quad (8)$$

where $\mathbf{H}_k \in \mathbb{C}^{N_r \times N_t}$ is the channel matrix between the k th ED and the ES with the assumptions of $\mathbb{E} \left\{ \mathbf{H}_k \mathbf{H}_k^H \right\} = N_t \mathbf{I}_{N_r}$

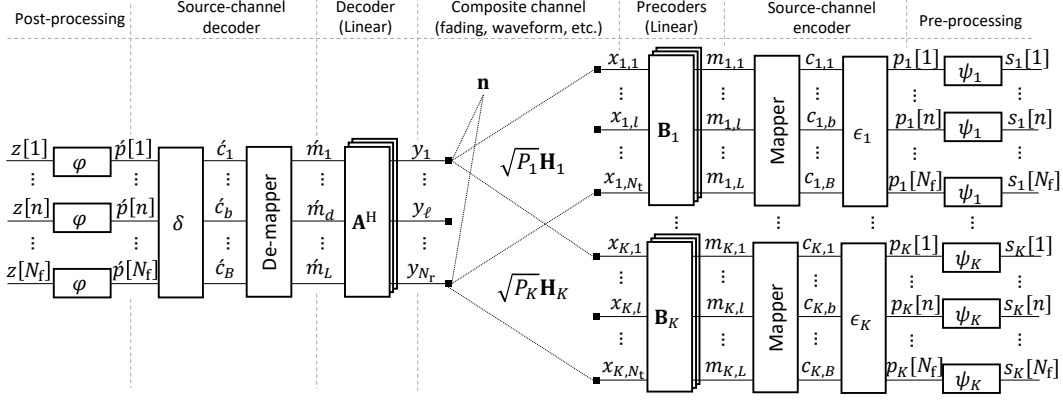


Fig. 2. A generalized model for an OAC method. The domains of the transmitted vectors $\mathbf{x}_k, \forall k$, and the received vector \mathbf{y} can be time, frequency, space, etc, depending on the OAC method.

and each element of \mathbf{H}_k is modeled as a zero-mean symmetric complex Gaussian random variable, unless otherwise stated, $\mathbf{n} = [n_1, \dots, n_{N_r}]^T \in \mathbb{C}^{N_r} \sim \mathcal{CN}(\mathbf{0}_{N_r}, \sigma_n^2 \mathbf{I}_{N_r})$ is the zero-mean symmetric noise vector with the variance σ_n^2 , N_r is the number of available dimensions at the ES, and $P_k \in \mathbb{R}$ denotes the received signal power for the k th ED, which is a function of the large-scale channel model, power control, waveform, power amplifier (PA) non-linearity, and adjacent-channel-leakage ratio (ACLR) requirements (see Section IV-B for further discussions). The receiver at the ES processes the superposed vector \mathbf{y} with a linear decoder $\mathbf{A}^H \in \mathbb{C}^{L \times N_r}$ (e.g., to overcome the impact of channel on the superposition along with $\mathbf{B}_k, \forall k$) as

$$\begin{aligned} \hat{\mathbf{m}} &= [\hat{m}_1, \dots, \hat{m}_L]^T = \mathbf{A}^H \mathbf{y} \\ &= \sum_{k=1}^K \sqrt{P_k} \mathbf{A}^H \mathbf{H}_k \mathbf{B}_k \mathbf{m}_k + \mathbf{A}^H \mathbf{n}. \end{aligned} \quad (9)$$

By using N_{access} outputs of the linear decoders, the resource de-mapper \mathcal{M}^{-1} first constructs the superposed codeword $\hat{\mathbf{c}} = [\hat{c}_1, \dots, \hat{c}_B]^T \in \mathbb{C}^B$. Afterwards, the receiver calculates an estimate of the superposed pre-processed symbols as

$$\hat{\mathbf{p}} = [\hat{p}[1], \dots, \hat{p}[N_f]]^T = \delta \{ \hat{\mathbf{c}} \}, \quad (10)$$

where $\delta : \mathbb{C}^B \rightarrow \mathbb{R}^{N_f}$ is the decoder (e.g., constellation de-mapper, channel decoder, source decoder, or a combination of these operations) at the ES. Finally, the target functions are evaluated with the post-processing function as $\mathbf{z} = [z[1], \dots, z[N_f]]^T \in \mathbb{R}^{N_f}$ for $z[n] = \varphi(\hat{p}[n]) \in \mathbb{R}, \forall n \in \{1, \dots, N_f\}$.

In Fig. 2, we provide a block diagram based on aforementioned transmitter and receiver operations for OAC. It is worth noting that we do not specify the domains of the transmitted vectors $\mathbf{x}_k, \forall k$, and the received vector \mathbf{y} . Without loss of generality, the domain can be time, frequency, space and depends on the scheme. In addition, if the target function is based on Kolmogorov's superposition, $2K+1$ nomographic functions in (2) can be computed over orthogonal resources (see [36] for an example) with a general OAC scheme.

A. Metrics

In this subsection, we discuss widely used metrics for assessing OAC schemes.

1) *Error definitions*: Let $\hat{f}(\mathbf{s}[n])$ be an estimate of $f(\mathbf{s}[n])$ for $\mathbf{s}[n] \triangleq [s_1[n], \dots, s_K[n]]^T$, for $n \in \{1, 2, \dots, N_f\}$. The function-estimation error (FEE) can be expressed as

$$e_{\text{FEE}}(\hat{f}(\mathbf{s}[n])) \triangleq \hat{f}(\mathbf{s}[n]) - f(\mathbf{s}[n]). \quad (11)$$

In [39] and [65], for $f(\mathbf{s}[n]) \in [f_{\min}, f_{\max}]$, $\forall n$, a normalized FEE is defined by

$$e_{\text{NFEE}}(\hat{f}(\mathbf{s}[n])) \triangleq \frac{e_{\text{FEE}}(\hat{f}(\mathbf{s}[n]))}{f_{\max} - f_{\min}}. \quad (12)$$

2) *Average error*: The classical mean-squared error (MSE) [66], [67], normalized MSE, and Bayesian MSE for computation can be expressed as

$$MSE(\hat{f}(\mathbf{s}[n])) \triangleq \mathbb{E} \left\{ \|e_{\text{FEE}}(\hat{f}(\mathbf{s}[n]))\|_2^2 \right\},$$

and

$$NMSE(\hat{f}(\mathbf{s}[n])) \triangleq \frac{\mathbb{E} \left\{ \|e_{\text{FEE}}(\hat{f}(\mathbf{s}[n]))\|_2^2 \right\}}{\|f(\mathbf{s}[n])\|_2^2},$$

and

$$BMSE \triangleq \mathbb{E} \left\{ MSE(\hat{f}(\mathbf{s}[n])) \right\},$$

respectively. In [63], the mean-squared function error (MSFE) is defined by

$$MSFE \triangleq \frac{\mathbb{E} \left\{ \|e_{\text{FEE}}(\hat{f}(\mathbf{s}[n]))\|_2^2 \right\}}{\mathbb{E} \left\{ \|f(\mathbf{s}[n])\|_2^2 \right\}}, \quad (13)$$

where the expectation is over both $\mathbf{s}[n], \forall n$, and the channel.

3) *Outage probability*: The outage probability provides a statistical view of the computation error as compared with MSE. By using (12), it can be defined as the probability that the normalized FEE is larger than or equal to ϵ [39] [65], i.e.,

$$P_{\text{out}}(\epsilon) \triangleq \Pr \left(|e_{\text{NFEE}}(\hat{f}(\mathbf{s}[n]))| \geq \epsilon \right). \quad (14)$$

Based on [4], for a given ϵ , the block outage probability may also be defined by

$$P_{\text{bout}}(\epsilon) \triangleq \Pr \left(\bigcup_{n=1}^{N_f} \sup |\hat{f}(\mathbf{s}[n]) - f(\mathbf{s}[n])| > \epsilon \right). \quad (15)$$

4) *Computation error rate*: Computation error rate (CER) is analogous to the bit error rate in communication systems. It can be used for assessing the computation when the arguments of the functions are discrete values. Let $s_k[n]$ be a discrete random variable, $\forall k, n$. The CER can be defined as

$$P_{\text{cer}} \triangleq \Pr \left(\hat{f}(\mathbf{s}[n]) \neq f(\mathbf{s}[n]) \right). \quad (16)$$

If N_f functions are taken into account for the error-rate calculation, as done in [3] and [68], the block-computation error rate (BCER) can be expressed as³

$$P_{\text{bcer}} \triangleq \Pr \left(\bigcup_{n=1}^{N_f} \hat{f}(\mathbf{s}[n]) \neq f(\mathbf{s}[n]) \right). \quad (17)$$

5) *Computation rate and throughput*: Computation rate \mathcal{R} and computation throughput R can be defined as the number of functions computed per channel use [3], [4], [68] and the number of functions computed per second, respectively. They can be expressed as

$$\mathcal{R} = \frac{N_f}{D} \text{ [functions/dimension]}, \quad (18)$$

and

$$R = \frac{N_f}{T} \text{ [functions/second]}, \quad (19)$$

where $D = 2N_{\text{access}}N_r$ and T are the number of real dimensions and the interval used for computing N_f functions, respectively.⁴ It is worth nothing that the number of real dimensions for a single-input-single-output scenario is approximately equal to $2WT$ for given bandwidth W and time interval T [69, Section 4.6]. Hence, for S spatial streams, the computation throughput can be approximately calculated as $R \approx 2WS \times \mathcal{R}$.

Based on [3] and [68], achievable computation rate can be defined as follows:

Definition 5 (Achievable computation rate [3], [68]). Let $s_k[n]$ be a discrete random variable, $\forall k, n$. The rate \mathcal{R} is said to be achievable if there exists a sequence of length- B block codes such that $\lim_{B \rightarrow \infty} P_{\text{bcer}} = 0$.

In [7], the computation of modulo- p sum function, i.e., $f(\mathbf{s}[n]) = \bigoplus_{k=1}^K q_k s_k[n]$, $\forall n$, for $s_k[n], q_k \in \mathbb{F}_p$, is investigated over Gaussian channel, i.e., $\hat{c}_b = \sum_{k=1}^K h_k c_{k,b} + n_b$ (see Fig. 2). For $n_b \in \mathbb{R}$, in [7, Theorem 2], Nazer and Gastpar show that achievable computation rate is

$$\mathcal{R} < \mathcal{R}^{\text{comp}} = \frac{\frac{1}{2} \log_2^+ \left(\left(\|\mathbf{a}\|_2^2 - \frac{P(\mathbf{h}^T \mathbf{a})^2}{\sigma_n^2 + P\|\mathbf{a}\|_2^2} \right)^{-1} \right)}{\log_2(p)}, \quad (20)$$

³In [3] and [68], (17) is defined as probability of error. To differentiate (17) from (16), we use a different terminology for (17) in this study.

⁴The dimensions can be in time, frequency, and/or space, depending on the resource utilization.

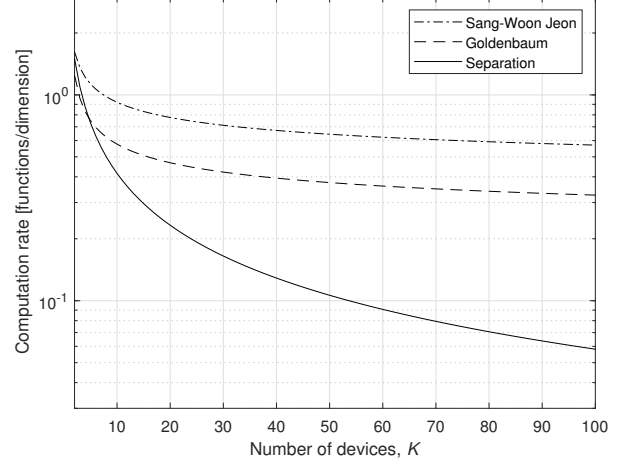


Fig. 3. Achievable computation rate for the arithmetic sum of K Bernoulli random variables in AWGN channel. The achievable computation rate with the separation of communications and computation can be dramatically lower than the ones with joint communications and computations.

where $\mathbf{a} = [a_1, \dots, a_K] \in \mathbb{Z}^K$ for $q_k = g^{-1}(a_k \bmod p)$, i.e., g^{-1} is a map from $\{0, 1, \dots, p-1\}$ to the corresponding elements in \mathbb{F}_p , and P is the average transmit power, $\mathbf{h} = [h_1, \dots, h_K] \in \mathbb{R}^K$. By observing the fact that, for a sufficiently large prime q , computing the modulo- q sum of K elements for $s_k[n] < p$ is equivalent to the arithmetic sum for $q > (p-1)K$ and using [1, Theorem 1] and (20) for $a_k = 1, \forall k$, Jeon, Chien-Yi, and Gastpar in [3] show that the achievable computation rate can be expressed as

$$\mathcal{R} < \mathcal{R}^{\text{comp}} = \frac{\frac{1}{2} \log_2^+ \left(\frac{1}{K} + \min_{\forall k} \frac{|h_k|^2 P}{\sigma_n^2} \right)}{H(f(\mathbf{s}[n]))}, \quad (21)$$

where $H(\cdot)$ is the entropy function and $s_k[n]$ is a discrete random variable, $\forall k, n$.

In [4], achievable computation rate is defined as follows:

Definition 6 (Achievable computation rate [4]). The parameter $\mathcal{R}^{\text{comp}}(f, \epsilon)$ is said to be an achievable computation rate for f and ϵ , if there exists a scheme that fulfills $P_{\text{bout}}(\epsilon) < \delta$ for every rate $\mathcal{R} < \mathcal{R}^{\text{comp}}(f, \epsilon)$ and every $\delta > 0$.

Based on Definition 6 and using the properties of nested lattice codes as done in [1] and [7], for a real-valued additive white Gaussian noise (AWGN) channel and arithmetic sum, in [4, Theorem 5 with Equation (54)], Goldenbaum shows that

$$\mathcal{R} < \mathcal{R}^{\text{comp}}(f, \epsilon) = \frac{\frac{1}{2} \log_2^+ \left(\frac{P}{\sigma_n^2} \right)}{\log_2(2^{b_0(f, \epsilon)} - 1) + \log_2 K}, \quad (22)$$

where $b_0(f, \epsilon)$ is the number of bits defined in Section III-C2a for given function f and the amount of maximum distortion ϵ .

In Fig. 3, we demonstrate the achievable computation rates for a given number of EDs based on the example given in [3] for arithmetic sum. Suppose the symbols $s_k[n]$, $\forall k, n$, are independent and identically distributed (IID) Bernoulli

random variables with the probability $1/2$ and the signal-to-noise ratio (SNR) is 15 dB. From [70], $H(f(s[n]))$ can be calculated as $H(f(s[n])) = K - 2^{-K} \sum_{k=1}^K \binom{K}{k} \log_2 \binom{K}{k} \leq \frac{1}{2} \log_2 (\pi e K / 2)$. Also, $b_0(f, \epsilon) = 1$ is sufficient for the representation of the symbols. The achievable computation rate for the separation can be calculated as $\frac{1}{2K} \log_2 (1 + KP/\sigma_n^2)$ [3], [71, Equation 6.13]. As can be seen from Fig. 3, the achievable computation rate with the separation of communications and computation can be dramatically lower than the ones with joint communications and computations. For example, if there are $K = 100$ EDs, OAC promises approximately 10 times faster reliable computations than the one with separation. For this example, Goldenbaum's result is more conservative than Jeon's rate as Goldenbaum's expression implicitly assumes equiprobable final outcomes. In [42, p. 4], for the same scenario, it is argued that the EDs can send significantly less information to the ES if the objective is to compute the sum function. This is because the entropy of the computed function is much smaller than the amount of information that needs to be transferred to the ES with the separation, i.e., $H(f(s[n])) \leq \sum_{k=1}^K H(s_k[n]) = K$.

In [68], [72], to improve the computation rate, a construction of the target function via local functions is proposed. In [68], the authors assume that the channel coefficients are IID random variables and select a subset of EDs with largest channel gains to compute local functions and gradually calculates the target function over fast fading channels. It is shown that non-vanishing computation rate is achievable even if the number of ED in the network increases. In a recent work [73], nested lattice codes are utilized along with stochastic quantization for AWGN channel. A theoretical comparison between uncoded OAC, coded OAC, and separation is provided in terms of distortion under Gaussian channels. In [74], the computation rates for both homogeneous and heterogeneous networks under large-scale fading are studied. The reader is also referred to [17] for the computation rates for uncoded and coded physical layer network coding strategies.

B. Classification criteria: Availability of CSI

One of the challenges for calculating (1) with an OAC method arises due to the fact that the impact of multi-path distortions on the transmitted symbols from the EDs, i.e., $\mathbf{H}_k \mathbf{x}_k$, occur before the superposition as expressed in (8). Hence, an estimator that estimates the output of the function at the ES can be unrealized, i.e., it may not be written solely as a function of the received symbols. For example, consider a scenario where \mathbf{H}_k is IID and follows Rayleigh fading and the power control ensures that the average received signal powers are perfectly aligned, e.g., $P_k = 1, \forall k$. Since the superposed symbol at the ES in this case cannot be expressed as

$$\mathbf{y} = \sum_{k=1}^K \mathbf{H}_k \mathbf{x}_k + \mathbf{n} = \mathbf{H} \sum_{k=1}^K \mathbf{x}_k + \mathbf{n}, \quad (23)$$

where $\mathbf{H} \in \mathbb{C}^{N_r \times N_t}$ is a matrix independent of the vector $\mathbf{x}_k, \forall k$ (i.e., there is no uniform fading matrix \mathbf{H} [66]), an equalizer that relies on the availability of \mathbf{H} to obtain $\sum_{k=1}^K \mathbf{x}_k$ cannot be realized. Given this observation, in this subsection,

we classify the methods in the state-of-the-art based on how they deal with the fading due to the wireless channel through the precoders $\mathbf{B}_k, \forall k$, and the decoder \mathbf{A} . We group them based on the availability of CSI at the transmitter (CSIT) and CSI at the receiver (CSIR). For simplifying the classification, we assume $P_k = 1, \forall k$. We also provide corresponding equations for different strategies in TABLE II when the real part of the superposed symbol is used for computation.

1) *CSIT: Available, CSIR: Not Available*: In this category, we assume that all EDs have their own CSI (i.e., the k th ED knows \mathbf{H}_k , but not the set $\{\mathbf{H}_{k'} | k' \neq k\}$) and the CSI is not available to the ES, i.e., no CSIR. Hence, the EDs cannot make coordinated transmissions. However, each ED can pre-distort its own transmitted symbols under an average transmit power constraint or an instantaneous transmit power constraint by designing the precoders, i.e., $\mathbf{B}_k, \forall k$, such that the superposed symbol at the receiver is a good approximation to the desired value. In this category, the equalization used in traditional communication is shifted from the receiver to the transmitter. The computation rate of these schemes can be as high as $\mathcal{R} = 1$ function/dimension if both imaginary and real part of the received symbols are exploited.

a) *Channel inversion*: Truncated-channel inversion (TCI) is a pre-equalization technique considered in many studies in the literature, e.g., [75]–[87]. In this approach, to reverse the effect of the wireless channel on the transmitted symbols, the symbol is multiplied with the inverse of the channel coefficient if the absolute square of the corresponding channel coefficient is larger than a pre-set threshold t . Hence, TCI is inline with zero-forcing (ZF) [88]–[90] (or pseudo-inverse of the channel matrix in general for $N_r \leq N_t$). Three potential issue can arise with TCI: 1) Due to the inversion, the transmit power can increase instantaneously. As a result, it can cause instantaneous spectral growth for a non-linear hardware. 2) Due to the truncation, some of the EDs may not participate in the computation, e.g., $s_k = 0$ for a non-participating ED. The implication of non-participating EDs on the performance depends on the application. 3) A power normalization that takes the average transmit power into account needs to be applied to the symbols, which is a function of the channel statistics. In the literature, the power control factor η_k for TCI is often designed based on the average transmit power after the truncation for Rayleigh fading channel (See [75, Eq. 13] and [77, Eq. 13] and the corresponding encoding in TABLE II), i.e.,

$$\eta_k = \frac{1}{\text{Ei}(t)}, \quad (24)$$

where $\text{Ei}(\cdot)$ is the exponential integral defined as $\text{Ei}(t) \triangleq \int_t^\infty \frac{1}{x} \exp(-x) dx$. Note that TCI is also mentioned in Goldenbaum's early work in [39, Remark 4], but not analyzed. In [91], TCI is investigated in a scenario where the same symbol is transmitted over different subcarriers to achieve a diversity gain.

b) *Phase correction*: Phase correction (PC) is a pre-equalization strategy to achieve a coherent superposition by rotating the phase of the transmitted symbols based on the amount of the phase distortion due to the channel [10], [90],

TABLE II
COMPUTATION UNDER FADING CHANNEL

Category	Method	N_t	N_r	N_f	Structure of channel \mathbf{H}_k	Linear precoder \mathbf{B}_k	Linear decoder \mathbf{A}	Encoder $\mathbf{e}_k\{\mathbf{p}_k\}$	Decoder $\delta\{\hat{\mathbf{e}}\}$	Rate \mathcal{R} ($N_{\text{access}} = 1$)	$\psi_k(x)$ & $\varphi(x)$	Calculated function	Target function
CSIT: ✓ CSIR: ✗	Zero forcing	1	1	1	h_k	$\sqrt{\eta_k} \frac{h_k^*}{ h_k ^2}$	1	p_k	$\hat{\mathbf{e}}$	$\frac{1}{2}$	x	$\Re \left\{ \sum_{k=1}^K \sqrt{\eta_k} s_k + n \right\}$	$\sum_{k=1}^K s_k$
	Truncated channel inversion	1	1	1	h_k	$\sqrt{\eta_k} \frac{h_k^*}{ h_k ^2} \mathbb{I} [h_k ^2 > t]$	1	p_k	$\hat{\mathbf{e}}$	$\frac{1}{2}$	x	$\Re \left\{ \sum_{k=1}^K \sqrt{\eta_k} \mathbb{I} [h_k ^2 > t] s_k + n \right\}$	$\sum_{k=1}^K s_k$
	Phase correction	1	1	1	h_k	$\frac{h_k^*}{ h_k }$	1	p_k	$\hat{\mathbf{e}}$	$\frac{1}{2}$	x	$\Re \left\{ \sum_{k=1}^K h_k s_k + n \right\}$	$\sum_{k=1}^K s_k$
	Maximum ratio transmission	N	1	1	$[h_{k,1}, \dots, h_{k,N}]$	$\sqrt{\eta_k} \mathbf{h}_k^H$	1	p_k	$\hat{\mathbf{e}}$	$\frac{1}{2}$	x	$\Re \left\{ \sum_{k=1}^K \sqrt{\eta_k} \ \mathbf{h}_k\ _2^2 s_k + n \right\}$	$\sum_{k=1}^K s_k$
	Amplitude correction + energy estimation	N	N	1	$\text{diag} \{ [h_{k,1}, \dots, h_{k,N}] \}$	$\text{diag} \left\{ \left[\frac{\sqrt{\eta_k}}{ h_{k,1} }, \dots, \frac{\sqrt{\eta_k}}{ h_{k,N} } \right] \right\}$	$\frac{1}{N} \mathbf{y}$	$\begin{bmatrix} \sqrt{g(p_k)} \times \\ e^{j\theta_1}, \dots, e^{j\theta_N} \end{bmatrix}^T$ g is affine	$g^{-1}(\hat{\mathbf{e}})$	$\frac{1}{2N}$	x	$g^{-1} \left(\Re \left\{ \sum_{k=1}^K \eta_k g(s_k) + \text{noise} + \text{inter.} \right\} \right)$	$\sum_{k=1}^K s_k$
CSIT: ✓ CSIR: ✓	ZF coordination	N	M	L	$\begin{bmatrix} h_{k,1,1}, \dots, h_{k,N,1} \\ \vdots \\ h_{k,1,M}, \dots, h_{k,N,M} \end{bmatrix}$	(25)	(28)	\mathbf{p}_k	$\hat{\mathbf{e}}$	$\frac{L}{2M}$	x	$\Re \left\{ \sum_{k=1}^K s_k + (\mathbf{A}^*)^H \mathbf{n} \right\}$	$\sum_{k=1}^K s_k$
	MMSE coordination	N	M	L	$\begin{bmatrix} h_{k,1,1}, \dots, h_{k,N,1} \\ \vdots \\ h_{k,1,M}, \dots, h_{k,N,M} \end{bmatrix}$	(29)	(29)	\mathbf{p}_k	$\hat{\mathbf{e}}$	$\frac{L}{2NM}$	x	$\Re \left\{ \sum_{k=1}^K (\mathbf{A}^*)^H \mathbf{H}_k \mathbf{B}_k^H s_k + (\mathbf{A}^*)^H \mathbf{n} \right\}$	$\sum_{k=1}^K s_k$
CSIT: ✓ CSIR: ✓	Channel hardening via aggregated CSI	1	M	1	$[h_{k,1}, \dots, h_{k,M}]^T$	1	$\frac{1}{M} \sum_{k=1}^K \mathbf{h}_k$	p_k	$\hat{\mathbf{e}}$	$\frac{1}{2M}$	x	$\Re \left\{ \sum_{k=1}^K \frac{\ \mathbf{h}_k\ _2^2}{M} s_k + \frac{1}{M} \sum_{k=1}^K \mathbf{h}_k^H \mathbf{n} + \text{inter.} \right\}$	$\sum_{k=1}^K s_k$
CSIT: ✗ CSIR: ✗	Channel hardening + energy estimation	N	NM	1	$\begin{bmatrix} \text{diag} \{ [h_{k,1,1}, \dots, h_{k,N,1}] \} \\ \vdots \\ \text{diag} \{ [h_{k,1,M}, \dots, h_{k,N,M}] \} \end{bmatrix}$	\mathbf{I}_N	$\frac{1}{NM} \mathbf{y}$	$\begin{bmatrix} \sqrt{g(p_k)} \times \\ e^{j\theta_1}, \dots, e^{j\theta_N} \end{bmatrix}^T$ g is affine	$g^{-1}(\hat{\mathbf{e}})$	$\frac{1}{2NM}$	x	$g^{-1} \left(\Re \left\{ \sum_{k=1}^K \frac{\text{tr}(\mathbf{H}_k^H \mathbf{H}_k)}{NM} g(s_k) + \text{noise} + \text{inter.} \right\} \right)$	$\sum_{k=1}^K s_k$
	Orthogonal signaling	2	2	1	$\text{diag} \{ [h'_k, h''_k] \}$	\mathbf{I}_2	\mathbf{I}_2	$\begin{bmatrix} 1 [p_k = 1] \\ 1 [p_k = -1] \end{bmatrix}$	Energy comparator	$\frac{1}{4}$	$\text{sign}(x)$	$\text{sign} \left(\left[\sum_{k=1}^K h'_k + n_1 \right]^2 - \left[\sum_{k=1}^K h''_k + n_2 \right]^2 \right)$	$\text{sign} \left(\sum_{k=1}^K \text{sign}(s_k) \right)$

[92]–[95]. The main advantage of this approach is that the power normalization due to the pre-equalization is not needed. On the other hand, PC does not correct the amplitude of the superposed symbols. For some applications, this is not an issue. For example, in [96], it is shown that amplitude alignment is not necessarily the best strategy for FEEL. In [92], it is emphasized that correcting the phase with an error less than $\pi/2$ can be sufficient to yield a constructive aggregation at the receiver. The PC is also utilized with broadband analog aggregation (BAA) in [97] and one-bit broadband digital aggregation (OBDA) in [98] for FEEL. In [99], PC is applied only for the real part of the symbols, which corresponds to a sign multiplication.

c) *Amplitude correction and energy estimation*: In [37]–[39], [100], Goldenbaum and Stańczak propose to calculate the energy of a sequence of superposed symbols along with a channel inversion to compute a general nomographic function. In this approach, the output of the pre-processing function is processed further with a function g that results in a non-negative value and afterwards the *square root* of the resulting value is multiplied with a sequence of length N as $\sqrt{g(p_k)} \times [e^{j\theta_1}, \dots, e^{j\theta_N}]$. At the receiver, the energy of the received sequence is calculated to achieve the OAC and the superposed symbol is processed with the inverse function g^{-1} (see TABLE II for the final expression). Three interesting observations were made: 1) Only amplitude correction is needed as the receiver calculates the energy of the symbol. This implies that the EDs need only modulus CSI [101, Proposition 1]. 2) The sequences for the proposed scheme should be designed to harness interference as a common goal, instead of eliminating the interference as in a traditional code division multiple access systems [37]. The need for a sequence set that should satisfy the property of mutually-orthogonal complementary codes or Z-complementary code set in general (e.g., [102, Eq. 2]). In [39], unimodular sequences with

random phases are adopted to reduce the interference. 3) As the ES calculates the energy of the received sequence, the proposed scheme is not sensitive to time and phase synchronization errors (see [39, Figure 2] for an illustration). By following Goldenbaum's work [39], in [65], it is assumed that the range space of each pre-processing function is a compact subset of non-negative reals. At the EDs, amplitude correction with truncation is applied to the output of the pre-processing function. To ensure both peak and average transmit power constraints, a sequential symbol power adaptation strategy that uses only the observed channel coefficients is proposed. At the ES, the energy of the superposed sequence is calculated to compute the nomographic function. Note that truncation is also used in [103] to realize Goldenbaum and Stańczak's scheme in practice.

d) *Maximum-ratio transmission without CSIR*: With maximum-ratio transmission (MRT) for traditional communications, a symbol is transmitted on the strongest eigenmode of the channel matrix and the received signals are combined using maximum-ratio combining (MRC), which requires both CSIT and CSIR [104]. In [105], MRT without CSIR is proposed for a scenario with single-antenna ES and EDs. In this approach, the symbols are multiplied with the conjugate of the channel coefficients. Hence, the transmit power can be more effectively utilized as compared to that of PCs if the symbols at the ED observe channel coefficients with different magnitudes. However, the norm-square of the channel appears on the calculated function (see TABLE II). The power control factor for this approach can be designed based on average transmit power (i.e., $\eta_k = 1/N_t$) or instantaneous transmit power (i.e., $\eta_k = 1/\|\mathbf{h}_k\|_2^2$ for $N_t > 1$) [106].

e) *What can go wrong?*: The methods in this category requires an *accurate* CSITs at the EDs. However, as discussed in [39], this can impose stringent requirements on the underlying mechanisms such as time and phase synchronizations, channel

estimation, and channel prediction, which can be challenging to satisfy without a clock synchronization and/or under the non-stationary channel conditions in mobile wireless networks [107], [108]. A sample-level precise synchronization (i.e., not just within the cyclic prefix (CP) duration of an orthogonal frequency division multiplexing (OFDM) symbol) is needed for the methods that are sensitive to the phase distortion as the CSI is a function of the synchronization point at the ES and the time-of-arrivals of the transmitted signals from the EDs. The second challenge is that it is not trivial to extend these methods to the cases with $N_r > N_t$ (e.g., an ES with multiple antennas or a multi-cell computation) [109]. This is due to the fact that the precoder cannot achieve a channel inversion for a random channel matrix without interference (i.e., $\mathbf{H}_k \mathbf{B}_k \neq \mathbf{I}_{N_r}$ for $N_r > N_t$). One potential solution to this issue is a coordination among the EDs (e.g., through some orchestration by an ES or multiple ESs) as done in uniform focusing, which unfortunately requires some knowledge on CSIR.

2) *CSIT: Available, CSIR: Available*: In this category, we assume that the CSI is available at both ES and EDs. Hence, it is the most flexible framework for optimizing the OAC performance as the precoders, i.e., $\mathbf{B}_k, \forall k$, and the decoder, i.e., \mathbf{A} , can be designed jointly.

a) *ZF and MMSE coordinations*: For ZF coordination [63], [66], [110]–[112], the noise at the ES is ignored. In this case, if $\mathbf{A}^H \mathbf{H}_k \mathbf{H}_k^H \mathbf{A}$ is an invertible matrix, $\forall k$, for a given $\mathbf{A} \triangleq \mathbf{A}_n / \sqrt{\eta}$ for any $\mathbf{A}_n \in \mathbb{C}^{L \times N_r}$ such that $\text{tr}\{\mathbf{A}_n^H \mathbf{A}_n\} = L$, the precoder $\mathbf{B}_k, \forall k$, can be obtained as

$$\mathbf{B}_k = (\mathbf{A}^H \mathbf{H}_k)^{\dagger} = \sqrt{\eta} (\mathbf{A}_n^H \mathbf{H}_k)^H (\mathbf{A}_n^H \mathbf{H}_k \mathbf{H}_k^H \mathbf{A}_n)^{-1}, \quad (25)$$

where $\max_k \text{tr}\{\mathbf{B}_k \mathbf{B}_k^H\} \leq P_0$ must hold true for a given maximum transmit power P_0 . By evaluating the condition further, the power control factor η can be obtained as

$$\eta = \frac{P_0}{\min_k \text{tr}\{(\mathbf{A}_n^H \mathbf{H}_k \mathbf{H}_k^H \mathbf{A}_n)^{-1}\}}. \quad (26)$$

Hence, the corresponding MSE of the superposed modulation symbols can be expressed as

$$e(\eta, \mathbf{A}_n) \triangleq \mathbb{E} \left\{ \left\| \hat{\mathbf{m}} - \sum_{k=1}^K \mathbf{m}_k \right\|_2^2 \right\} = \sigma_n^2 \frac{\text{tr}\{\mathbf{A}_n^H \mathbf{A}_n\}}{\eta}. \quad (27)$$

By substituting η into (27), the optimization problem for ZF coordination can be written by

$$\begin{aligned} \mathbf{A}_n^* &= \arg \max_{\mathbf{A}_n} \min_k \text{tr}\{(\mathbf{A}_n^H \mathbf{H}_k \mathbf{H}_k^H \mathbf{A}_n)^{-1}\} \\ \text{s.t. } &\text{tr}\{\mathbf{A}_n^H \mathbf{A}_n\} = L. \end{aligned} \quad (28)$$

Since $\mathbf{A}^H \mathbf{H}_k \mathbf{H}_k^H \mathbf{A}$ is assumed to be an invertible matrix, $\forall k$, the maximum number of computable functions is $L \leq \min\{N, M\}$. The computation rate can be calculated as L/M if both real and imaginary parts of the symbols are used for computation. If \mathbf{B}_k and \mathbf{A} represent the precoder and decoder for a multi-antenna system, respectively, $S = L$ spatial streams via multiple antennas can be utilized to compute L functions in parallel, i.e., a higher computation throughput as discussed in Section III-A5. Also, note that the design problem for OAC

is the dual of the beamforming optimization for the downlink (DL) multi-casting [66], [110].

In [66], [111], [112], ZF coordination is investigated for a scenario with single-antenna EDs and a multiple-antenna ES. In [66], an algorithmic approach based on semidefinite relaxation is considered to solve (28). In [111] and [112], ZF-coordination is studied based on device subset selection. In [112, Theorem 1], a closed-form solution is provided when only a single ED transmits with the maximum power under certain channel conditions. The case where both EDs and ES have multiple antennas are studied in [63] and [110]. In [63], ZF coordination is investigated for $\mathbf{A}_n^* = \mathbf{I}_L$ and $N_t \geq N_r = L$. An approximate solution for $\mathbf{A}_n^H \mathbf{A}_n = \mathbf{I}_L$ is provided in [110, Eq. 14].

With minimum mean-squared error (MMSE) coordination [67], [112]–[114], the main goal is to minimize the MSE of the superposed modulation symbol vector $\hat{\mathbf{m}}$, where the MSE can be written as a function of \mathbf{A} and $\mathbf{B}_k, \forall k$, by

$$\begin{aligned} e(\mathbf{A}, \{\mathbf{B}_k\}) &\triangleq \mathbb{E} \left\{ \left\| \hat{\mathbf{m}} - \sum_{k=1}^K \mathbf{m}_k \right\|_2^2 \right\} \\ &= \mathbb{E} \left\{ \left\| \sum_{k=1}^K (\mathbf{A}^H \mathbf{H}_k \mathbf{B}_k - \mathbf{I}_L) \mathbf{m}_k + \mathbf{A}^H \mathbf{n} \right\|_2^2 \right\} \\ &= \sum_{k=1}^K \text{tr}\{(\mathbf{A}^H \mathbf{H}_k \mathbf{B}_k - \mathbf{I}_L)(\mathbf{A}^H \mathbf{H}_k \mathbf{B}_k - \mathbf{I}_L)^H\} \\ &\quad + \sigma_n^2 \text{tr}\{\mathbf{A}^H \mathbf{A}\}, \end{aligned}$$

for $\mathbb{E}\{\mathbf{m}_i \mathbf{m}_j^H\} = \delta_{ij} \mathbf{I}_L, \forall i, j$. For MMSE coordination, the optimization problem can be expressed as

$$\begin{aligned} (\mathbf{A}^*, \{\mathbf{B}_k^*\}) &= \arg \min_{\mathbf{A}, \{\mathbf{B}_k\}} e(\mathbf{A}, \{\mathbf{B}_k\}) \\ \text{s.t. } &\text{tr}\{\mathbf{B}_k \mathbf{B}_k^H\} \leq P_0, \forall k \end{aligned} \quad (29)$$

The MMSE coordination differs from the ZF coordination in that it leads to a combination of maximum power transmission and channel inversion across the EDs, and the optimal precoders and decoder are functions of the noise variance at the ES. In [113] and [115], the authors investigate MMSE-coordination for a scenario with single-antenna ES and EDs. [113] extends the optimization problem to time-varying channels while [115] investigates the effect of imperfect CSI on computation and provide several closed-form solutions based on some approximations. In [67] and [112], a scenario where the EDs are equipped with a single antenna while ES has multiple antennas is considered. It is shown that the MMSE coordination is related to device subset selection. In [114], a single function, i.e., $L = 1$, is aim to be computed in multiple-input-multiple-output (MIMO) channel and an iterative algorithm described in [114, Eqs. 11-13] is adopted for MMSE coordination. In [116], MMSE coordination is considered by taking the normalization of the parameters into account for distributed sensing.

In the literature, the optimization of the linear precoders and decoder have been investigated for various interesting applications and scenarios. In [117], analog beamforming is

investigated for OAC, where the main objective is to minimize a bound on the loss function for FEEL, instead of MSE. In [118], the scenario is extended to a multi-cluster network and uniform forcing is investigated under inter-cluster interference in selective fading. In [119], the receive beamforming is optimized based on antenna selection. In [120], the same scenario is investigated with the consideration of a relay network with multiple antennas and the beamforming vectors at the EDs, ESs, and relays are jointly optimized. To calculate multiple linear functions, the design of beamforming vectors at the ES and ED is discussed in [121]. In [122], a general distribution optimization problem is investigated when the radios are equipped with a large number of antennas for transmission and full-duplex capability. Beamforming vectors are proposed to be optimized to support multiple concurrent computations. In [123], [124], several channel inversion techniques along with scheduling are investigated when there are multiple antennas at the ES. For a given maximum tolerable computation error [123] or FEEL performance [124], greedy scheduling algorithms are proposed. In [125], the authors design the precoders at the EDs and the decoder at the ES with the considerations of both spatial correlation and heterogeneous data correlation to minimize MSE further. In [126], simultaneous federated learning with OAC and information transmission is studied.

b) Diversity-oriented techniques: In the literature, there are methods that exploit time and/or frequency diversity techniques to improve the performance of OAC based on pre-equalization. For example, in [127], a WSN scenario, where each sensor sends a symbol over multiple subcarriers, is considered. The pre-equalization vector at the sensors and the aggregation vector that combines the copies at the fusion center are jointly optimized such that MSE is minimized under a power constraint. The utilized precoder and combining vectors are similar to the ones with multiple antennas [111] since the effective channel can be expressed as a diagonal MIMO matrix. In [128], a space-time approach for multiple EDs and ESs is also investigated to minimize MSE of the computation. Similarly, in [129], a multi-slot OAC is proposed for fast-fading channels and time diversity is exploited to mitigate the impact of fading channel on OAC.

In [130], an OAC strategy using a space-time line code (STLC) [106] is proposed to achieve a receive diversity gain. In this approach, each ED is equipped with a single antenna while the ES has two antennas. Each ED performs two STLC symbol transmissions back-to-back as a function of the CSI, where STLC symbols are generated from the same sensor information. The ES combines the received symbols at different time slots and antennas blindly. Nevertheless, the power normalization factor still needs to be known at the EDs, where the ES calculates the factor based on the feedback transmitted from all EDs in orthogonal channels.

c) Channel manipulation: One way of achieving favorable propagation conditions for OAC is to manipulate multi-path channel itself with technologies like reconfigurable intelligent surfaces (RIS) [131]. For example, in [132], RIS is utilized to boost or null the received signal power at desired locations. In [133], device selection for OAC is studied along with RIS with the availability of CSIT. In [134], the RSI

phase shifts are exploited for over-the-air model aggregation with the consideration of the cascaded channel coefficients to eliminate the need for CSI at the EDs. In [135], multiple RISs are investigated for a similar scenario. In [136] and [137], the authors consider the optimization problem of transceiver design and RIS phase selection with the consideration of imperfect CSI. In [138], the sign stochastic gradient descent (signSGD) is exploited for OAC along RIS. In [139], average MSE with respect to a target function is minimized by jointly optimizing the RIS phase-shift vector and the transmission and reception scaling factors of ED. In [140], RIS is proposed to compute convolution over the air to realize a convolution neural network (CNN) in wireless channel. In [141], the authors investigate joint optimization problem with respect to the transmit power, denoising factor, and RIS phase-shifts for a graph neural network. We refer the reader to [142] and the references therein for further optimization frameworks on phase shift design.

d) What can go wrong?: The methods in this category can introduce a major computation complexity to both EDs and ES. They are also prone to the imperfections caused by underlying enabling mechanism, e.g., imperfect coordination among EDs within the coherence time, and phase, time, and frequency synchronization errors. Hence, the OAC performance of these methods is a strong function of how much the underlying link-layer procedures in practice can make the assumptions (e.g., accurate and fresh CSI estimates at both ES and ED within the coherence time) hold.

3) *CSIT: Not available, CSIR: Available:* This category is dedicated to the blind EDs, i.e., EDs cannot access the CSI, but the ES has some knowledge about the CSI. The methods in this category particularly rely on channel hardening techniques.

a) Channel hardening by using the aggregated CSI: One way of achieving channel hardening for OAC is to use an estimate of the superposed channel, i.e., the sum of the channel gains from all the EDs (i.e., $\sum_k \mathbf{h}_k$) to derive the linear decoder \mathbf{A} at the ES [143]–[147]. Since the CSI between each ED and ES is not needed with this strategy, the channel estimation overhead significantly reduces at the expense of some interference due to the uncoordinated transmissions of the EDs. In [143], [144], this approach is adopted based on multiple antennas at the ES. It is assumed that the ES has a noisy estimate of the aggregated channel from all the devices to each antenna and employs MRC. It is shown that the variance of interference on the superposed symbol is scaled by $(K - 1)/N_r$, where N_r is the number of antennas at the ES [143], [144]. In [148], the same scenario is investigated for time-varying channels and it is shown that the time-variation in typical wireless channels does not reduce the FEEL performance and the inter-carrier interference reduces with increasing number of receive antennas.

b) Advanced receivers: In [149], [150], digital OAC problem is interpreted as a multi-user detection problem. Considering an asynchronous multi-user OFDM scenario, it is demonstrated that multi-user detection algorithms can be applied to the superposed signals for convolution code or low-density parity check (LDPC). In [151], a similar multi-user detection and aggregation approach is considered for Long-

Range (LoRa) network. In [152], it is proposed to separate the transmitted signal of each client from the superposed signals so that independent sparsification patterns can be applied at the EDs by assuming that the number of antennas are larger than the number of EDs.

c) *What can go wrong?*: Channel hardening relies on the existence of a large number of degrees-of-freedom (DoF) at the ES, i.e., N_r , to decrease the variance of interference, which can increase the cost and decrease the computation rate \mathcal{R} as can be seen from Table II. Also, if N_r is larger than or equal to KN_t and the complete CSIR is available at the ES, the separation of computation and communication tasks can more reliable than the OAC as the number of observations can be larger than or equal to the number of unknowns. The main limitation of advanced receivers for the detection of codewords from the superposed signals is that it is not trivial to extend the computation to a large number of EDs as the computation and storage complexity can be prohibitively high.

4) *CSIT: Not available, CSIR: Not available*: The methods in this category is the most restrictive in the sense of optimization as the CSI is available neither at the EDs nor the ES. Although this appears as a prohibiting factor for a reliable OAC, the main benefits gained by not using CSI are the robustness against time-variation of the wireless channel and synchronization errors and a major overhead reduction as compared to the methods relying on the availability of CSIT or CSIR.

a) *Orthogonal signaling*: In [153]–[156], the authors consider distributed training by the MV with signSGD [157] and calculate the MV based on orthogonal signaling at the EDs and non-coherent detection at the ES. Since the arguments and the output of the nomographic function in this specific application consist of discrete states, i.e., $\{-1, 1\}$, the schemes in [153]–[155], [158], and [159] use frequency-shift keying (FSK) over OFDM, pulse-position modulation (PPM), and chirp-shift keying (CSK) over discrete Fourier transform (DFT)-spread OFDM (DFT-s-OFDM), where the symbols are determined based on $\text{sign}(s_k)$. An energy comparator is used to detect the MV at the ES. The authors show the efficacy of this approach for distributed learning under time synchronization errors without requiring phase synchronization. Since these schemes do not use CSIT and CSIR, they can also be used for multi-cell computation, where there are multiple fusion nodes [156]. The authors in [160] also propose to use orthogonal resources for negative and positive-valued measurements. Note that the distributed training based on MV with signSGD is considered in [77] and [138], where the OAC relies on TCI discussed in Section III-B1a and use of RIS, respectively. However, the phase synchronization is needed for these methods as [77] and [138] propose to use the same resource for negative and positive gradients.

The keying idea is generalized in [161], [162] to compute general nomographic functions by using balanced numerals. With similar motivations, i.e., robustness against synchronization errors, Valenti and Ferrent study FSK for physical-layer network coding (PLNC) in [163], [164], where the target function is the XOR of the transmitted bits from two devices. In [165], a positional encoding for OAC without using CSI

is discussed. Based on the fraction of time slots occupied by among a fixed number of available slots, the activated classes that encodes temperature ranges are estimated. In [166], a codebook for TBMA is proposed to be designed via a neural network with the considerations of channel and source statistics.

b) *Channel hardening and energy estimation*: In [101], Goldenbaum and Stańczak re-evaluate their scheme presented in [39] when there is no CSIT under a scenario where the receiver is equipped with multiple antennas. In this approach, each ED transmits a sequence as discussed in Section III-B1c. However, it does not apply any amplitude correction and the receiver at the ES calculates the energy of the received sequence over the multiple antennas. One of the main conclusions drawn for this approach is that the rapid changes of the channel coefficients can be beneficial to improve the convergence when CSIT is not available for IID small-fading. Note that a similar approach is also adopted in more recent work in [57], [167], [168], and [54, Section VI]. To mitigate the channel fading coefficients on OAC, averaging over multiple antennas are investigated in [161], [169]. The impact of uncompensated channel along with multiple transmissions is discussed for collaborative decision making in [95].

c) *Joint channel and parameter estimation*: In [170], the blind OAC is interpreted as a joint channel and parameter estimation problem. To estimate the channel coefficients and parameters, a randomly initialized Wirtinger flow is proposed. It is demonstrated that the proposed approach results in small estimation errors with sufficient samples.

d) *What can go wrong?*: The error rate or MSE with orthogonal signaling can be worse than the methods relying pre-equalization or multi-antenna techniques as the impact of channel on the symbol is not compensated. To reduce the estimation errors, averaging can consume time, frequency, or space resources (i.e., a lower computation rate) while introducing a complex algorithm to the ES can increase the receiver complexity.

C. Classification criteria: Encoding

The classification in this category particularly concerns about how the outputs of the pre-processing functions are processed before the linear encoders takes place to overcome the fading channel. We group the approaches under analog encoding and digital encoding. While analog encoding deals with the continuous-valued symbols to realize the desired nomographic function (over an analog modulation), digital encoding uses some form of quantization, compression, and/or source-channel coding for the same goal (over a digital modulation).

1) *Analog encoding*: In the literature, a majority of the OAC methods exploit the available DoF without a particular encoding as long as the reliable superposition is maintained under the fading channel with aid of the precoders $\mathbf{B}_k, \forall k$, and the decoder \mathbf{A} . Nevertheless, it has been shown that an additional processing can still be helpful for certain goals.

a) *Linear analog encoders:* A linear analog encoder for OAC can be defined as

$$\epsilon_k\{\mathbf{p}_k\} = \mathbf{G}\mathbf{p}_k, \forall k, \quad (30)$$

where \mathbf{G} is a $B \times N_f$ matrix for $B < N_f$ (i.e., compression) [171]. Hence, the encoder projects the vector \mathbf{p}_k into a lower dimensional space and reduces the number of resources to be utilized to compute N_f . A linear encoder is suitable operation for OAC because the sum of the projected vectors is identical to the projection of the sum of vectors.

Linear encoders are especially applied to the applications where the pre-processed symbol vector \mathbf{p}_k is inherently sparse or can be sparsified with a tolerable distortion. For example, in [172] and [76], for distributed learning, the EDs sparsify their gradient estimates before they project them into a lower dimensional space with (30). These projections are directly used with an analog OAC scheme. At the ES, an approximate message passing algorithm is proposed to recover the superposed symbols. In [171], with a similar motivation, \mathbf{G} is constructed randomly from the rows of the rotated Walsh-Hadamard matrix. At the ES, the projected vector is mapped to the superposed symbol based on a general norm-minimization problem, i.e., $\hat{\mathbf{p}} = \delta\{\hat{\mathbf{c}}\} = \arg \min_{\mathbf{p}'} \|\hat{\mathbf{c}} - \mathbf{G}\mathbf{p}'\|_2$. It is shown that linear analog encoders in AWGN channel can perform well at low SNRs. [173], the sparsification is achieved by selecting k gradients with the greatest magnitudes, where k is a predetermined integer. In this study, discrete cosine transform matrix is used for the compression. In [152], a similar compression approach is considered for the model updates and the measurement matrix is constructed based on IID Gaussian distribution.

One of the concerns on OAC with sparsification is that the sum of the sparse vectors may not be sparse after the aggregation, i.e., the sparsity level can deteriorate depending on the number of EDs. In [152], the authors study a uniform sparsity pattern and independent sparsity patterns for FEEL and show that a higher test accuracy can be achieved when the EDs decide their own sparsity pattern, especially when the data distribution is heterogeneous.

b) *Affine analog encoders:* In [38], [39], [54], [89], [148], [174], [175], it is proposed to process the output of the pre-processing function with an affine function as

$$\epsilon_k\{p_k[n]\} = ap_k[n] + b, \forall k \quad (31)$$

for $a, b \in \mathbb{R}$, where a and b are chosen such that the output of the encoder always results in a non-negative value (see [54, Eq. (28)] for an example under a power normalization constraint and discussions in Section III-B1c). Hence, the sign ambiguity at the receiver is eliminated. After the energy calculation of the received sequence at the receiver, the superposed symbol is processed with the inverse function $\delta = \epsilon^{-1}$. Note that the encoder needs to be restricted to be an affine function to be able to calculate the desired nomographic function [39, Proposition 1].

As discussed in Section III-B1c, the encoder proposed in [39] multiplies the square-root of the affine function with a

sequence as

$$\epsilon_k\{p_k[n]\} = \sqrt{ap_k[n] + b} \times [e^{j\theta_1}, \dots, e^{j\theta_N}], \forall k. \quad (32)$$

The fundamental reason for the square-root operation is that the OAC relies on the estimation of energy of sequence at the receiver.

c) *Non-linear encoders:* In [77], [79], [94], [145], [152], [173], [176], [177], the imaginary and real parts of the symbols are proposed to be utilized as

$$\epsilon_k\{p_k[n], p_k[n+1]\} = p_k[n] + jp_k[n+1], \quad (33)$$

for all odd positive n . Therefore, the spectrum efficiency of the transmission is improved as B is equal to $\lceil N_f/2 \rceil$.

2) *Digital encoding:* In this subsection, we discuss the methods that use some form of source and channel coding for OAC.

a) *Encoding based nested lattice codes:* The linearity of the nested lattice codes are first used in [1] and [7] for achieving computation over Gaussian channels in finite fields (see Section III-A5 for further discussions). In [4] and [178], a digital OAC scheme along with a nested lattice coding is introduced to increase the reliability of the computation of N_f functions in a real-valued AWGN channel. To calculate $\sum_{k=1}^K p_k[n]$, $\forall n$, the steps taken at the k th ED, $\forall k$, based on [4, Proof of Theorem 5], can be listed as follows:

- Step 1 (Quantization): Let b_0 be the quantization parameter in bits, which is specified based on the amount of tolerable quantization error. The symbol $p_k[n]$, $\forall n$, is mapped to a positive integer $w_k[n] \in \{0, 1, \dots, 2^{b_0} - 1\}$ for a given b_0 . For example, for $b_0 = 3$ bits, $K = 3$ EDs, and $N_f = 4$ functions to be computed, suppose that the EDs' symbols within the range $[0, 1]$ are given by

$p_k[n]$	$n = 1$	$n = 2$	$n = 3$	$n = 4$
$k = 1$	1	1	0.9	0.4
$k = 2$	1	1	0	0.7
$k = 3$	1	1	0.2	0.1

(34)

By uniformly dividing the range $[0, 1]$ into 2^3 parts and using a natural code, the corresponding integers can be obtained as

$w_k[n]$	$n = 1$	$n = 2$	$n = 3$	$n = 4$
$k = 1$	7	7	6	3
$k = 2$	7	7	0	5
$k = 3$	7	7	1	1

(35)

- Step 2 (Source encoder): The integers obtained from the quantization step, i.e., $w_k[n]$, $\forall n$, are divided into S sub-sequences and each sub-sequence is mapped to a message as an integer. The procedure is as follows: Each sub-sequence contains $\tau = N_f/S$ integers for a given S . The τ integers in each sub-sequence is first assigned to the digits of a number, e.g., $(w_k[\tau] \dots w_k[2]w_k[1])_\beta$, in the base- β positional numeral system for $\beta \triangleq K(2^{b_0} - 1) + 1$. Afterwards, each number in base β is converted to an integer, e.g., $\sum_{t=1}^{\tau} w_k[t]\beta^{t-1}$. Note that the source encoding results in S messages, where the maximum value of a message is $(\beta^\tau - 1)/K$.

The reason for choosing β as a function of number of EDs is to eliminate a potential carry digit for the superposed message across K EDs so that $\sum_k (w_k[\tau] \dots w_k[2] w_k[1])_\beta$ can be expressed as $(\sum_k w_k[\tau] \dots \sum_k w_k[2] \sum_k w_k[1])_\beta$. For example, consider the integers in (35). Suppose that the source encoder results in $S = 2$ messages. Hence, each message is calculated over $\tau = N_f/S = 2$ integers by mapping them to the digits of a number in a positional numeral system. The corresponding numbers are then converted to the messages as

$$\begin{array}{c|c|c} k=1 & (77)_\beta & (63)_\beta \\ k=2 & (77)_\beta & (05)_\beta \\ k=3 & (77)_\beta & (11)_\beta \end{array} \xrightarrow{\text{From base } \beta \text{ to base 10}} \begin{array}{c|c|c} k=1 & 161 & 135 \\ k=2 & 161 & 5 \\ k=3 & 161 & 23 \end{array}, \quad (36)$$

for $\beta = K(2^{b_0} - 1) + 1 = 22$. Hence, the sum of the messages across $K = 3$ EDs can be calculated without a carry digit, e.g., the sum $(77)_{22} + (77)_{22} + (77)_{22}$ is $(21, 21)_{22} \equiv (483)_{10}$ for $n = 1$. Note that the maximum value of the superposed message for this example is $\beta^\tau - 1 = 483$ while the maximum value of a message is $(\beta^\tau - 1)/K = 161$ as can be seen from (36).

- Step 3: (Channel encoder): A nested lattice code from \mathbb{Z}_p^S to \mathbb{R}^B is constructed for a prime $p \geq \beta^\tau$. The S messages calculated from the previous step are used to calculate the codeword $\mathbf{c}_k \in \mathbb{C}^B$ with the corresponding generator matrix $\mathbf{G} \in \mathbb{R}^{B \times S}$ of the lattice under an average power constraint. For example, the codewords at EDs for the messages in (36) can be calculated as

$$\mathbf{c}_{k=1} = \mathbf{G} \begin{bmatrix} 161 \\ 135 \end{bmatrix}, \mathbf{c}_{k=2} = \mathbf{G} \begin{bmatrix} 161 \\ 5 \end{bmatrix}, \mathbf{c}_{k=3} = \mathbf{G} \begin{bmatrix} 161 \\ 23 \end{bmatrix}. \quad (37)$$

The ES receives the sum of the codeword, i.e., $\hat{\mathbf{c}}$. For example, for the codewords in (37), $\hat{\mathbf{c}}$ can be expressed as

$$\hat{\mathbf{c}} = \sum_{k=1}^3 \mathbf{c}_k.$$

The superposed vector $\hat{\mathbf{c}}$ at the ES is processed as follows:

- Step 1 (Channel decoder): By using an Euclidean nearest neighbor decoder, the decoder obtains the message, which corresponds to the superposed message due to the linearity of the code. For example, for the codewords in (37), $\hat{\mathbf{c}}$ can be expressed as

$$\hat{\mathbf{c}} = \mathbf{G} \begin{bmatrix} 483 \\ 163 \end{bmatrix}.$$

and the decoder results in 483 and 163 as the superposed messages if there is no error.

- Step 2 (Source decoder): Each superposed message is expressed in base β to obtain the sum of the quantization results, e.g., $(\sum_k w_k[\tau] \dots \sum_k w_k[2] \sum_k w_k[1])_\beta$. For example, $(483)_{10} \equiv (21, 21)_{22}$ and $(163)_{10} \equiv (79)_{22}$. Hence, the source decoder returns $\hat{\mathbf{p}} = [\hat{p}[1], \hat{p}[2], \hat{p}[3], \hat{p}[4]]^T = [21, 21, 7, 9]^T$, i.e., the sums of the values on each column in (35).

b) Encoding based on numeral systems: In [179], pulse-amplitude modulation (PAM) is utilized with a radix-based encoding. In this approach, the binary representation of a parameter p_k is first partitioned into subgroups. Afterwards, the decimal representation of the bits on each subgroup is mapped to a PAM symbol to achieve a processing gain (see [179, Fig. 4]). This approach generalizes the encoder that encodes p_k into a M -PAM symbol after p_k is quantized into $\log_2 M$ bits [171, Eq. (13)]. Note that the PAM can be extended to square M -quadrature amplitude modulation (QAM) constellations, where real and imaginary part of the constellation dedicates to two symbols, as done for gradient aggregation for FEEL in [81].

In [13], the authors propose to calculate $\sum_{k=1}^K p_k$ where $p_k = w_k s_k$ for non-negative integers s_k, w_k . They consider the binary representation of each symbol and map each bit to a binary phase shift keying (BPSK) symbol. By using the linearity of the decomposition, the weights w_k are incorporated to the transmit power at the source nodes to calculate the weighted sum. The main observation is that the received symbol is a point in a non-standard PAM after the superposition. The destination node exploits the discrete nature of the superposition to compute the arithmetic sum. The authors also derive the CER (See Section III-A).

In [161], [162], the authors propose to utilize the balanced number systems for OAC to represent a negative parameter efficiently. A balanced numeral system consists of negative numerals, i.e., signed digit. Hence, it can represent a negative number without using dedicated sign symbol. In this method, the parameters are first represented in a balanced number system. For each numeral, one of the corresponding OFDM subcarriers are activated. At the receivers, the sum of the parameters is estimated. MSE is also analyzed for multiple antennas at the receiver. If only a single digit is used with balanced ternary system, the encoding in [161], [162] corresponds to keying methods discussed in [153]–[156]. The proposed encoding method in [153]–[156] is designed for calculating the MV (see TABLE I). Since the nomographic function for the MV consist of discrete states, the modulation symbols are determined based on keying methods such as FSK, CSK, and PPM and non-coherent detectors are used to obtain the MV at the ES. Note that the same nomographic function is targeted to be computed in [77] based on TCI. In [158], it is shown that using a tri-state encoder (i.e., $\{-1, 0, 1\}$) that eliminates the EDs with small gradients from the MV computation) can largely address the bias due to the data heterogeneity and imperfect power control in the learning when OAC is used for FEEL. In [159], CSK is extended to M -ary CSK. The sign of $\log_2 M$ parameters are mapped to a chirp index and the authors show how to calculate MVs for this specific encoding by exploiting the binary representations of the indices.

In [169], the authors propose to encode a local gradient vector of length L into a sequence in an orthogonal sequence set of size $2L$ for OAC, where the encoding relies on stochastic quantization. In this scheme, the transmitted sequence is chosen with the probability that is proportional to the magnitude of the elements of the normalized local gradient vector (i.e., the coefficients derived from the decomposition of the normalized

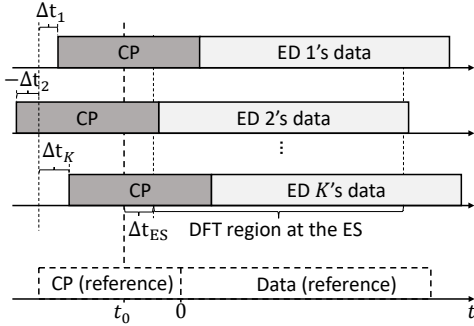
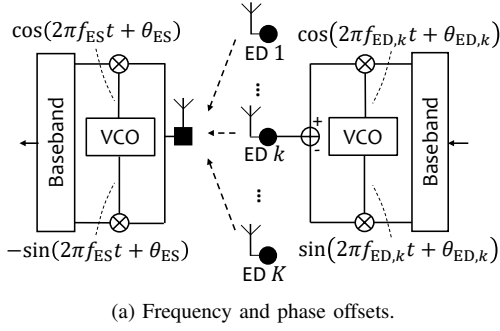


Fig. 4. Synchronization imperfections in time and frequency.

local gradient vector over a scaled cross polytope constructed over standard basis vectors). At the receiver, the received signal is correlated with each sequence in the set to estimate the probabilities. By combining the results over realizations, the superposed gradient vector is obtained. It is worth noting that this scheme also separate the sign information to the orthogonal resources as in [153]–[156], but it differs from these studies as it targets a continuous-valued computation through probabilistic choice of the activated resource over $2L$ resources. In [180], the same idea is investigated for consensus problem.

IV. WHAT ARE THE ENABLING MECHANISMS FOR OAC?

In this section, we discuss the underlying mechanisms that maintain reliable computations and address security issues.

A. Synchronization

To elaborate the effect of synchronization impairments on OAC, let f_{ES} and $f_{ED,k}$ denote the carrier frequencies at the ES and the k th ED, respectively, where the phase of the corresponding oscillators are θ_{ES} and $\theta_{ED,k}$, as shown in Fig. 4(a). Thus, the carrier frequency offset (CFO) and the phase offset (PO) between k th ED and the ES are $\Delta f_k = f_{ED,k} - f_{ES}$ and $\Delta \theta_k = \theta_{ED,k} - \theta_{ES}$, respectively. Similarly, time offset (TO) between transmitter and receiver can be described as the following: Let t_0 denote the ideal synchronization point at the ES. Assume that the synchronization point at the ES and the time-of-arrival instant of the k th ED's signal at the ES location deviate by Δt_{ES} seconds and $\Delta t_{ED,k}$ seconds, respectively. Thus, the overall TO can be expressed as $\Delta t_k = \Delta t_{ED,k} - \Delta t_{ES} - t_0$.

Let $s_k(t) \in \mathbb{C}$ be the baseband signal for the k th ED to be transmitted. Hence, the passband signal of the k th ED from the perspective of the ES can be expressed as

$$s'_k(t) = \Re\{s_k(t - \Delta t_k)e^{j2\pi(f_{ES} + \Delta f_k)(t - \Delta t_k)}e^{j\Delta \theta_k}\}. \quad (38)$$

Assume that the impulse response of the multi-path channel in the passband is given by

$$h'_k(\tau) = \sum_{p=1}^P a_{k,p} \delta(\tau - \tau_{k,p}), \quad (39)$$

where P is the number of paths, $a_{k,p} \in \mathbb{R}$ and $\tau_{k,p} \in \mathbb{R}$ are the p th path gain and path delay for the k th ED, respectively [181, Chapter 2]. The received passband signal for the k th ED can then be expressed as

$$r'_k(t) = h'_k(\tau) \otimes s'_k(t) = \Re\{e^{j2\pi f_{ES}t} r_k(t)\} \quad (40)$$

where $r_k(t)$ is the received complex baseband signal given by

$$r_k(t) = \sum_{p=1}^P a_{k,p}^b s_k(t - \tau_{k,p} - \Delta t_k) e^{j2\pi \Delta f_k t} \quad (41)$$

for $a_{k,p}^b \triangleq a_{k,p} e^{-j(2\pi f_{ES}(\tau_{k,p} + \Delta t_k) - \Delta \theta_k)} e^{-j2\pi \Delta f_k(\tau_{k,p} + \Delta t_k)}$. Hence, based on (41), we can infer the followings:

- The timing errors at the EDs or ES do not only cause a translation in time, but also phase rotation.
- The CFO causes phase error accumulation that grows over time.
- An additional phase rotation is introduced due to the CFO, depending on the time offset and path delays.

Now, assume that the OAC is based on OFDM. For $t \in [0, T_{\text{sym}})$, we can express the baseband signal for the k th ED as $s_k(t) = \sum_{\ell=0}^{M-1} x_{k,\ell} e^{j2\pi \frac{\ell}{T_{\text{sym}}} t}$, where the T_{sym} is the symbol duration, M is the number of active subcarriers, and $x_{k,\ell}$ are the transmitted symbol as given in (7). Assume that the channel is ideal, i.e., $P = 1$, $a_{k,p} = 1$, and $\tau_{k,p} = 0$, $\forall k$. Assume that the ideal synchronization point where the N -point DFT is started to be applied to the received baseband signal is within the CP duration, i.e., at $t_0 \leq 0$, as illustrated in Fig. 4(b).⁵ Under the synchronization impairments, the received symbol on the ℓ th subcarrier at the ES can be expressed in (42), where $\eta_{FO,k} \triangleq \Delta f_k T_{\text{sym}}$ and $\eta_{TO,k} \triangleq \Delta t_k / T_{\text{sym}}$ are the normalized CFO and TO for the k th ED, respectively, and $D_N(x) \triangleq \frac{1}{N} \sum_{n=0}^{N-1} e^{j2\pi \frac{n}{N} x} = \frac{e^{j\pi x \frac{N-1}{N}} \sin(\pi x)}{N \sin(\pi x / N)}$ is the Dirichlet sinc kernel. As can be seen from (42), the existence of CFO causes inter-carrier interference while TO due to the imperfect time-of-arrivals or the synchronization errors at the ES results in phase rotations *scaled* with the subcarrier index. On the other hand, the residual PO leads to a distortion independent from the subcarrier index. A similar observations on CFO, TO, and PO are also made in [176, Section VI], [182], and [150].

Since the PO, TO, and CFO affect the received signal jointly, the key OAC-related metrics such as computation rate or MSE for the computation discussed in Section III-A are

⁵In practice, an OFDM receiver intentionally backs off some duration for the DFT calculation to avoid samples from the following OFDM symbol.

$$\begin{aligned}
y_\ell &= \frac{1}{N} \sum_{n=0}^{N-1} \sum_{k=1}^K \mathbf{r}_k(t) \Big|_{t=\frac{n}{N}T_{\text{sym}}} e^{-j2\pi \frac{n}{N}\ell} \\
&= \frac{1}{N} \sum_{n=0}^{N-1} \sum_{k=1}^K e^{-j(2\pi f_{\text{ES}}\Delta t_k - \Delta\theta_k)} e^{-j2\pi f_k \Delta t_k} \mathbf{s}_k(t - \Delta t_k) e^{j2\pi f_k t} \Big|_{t=\frac{n}{N}T_{\text{sym}}} e^{-j2\pi \frac{n}{N}\ell} \\
&= \frac{1}{N} \sum_{n=0}^{N-1} \sum_{k=1}^K e^{-j(2\pi f_{\text{ES}}\Delta t_k - \Delta\theta_k)} e^{-j2\pi f_k \Delta t_k} \sum_{l=0}^{M-1} x_{k,l} e^{j2\pi \frac{l}{T_{\text{sym}}}(t - \Delta t_k)} e^{j2\pi f_k t} \Big|_{t=\frac{n}{N}T_{\text{sym}}} e^{-j2\pi \frac{n}{N}\ell} \\
&= \sum_{k=1}^K \sum_{l=0}^{M-1} x_{k,l} e^{-j(2\pi f_{\text{ES}}\Delta t_k - \Delta\theta_k)} e^{-j2\pi \eta_{\text{FO},k} \eta_{\text{TO},k}} e^{-j2\pi l \eta_{\text{TO},k}} \frac{1}{N} \sum_{n=0}^{N-1} e^{j2\pi \frac{n}{N}(l - \ell + \eta_{\text{FO},k})} \\
&= \sum_{k=1}^K x_{k,\ell} \underbrace{e^{-j(2\pi(\eta_{\text{FO},k} + \ell)\eta_{\text{TO},k} + 2\pi f_{\text{ES}}\Delta t_k - \Delta\theta_k)} D_N(\eta_{\text{FO},k})}_{\text{distortion}} + \underbrace{\sum_{k=1}^K \sum_{\substack{l=0 \\ l \neq \ell}}^{M-1} x_{k,l} e^{-j(2\pi(\eta_{\text{FO},k} + \ell)\eta_{\text{TO},k} + 2\pi f_{\text{ES}}\Delta t_k - \Delta\theta_k)} D_N(\eta_{\text{FO},k} + l - \ell)}_{\text{inter-carrier interference}} .
\end{aligned} \tag{42}$$

also affected. However, how these metrics are affected under such offsets is not well-assessed in the literature. It is also worth emphasizing that the sensitivity of the computation to the residual offsets depends on the scheme and the function desired to be computed. For instance, for an OAC scheme that requires phase synchronization among the EDs, the PO, TO, and CFO need to be compensated very accurately, particularly for analog aggregation. Hence, this scheme would require a sample-level synchronization and MSE would be sensitive to synchronization errors (See Section III-B1e). On the other hand, if the target function is an MV computation and the OAC scheme relies on keying approaches along with a non-coherent detection, it is demonstrated that maintaining the synchronization within the CP range can be sufficient. For such a scheme, MSE does not increase with the sample-level synchronization errors as demonstrated in [183] (See also Section III-B4a).

In practice, it is challenging to mitigate the impacts of random TOs, CFOs, and POs on an OFDM-based OAC. However, in the case that the offsets change slow, they can be mitigated through control loops. For example, in [182], the residual TO and PO are estimated by tracking the phase in the frequency domain before the OAC takes place. A protocol that feeds back the estimates of TO and PO to the EDs are proposed, where the ED can compensate the residual errors. It is also worth noting that the residual CFO estimation errors cause the phase error accumulation for the packets with many OFDM symbols. To mitigate the error accumulation, extra signaling or better high-precision clocks can be utilized [150].

In the literature, the synchronization for OAC is also investigated for waveforms different from OFDM. For instance, in [176], [184], [185], the analyses are performed for a single-carrier (SC) waveform constructed with a rectangular pulse shape.⁶ In [176] and [184], to estimate the sum of the parameters under time-synchronization errors, a post-processing

called whitened matched filtering and sampling is proposed assuming that the ES knows the TO for each ED. In [185], the same setup is investigated from the perspective of Bayesian approaches. In [89], sinc kernel is considered for waveform and it is proposed to recover the summation of the parameters by solving a convex semi-definite program without any prior information on the misalignment. Note that, in [89], [176], [184], [185], the channel is not frequency selective and overall phase rotation is assumed to be compensated via channel inversions at the EDs and decoupled from the TO.

The non-coherent OAC approaches discussed in Section III-B4 provide robustness against PO as these methods do not convey the information in the phase. In [154] and [155], in order to mitigate the interference between the adjacent symbols due to the random TOs, a guard time between adjacent PPM or CSK symbols (based on DFT-s-OFDM) is proposed, respectively. Also, a larger energy calculation window than the corresponding bins at the transmitter is used for the energy calculations to accommodate the jitter, respectively.

B. Power Management

In this section, we investigate power management under two categories: In the first category, we discuss power management from the perspective of receiver, e.g., power alignment at ES via power control. In the second category, we discuss the power management from the perspective of transmitters and focus on the issues related to peak-to-average power ratio (PAPR) and output-power back-off (OBO).

1) *Receiver side:* For power control, a perfect amplitude alignment at the ES to ensure fairness or an accurate computation, or a policy that minimizes of an application-specific metric are two main objectives one can consider. In the former case, the link with the worst channel condition may dominate the performance of computation [96]. On the other hand, the latter one requires a well-defined metric to be taken into account and the power control strategy becomes a function of the application. In this case, the policy can be quite diverse. For example, in [96], it is shown that the power

⁶A single carrier waveform synthesized based on a rectangular pulse shape corresponds to the direct-current (DC) subcarrier of OFDM. Inclusion of a guard period or a CP duration depends on the design.

alignment for gradient aggregation is not always necessary for the convergence of FEEL. As another example, in [82], the authors consider an online power control mechanism with the considerations of saddle regions for distributed principal component analysis (PCA) computation. In [186] and [187], for static fading channels, channel inversion that minimizes MSE for multiple transmissions is studied. It is shown that the optimal channel inversion coefficient is a function of the number of re-transmission. In [188], channel inversion that particularly minimizes the bias for a given number of re-transmissions is investigated for fast-fading channels (i.e., time diversity). In [189], it is shown that the optimal power allocation policy across OFDM subcarriers for channel inversion yields a proportional fairness scheme. In another application, Byzantine attacks are taken into account for power control [190]. We refer the reader for a comprehensive treatment on various power control methods for FEEL to [24] and references therein.

Most of the state-of-the-art power control strategies for OAC rely on a small-scale channel model when a precoding such as TCI is employed at the EDs (e.g., see [82], [190]–[192]). On the other hand, the power control is also related to large-scale models and interactions between the adjacent cells. In [193], inter-cell interference in a scenario where OACs occurs at different cells concurrently is taken into account and the optimal policies for controlling devices' transmit power are investigated to minimize the MSE of computed function. In [194], assuming that the inter-cell interference is harmful to the OAC, the beamforming vectors and transmit powers are optimized with the consideration proportional fairness at different cells. In [195], inter-cell interference is investigated in both UL and DL directions for a channel-inversion based OAC. In the literature, it is also shown that inter-cell interference can actually be harnessed for OAC, as discussed in Section IV-C.

When there is a large number of devices participating in the computation, the dynamic range of a superposed signal at the ES can exceed the dynamic range of the receiver [160], [176], [196]. Reducing the transmit powers of the EDs or designing adaptive gain control for OAC are two potential solutions to address this issue. In [160], a randomization approach is proposed to spread the energy. In [196], the MSE minimization of OAC under a sum-power constraint is studied, where one of the motivations is to reduce the potential interference due to the superposed signals. In [136], the sum-power constraint is introduced for energy saving.

2) *Transmitter side*: The dynamic range of the transmitted signals is directly related to the power management in a network. A large PAPR can cause a reduced cell size due to the power back-off, a higher adjacent channel interference due to the saturation, and a reduced battery life in order to accommodate the instantaneous power fluctuations. In the literature, a few OAC schemes is analyzed from the perspective of PAPR. In [153], the randomization symbols are used to reduce the PAPR for FSK-based MV (FSK-MV) computation. It is demonstrated that if the parameters are highly correlated in the frequency domain (e.g., the elements of a stochastic gradient vector at one iteration can be highly-correlated due to the over-parameterized neural networks [197]), modulating

the subcarriers with the parameters without any precaution can cause OFDM symbols with large PAPRs. In [117], [154] and [155], the properties of SC waveform and chirps are exploited to mitigate PAPR for OAC. In [155], a basic model is proposed to relate OBO to the cell size under power control: Let P_{ref} and OBO_{ref} be the average transmit signal power in Watts and the OBO in dB, when the link distance between the ES and an ED is r_{ref} meters, respectively. Also, let OBO_{min} be the minimum OBO that does not violate ACLR or the spectrum-emission mask requirements. Based on the simplified path loss model, the received signal for the k th ED can be expressed as

$$P_k = \begin{cases} \left(\frac{r_k}{r_{\text{ref}}}\right)^{-\alpha+\beta} P_{\text{ref}}, & r_{\text{ref}} \leq r_k < r_{\text{max}} \\ \left(\frac{r_{\text{max}}}{r_{\text{ref}}}\right)^{-\alpha+\beta} P_{\text{ref}}, & r_k \geq r_{\text{max}} \end{cases}, \quad (43)$$

where r_k is the link distance between k th ED and ES, α is the path loss exponent, $\beta \in [0, \alpha]$ is a coefficient that determines how much path loss is compensated via power control, and r_{max} is the maximum link distance beyond which the ED is unable to increase the average transmit power and it can be expressed as

$$r_{\text{max}} = r_{\text{ref}} \times 10^{\frac{OBO_{\text{ref}} - OBO_{\text{min}}}{10\beta}}. \quad (44)$$

The parameter r_{max} determines the region in which the average received signal powers of the EDs located in this area can be aligned at the ES location. Based on (44), a smaller OBO_{min} results in a larger r_{max} . However, to decrease OBO_{min} , a more linear PA or an OAC scheme with low instantaneous power fluctuations are needed. In [155], based on Rapp model, OBO_{min} values are obtained for OAC with TCI and CSK-based OAC and the trade-off between computation rate and cell size is emphasized. It is shown that the reduced-cell size due to the power back-off can deteriorate the performance of the computation due to the weak signals from the EDs with large link distances.

C. Architecture

In the literature, a majority of the papers on OAC consider either a single-cell scenario or a network where there is no cooperation among the cells. On the other hand, harnessing the interference among the cells with some coordination can also result in a more global computation while addressing large-scale fading of wireless channels. In Fig. 5, we illustrate several architectures for OAC. As compared to the single-cell scenario in Fig. 5(a), the interference due to the adjacent cells in a multi-cell scenario may be considered as harmful to the OAC as in Fig. 5(b) or harnessed for the computation as shown in Fig. 5(c). Similar to an UL, OAC can also be realized in DL as depicted in Fig. 5(d). In Fig. 5(e), we illustrate a two-tier hierarchical computation, where the intermediate ESs can be base stations while the final fusion node can be a satellite in a non-terrestrial network (see [198] for an example with a low-earth orbit satellite without hierarchical computation). Finally, Fig. 5(f) illustrates OAC in an adhoc network, e.g., to achieve consensus on the output of a function among the EDs, where the network topology can change over the time and the EDs

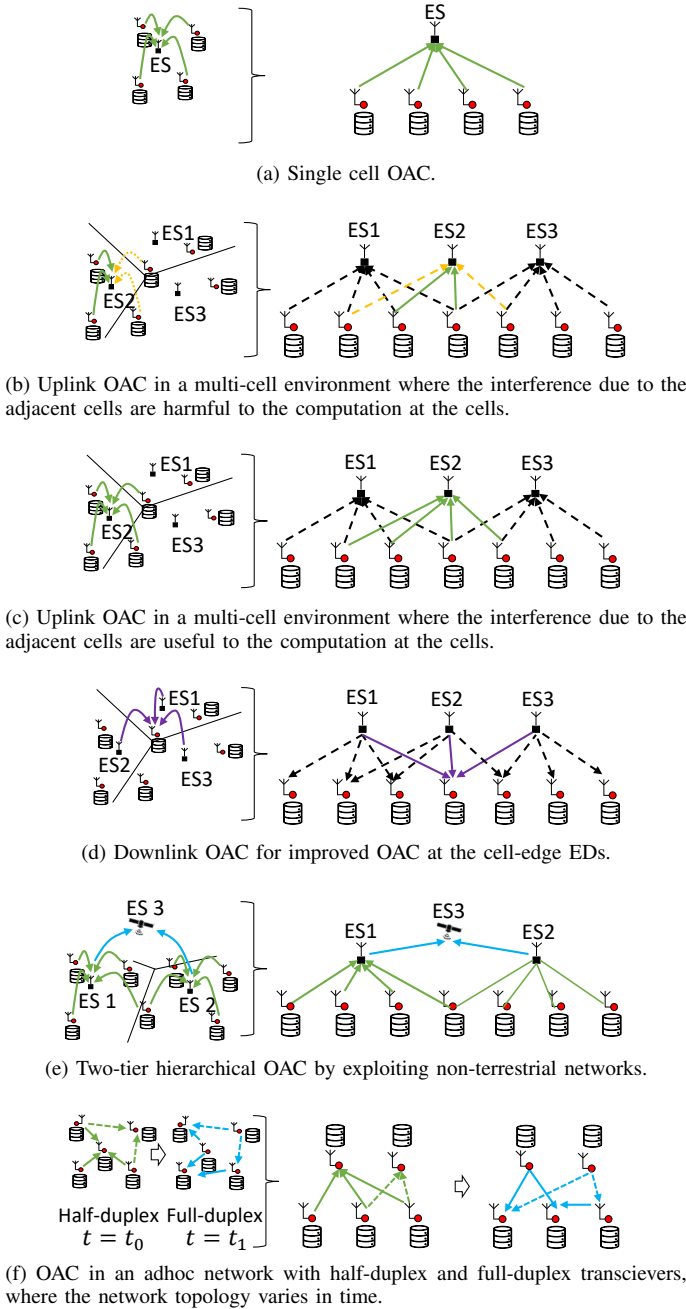


Fig. 5. Several architectures for OAC.

may perform OAC while transmitting to the other nodes with the consideration of full-duplex transceivers.

In [145], [146], hierarchical FEEL is investigated over multiple clusters to address the adverse effects of path loss on aggregation. In this approach, OAC is employed in each clusters, where the intermediate servers are connected to a global server to aggregate their results. In [199], hierarchical FEEL under data heterogeneity is addressed via a dynamic weighting approach. The scheme used in this paper is based on TCI. In [145], [146], [199], the impact of the inter-cluster interference is not taken into account. In [191], the inter-cluster interference is also exploited with OAC for hierarchical FEEL. In [200], it is proposed to use multiple clusters where the ESs

in clusters seek for a consensus for FEEL update with OAC, in addition to the OAC within the clusters among the EDs. In [68], to improve the robustness against signal attenuation for long distances, a multi-hop network is considered. In this strategy, computation occurs locally in the sensors through multiple hops till final aggregation occurs in a fusion center by exploiting the fact that a target function can be decomposed into locally computable functions.

In [2], the universality property, based on Theorem 5, is exploited to compute multiple functions in multiple sensor clusters, where each cluster is assigned to compute one of the target functions. In [156], interference among the base stations is exploited for computations. In this approach, OAC is used in both UL and DL by using FSK-MV calculation. It is shown that such an approach can improve the minimization of independent objective functions and leads to a better learning performance in larger area. In [201], similarly, multiple ESs are considered. Coherent OAC with TCI is considered and the analysis is performed under the harmful interference due to the downlink signals for ESs.

In [195], a cooperative multi-cell optimization framework is introduced to improve the average learning performance as compared to non-cooperative baseline schemes. In [122], a topology where all devices are connected with each other is investigated. The OAC relies on the existence of a large number of antennas and full-duplex capability. In [202], similarly, a full-duplex capability is assumed and various network topologies are investigated. In [203], OAC is applied to graph neural networks where each node in the graph locally processes the information. The OAC based on PC is investigated to improve communication efficiency and privacy. In [167], [168] a consensus protocol is proposed to achieve max-consensus in a clustered network. OAC is utilized across the clusters with the considerations of full-duplex [167] and half-duplex communications [168]. For general time-varying network topology, we refer the reader to [204] and the reference therein.

D. Channel Estimation

To achieve an accurate aggregation over fading channels, accurate and fresh CSI may need to be available at the EDs and/or the ES, depending on the OAC method. While an inaccurate estimate of CSI can cause an incoherent aggregation, the aging of CSI estimate due to the residual CFO or mobility can result in a larger overhead and limit the number of functions to be computed in one single packet.

For the OAC methods relying on precoding techniques, each ED needs its own UL CSI, which can be acquired through a DL signal for a time-domain duplexing system or transmitted back to the ED based on the estimates at the ES. While the former solution requires a calibration procedure, the latter causes an overhead that is scaled with the number of EDs and an increased latency. The inaccuracy due to the either of these methods may be modeled based on some error on the ground-truth CSI. Under this model, in [205], the authors derive an optimal transceiver design that minimize MSE with the consideration of multiple antennas at the ES with the

consideration of the imperfect CSI. In [192], a strategy takes the imperfect CSI at the EDs into account to determine the number of local update steps is proposed. In [206], the imperfect CSI is taken into account for joint device selection and transceiver design, where the main goal is to maximize the number of participating EDs under an MSE constraint. In [136], the imperfect CSI is evaluated along with RIS. In [115], an adaptive pilot retransmission policy that offers a trade-off between wireless resources and gain in the accuracy of the computations is proposed.

Some OAC methods use sum-channel estimate, rather than the UL CSI for each link. For instance, in [114], it is proposed to use a procedure that optimizes the beamforming vectors at the EDs and ES iteratively by exploiting the sum-channel CSI acquisition. In this method, the ES first transmits a set of reference symbols and broadcasts its current beamforming vector. After each ED estimates the DL channel and design its own beamforming vector, all the EDs transmits a set of common pilot symbols concurrently so that the ES can estimate the sum channel. The key observation is that the the ES can update its beamforming vector based on the sum channel. Common pilots are also employed in [144], [207] to estimate the sum channel for the methods relying on channel hardening or random orthogonalization over a large number of multiple antennas. In [207], the sum channel is also used as a precoder in the DL. Instead of using pilots in DL, an echo protocol where the ES broadcasts the received symbols for the sum-channel estimation back to the EDs with only processing is proposed. In the UL, the EDs design their channel inversion coefficients based on the received symbols in the DL.

E. Security

OAC relies on the superposition of the transmitted signals from the EDs. As discussed in [20], this fact has both positive and negative consequences as far as security is concerned. On one hand, the superposition in OAC promotes user privacy as the transmitted signals cannot be directly observed. On the other hand, it opens up potential adversaries to harm the computation, particularly through Byzantine attacks. This is because Byzantine attacks are launched by the nodes that are already part of the network. For example, for FEEL, if an ED's local data are deliberately labeled incorrect (i.e., one of the data poisoning attacks) or the sign of the gradients are flipped (i.e., one of the model poisoning attacks) by an adversary or due to the failure of a node, the whole learning process can be unreliable. This problem has been studied in the FL literature by identifying the Byzantine nodes or detecting anomalies in the local signals (see [208] and [190] and the references therein for further discussions on various attacks and defense mechanisms). However, if the aggregation is handled through an OAC scheme for the same scenario, well-known defense strategies that rely on the observation of local information cannot be utilized as the ES only observes the superposed signal, not the signals transmitted from different EDs.

1) *Byzantine Attacks*: One way of achieving resiliency against Byzantine attacks relies on geometric median, rather

than arithmetic mean, which can be expressed as

$$\mathbf{z}^* = \arg \min_{\mathbf{z}} \sum_{k=1}^K \alpha_k \|\mathbf{z} - \mathbf{p}_k\|_2, \quad (45)$$

where α_k is the weight factor for the k th parameter. It is well-known that the equation (45) can be solved with Weiszfeld algorithm. In [61] and [80], a modified Weiszfeld algorithm is proposed for achieving a smoothed geometric median aggregation against Byzantine attacks with OAC. To calculate the geometric median in (45), the following iterations are proposed to realize with OAC:

$$\mathbf{z}^{(n+1)} = \frac{\sum_{k=1}^K \beta_k \mathbf{p}_k}{\sum_{k=1}^K \beta_k}, \quad (46)$$

where β_k is defined as

$$\beta_k = \frac{\alpha_k}{\|\max(v, \mathbf{z}^{(n)} - \mathbf{p}_k)\|_2}, \quad (47)$$

and v is a chosen smoothing factor to prevent the denominator in (46) from yielding an unrealizable $\mathbf{z}^{(n+1)}$ value. The proposed scheme considers FEEL based on model aggregation, where the investigated OAC scheme is BAA with TCI (see Section III-B1a). In this approach, the k th ED transmits the scaled model parameters $\beta_k \mathbf{p}_k$ and the scalar β_k . The ES calculates (46) with OAC by using the estimates of the numerator and denominator parts and broadcast the vector $\mathbf{z}^{(n+1)}$. This procedure continues until a certain convergence is achieved. The proposed scheme have two main disadvantages: First, it can cause an additional delay as the algorithm should run exclusively for each communication round of FEEL. Second, it assumes that Byzantine users follow the proposed algorithm, which may not be the case in practice.

In [79], it is assumed that the ES has a reference data set and uses its own gradient as a reference vector to provide robustness against Byzantine ED. To this end, the network divides the EDs into multiple groups in orthogonal resources. By comparing distances between its own gradient and the received estimate of each group with OAC scheme that relies on analog aggregation and TCI. In this study, OAC based on BAA with channel inversion is used to reduce per-round communication latency for each group, rather than directly addressing Byzantine attack as done in [61] and [80].

In [190], the EDs transmit not only their standardized gradients (i.e., the variance and the mean of the local gradients is always set to 1 and 0, respectively), but also the variance that is used for the standardization. It is proposed to calculate the global gradient with a channel-inversion-based OAC while transmitting the variance information through orthogonal channels. Assuming that Byzantine attackers follow the standardization to avoid exposing themselves during the standardization stage, they would send the true mean and variance of their local gradients. Under this scenario, it is shown that TCI-based OAC for stochastic gradient descent (SGD) has limited defensive capability against Byzantine attacks as the TCI aligns the amplitude levels at the ES. The best effort approach, i.e., using maximum power, is proposed against Byzantine attacks. The main shortcoming of the proposed approach is

that Byzantine attacker can still transmit a non-standardized gradients while transmitting a valid variance information.

2) *Privacy*: Differential privacy is a well-established metric that measures the privacy of local data sets with respect to disclosed aggregate statistics [209]. A typical approach is to randomize the disclosed statistics by adding random noise, which causes a trade-off between accuracy and privacy. For OAC, random perturbations is added to the local model parameters or gradients before transmission for FEEL [93], [210], [211]. In [93], it is shown that the privacy leakage per user scales as $\mathcal{O}(1/\sqrt{K})$, compared to the orthogonal schemes. In [212], privacy is investigated with the consideration of random client participation and power misalignment. In [213, Lemma 3], it is shown that such an approach guarantees differential privacy and can be obtained without affecting the learning performance as long as the privacy constraint level is below a threshold. The authors also emphasize that although the channel inversion for OAC causes noise amplification under fading, it is beneficial for privacy. In [83], the privacy concern is addressed by incorporating channel perturbations into the optimization problem and introducing a framework that does not explicitly transmit the Hessian or the gradient to the ES. In [203], privacy-preserving signaling and privacy-guaranteed training algorithm along with OAC are investigated when a neural network is distributed across multiple nodes based on a graph. In [214], trade-offs between the data privacy and the training accuracy via power control optimization is investigated for channel inversion based OAC. In [215], differential privacy is evaluated when the devices with better channel conditions are scheduled for OAC during the training period of FEEL. In [216], it is proposed to use low-resolution analog-to-digital converters (ADCs) at the ES and digital-to-analog converter (DAC) at the EDs along with OAC for promoting the privacy further.

3) *Eavesdropping*: Eavesdropping is one of the potential issues of OAC as an eavesdropper can overhear the computation in the wireless channel. To address this issue, in [217], data confidentiality is investigated for TBMA. The key idea in this work is that the sensors that have weaker channel gains can be utilized to confuse as eavesdropper by exploiting the independence between the desired and eavesdropping channels. A similar idea where a group of EDs with weaker channel conditions are selected as jammers is utilized for FEEL in [218]. In [219], the pre-processed symbols transmitted from the EDs, i.e., $\{p_k[n], \forall k\}$, are intentionally distorted with jamming symbols such that the distortion can cause a substantial MSE degradation at the eavesdropper as compared to the one at the legitimate receiver, i.e., ES. The basic assumption exploited in this work is that the ES has either precise knowledge of the jamming symbols while the eavesdropper only has knowledge about the distribution of the jamming signal. Hence, under this assumption, the ES can cancel the jamming symbols or affected by less interference as compared to the eavesdropper. The proposed scheme is investigated for computing an arithmetic average over an AWGN channel. In [220], it is proposed to use a full-duplex transceiver at the ES so that a jamming noise is transmitted to degrade the eavesdropper's links. In [221], ES calculates an artificial

noise vector such that it is projected into the null-space of the channel vector after the simultaneous transmissions. The trade-off between the computation at the ES and the security against the eavesdropper is emphasized.

4) *Jamming*: In [222], it is proposed to use a common spreading code assigned by the ES to facilitate protected model aggregation. For this scenario, it is assumed that the adversarial user who is not aware of the spreading code. Hence, the interference due to the adversary is suppressed in the despreading/decoding process at the ES.

V. WHAT ARE THE APPLICATIONS OF OAC?

In this section, we discuss several applications of OAC in various fields, as illustrated in Fig. 6. We also discuss the state-of-the-art demonstrations of OAC for certain applications.

A. Distributed localization

Consider a scenario where many sensors are deployed in an area to identify the location of a radio source with emitting with a constant known power based on the received signal strength information (RSSI). OAC can provide a localization solution based on voting over OFDM as follows [159]:

- Step 0: The area is divided into a grid and all sensors know their positions and the grid structure.
- Step 1: Each sensor estimates the link distance between its location and source based on RSSI.
- Step 2: Each sensor marks the squares that intersect with the circle with the radius the estimated link distance.
- Step 3: Each sensor activates the corresponding OFDM subcarriers that represent the marked squares (i.e., vote).
- Step 4: All the sensors transmit simultaneously.
- Step 5: The ES determines the location of the source by detecting the subcarriers that has the largest magnitude (i.e., MV).

The steps above is an extension of a voting-based localization [223] with the consideration of OAC. With OAC, instead of using orthogonal channels to acquire the sensor information, the ES receives the superposed signal and obtains the locations of the radio without any extra computation. An example is illustrated in Fig. 6(a).

B. Wireless control systems

In control theory, a dynamic plant refers to a state-space model where the current states evolve in time. It can be modeled a set of first-order linear difference equations, e.g., $\mathbf{x}(t+1) = \mathbf{A}\mathbf{x}(t) + \mathbf{B}\mathbf{u}(t) + \mathbf{w}(t)$, where \mathbf{A} and \mathbf{B} are real-valued controllable matrices, $\mathbf{u}(t)$ is plant control action, $\mathbf{x}(t)$ is the plant state, and $\mathbf{w}(t)$ is the plant noise [12]. A simple example of a dynamic plant is a pendulum, where the vector $\mathbf{x}(t)$ represents the angular position and speed of the pendulum [224]. The vector $\mathbf{x}(t)$ may involve a large number of spatially-distributed state variables. For example, for a chemical plant, the state variables may be the temperature, humidity, pressure, flow amount, while they may be atmospheric pressure, thrust, drag, speed, and accelerations for an aircraft. In [12], a scenario where the stability of a dynamic plant is monitored by

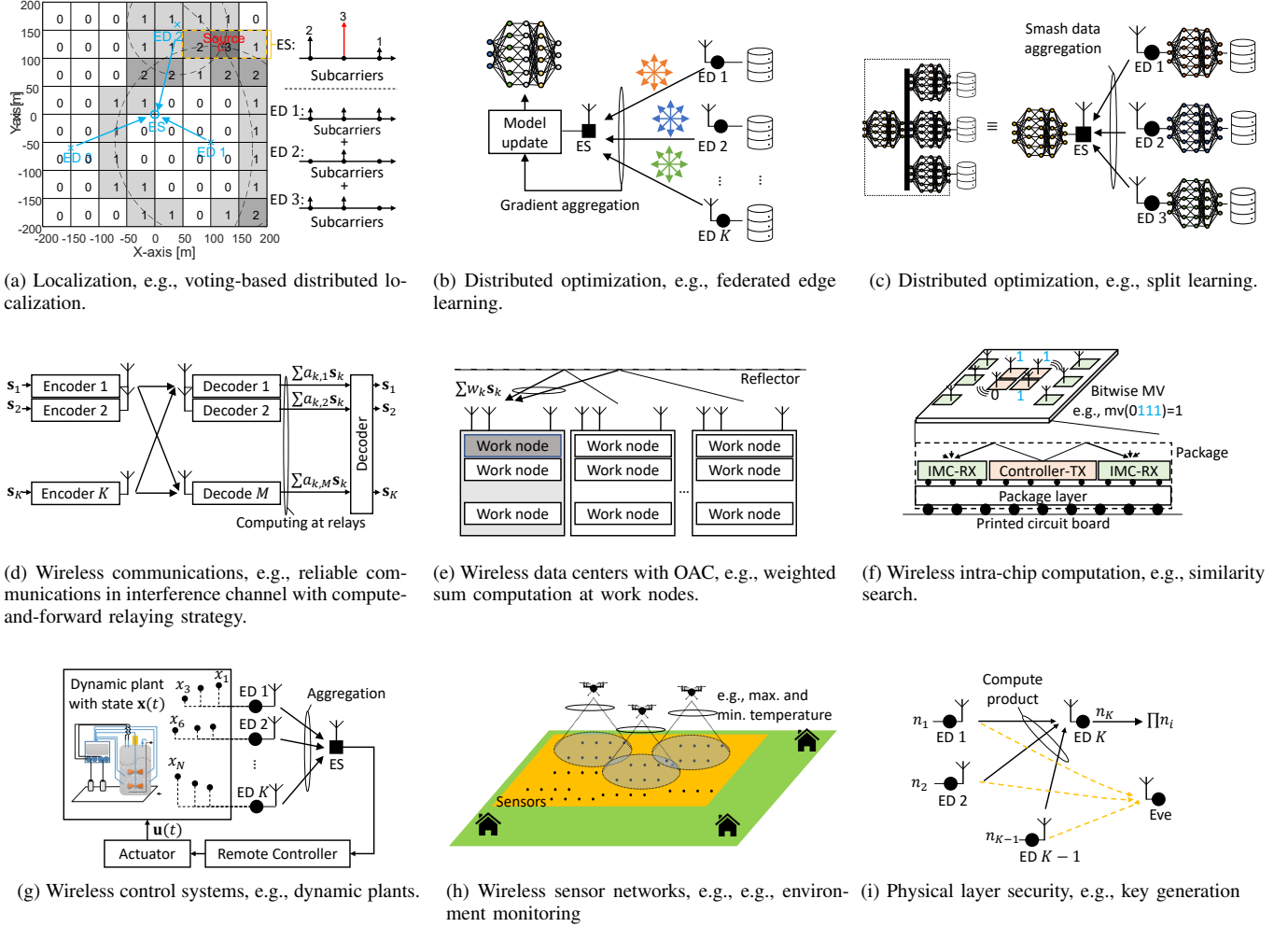


Fig. 6. Applications of OAC.

distributed sensors is considered. The main goal is to stabilize a potentially unstable plant over a limited wireless resources by acquiring the current state as quick as possible. By expressing the corresponding state-space equation of the dynamic plant by incorporating the multiple-access channel, OAC is exploited to support a large number of sensors. We also refer reader to [179], [224], [225] for further details to dynamic plants, where the main goal is recover the state vector $\mathbf{x}(t)$ by using OAC. In [226], OAC is applied to a general control system. The proposed scheme is concerned about the transmit power of sensors to minimize the effect of the wireless channel to the control system under a transmit power constraint. In [99], distributed consensus via OAC is applied to vehicle platooning control. OAC is utilized to calculate the average positions of the vehicles, needed for the calculation of the accelerator at each vehicular to stabilize the platoon. For OAC, the authors propose to multiply the parameter (a scaled version of the position of the vehicle) with the sign of the real part of the channel at the transmitters so that a coherent addition is obtained at the receiver. Only real part of the symbols are used for computation.

C. Wireless sensor networks

In [37], OAC is used for estimating the portion of inactive sensors in a network. For this application, all active sensors transmit the symbol 1 and the receiver estimates the number of active sensors from the received signal. If the ES knows the amount of sensors in the network, it immediately estimates what portion of sensors are inactive. An example of OAC for computing the arithmetic mean of temperatures measured by 250 sensors for environment monitoring can be found in [37]. In [62], several other applications of OAC like counting the number of sensors whose readings satisfying a certain threshold, variance of the measured temperatures, or the best linear fit to the observed measurements, i.e., regression, are given in the area of WSNs. With the motivation of environment sensing and radio map construction, product-of-experts-based Gaussian process regression over a distributed network is investigated in [90], where the investigated OAC schemes are based on ZF precoder and PC. In [116], the authors consider a distributed sensing application, where all the sensors observe a linear combination of the data. In [88], the mobility of unmanned aerial vehicles (UAVs) is exploited to improve the power alignment for ZF-based OAC.

Cluster scheduling, association, and UAV trajectory are jointly optimized with the motivation of aligning the signals within each cluster while mitigating the inter-cluster interference. UAV-based aggregation is also studied in [94]. Similarly, UAV trajectory optimization with the consideration of multi-slot OAC is investigated in [227]. In [86], the authors consider the freshness of the aggregated data in addition to MSE in a time-varying environment for OAC-based remote monitoring applications. In [160], OAC is considered for constructing the geographical heat distribution via low-power wide-area networks with the motivation of detecting forest fires.

D. Distributed optimization over wireless networks

One of the main motivations behind OAC is the convergence of communication and computing architectures as explicitly discussed in ITU's report for IMT-2030 [228]. The driving force for this trend is the advances in machine learning and artificial intelligence technologies such as federated learning and split learning, and their utilization over wireless networks. The major benefit gained from OAC for a distributed optimization problem is the considerable improvement in computation rate as compared to the traditional way of separating communication and computation tasks, particularly, when a large number of EDs participates in computation.

1) *Federated learning*: FL [26] is one of the most studied distributed learning frameworks. The task of model training is distributed across multiple EDs and the data uploading is avoided to promote user-privacy. Instead of data samples, EDs share a large number of local stochastic gradients or local model parameters with an ES for aggregation. For its implementation over a wireless network in general, i.e., FEEL, we refer the reader to [18]–[24].

For FEEL, if the communication and computation are considered as separate tasks, for each iteration, the ES needs to acquire the local model parameters (or gradients) from K EDs, separately, to compute $N_f \sim 10^6 - 10^8$ functions. Hence, $N_f K$ parameters need to be transferred in the UL and the latency grows linearly with the number of EDs for an orthogonal user multiple access scheme. On the other hand, with OAC, the cost is equal to the one with a single ED as all the EDs transmit simultaneously to compute N_f functions, e.g., the average of the local model parameters (or gradients). Hence, the training can be completed much faster if OAC is utilized.

One of the crucial choices for OAC to support FEEL is that the information needs to be transmitted in the UL and DL. This is because the UL information can be local gradients or local parameters, while the information broadcast to the EDs in the DL can be the updated model parameters or the aggregated gradients, leading to four different FEEL implementations. Although the gradients often have an unknown probability distribution that changes over the communication rounds [229], their magnitudes tend to decrease over iterations. Also, the gradients between adjacent communication rounds and across the devices, and the entries of a stochastic gradient vector at one iteration may have a high correlation, [177], [197], [230]. In addition, even if the signs of the gradients are transmitted, convergence can be achieved [157]. These

properties are exploited in the UL in several OAC papers, e.g., [77], [156], [158], [161], [162], [177], [197], [229]. In DL, the broadcasting updated model parameters can ensure that the EDs calculate the gradients based on the same model parameters. On the other hand, for multi-cell OAC, broadcasting aggregated gradients in the DL is shown to be useful for aggregation for EDs located at the cell edge [156] while promoting the personalization of the model parameters.

It is also worth noting that FEEL with OAC inherits the well-known problems in FL literature such as convergence under data and device heterogeneity, stragglers, data privacy, and various security issues. Hence, these application-specific challenges often need to be re-evaluated for a given OAC scheme. For example, it is more challenging to deal with Byzantine attacks when OAC is used for FEEL since the ES does not directly observe the gradients or the model parameters. Also, training can lead to biased learning due to the imbalanced averaged received signal powers [158], [161]

2) *Split learning*: In [231], the authors investigate the idea of splitting a neural network over the EDs and ES so that the EDs can conserve privacy of their local data sets while the computational burden is decreased at the ED's side. Under a simple configuration, the EDs train the network up to a specific layer called *cut layer*, and send the output of the cut layer, i.e., *smashed* data, with the labels to the ES. The ES completes the rest of forward step starting from a layer, called *aggregation* layer that concatenates and aggregates the EDs' smash data. Afterwards, the ES starts the back-propagation of the gradients from the last layer to the first layer of the ES network, and sends the gradients with respect to the smash data to the EDs. The forward and back-propagation continue until the network converges. The main advantage is that the EDs have fewer layers as compared with the ones in the FL [232]–[235]. Note that the model splitting also appears as *vertical FL* in the literature [236], where a neural network is divided and distributed across the network. User scheduling under fading channel for vertical FL is discussed in [237] without using OAC. The reader is also referred to the technical reports in [238], [239] for potential applications of split learning (SL).

SL is not heavily investigated in the state-of-the-art from the perspective of OAC. In [240], aggregation layer of SL is proposed to be realized with BAA along with channel inversion. In this approach, to accommodate OAC, weighted multiplication of the aggregation layer is moved to the EDs whereas the bias addition and activation is kept at the ESs. To address the fading, the users under deep fade are excluded from the training. Instead of gradient or local parameter aggregation, smash data aggregation takes place for the implementation of SL over a wireless network as shown in Fig. 6(c). In [241], [242], by exploiting channel reciprocity and considering the wireless channel as part of the neural network, i.e., a form of OAC for implementing a fully-connected layer over-the-air, forward-backward propagation for SL is investigated over MIMO channels. The key observation in this study is that the backward propagation can still be maintained by transmitting the gradients if the channel reciprocity is maintained.

3) *Other optimization frameworks*: In [203], a *graph neural network* where the devices correspond to edge of a graph

is investigated. With a graph neural network, each node aggregate information from the neighborhood in the graph. In this study, OAC is exploited to improve computation rate while increasing the privacy. In [243], *message passing neural network*, i.e., a framework of graph neural network that uses the graph convolution by updating the graph embedding via message passing and aggregation, is discussed along with OAC. In [82], OAC is utilized to perform PCA when the data is not centralized. The authors express the centralized PCA problem as a minimization problem. By using the corresponding gradients of the objective function, it is proposed to solve the minimization problem by aggregating the gradients over the air along with TCI. In [244], it is proposed to obtain a cooperative solution of a linear algebraic equation by exploiting OAC, where each agent knows only a subset of the equations. In [87], distributed primal-dual optimization is investigated along with TCI-based OAC, and applied to the energy management of a smart grid system.

In the literature, it is worth noting that there are many other statistical methods, e.g., independent component analysis, k-means, k-SVD, that can benefit from OAC. Exploration of such algorithms with the consideration of OAC is currently an open topic.

E. Wireless data center networks

A data center network (DCN) manages communications among the work nodes across data centers to store or process the files in parallel manner. It is often implemented through a high-bandwidth wired network. On the other hand, a wired DCN has limited flexibility, cabling complexity, device cost, which affects the scalability of DCNs. To address this issue, in [13], OAC is proposed to compute arithmetic mean of the symbols at K source nodes for a wireless DCN.

F. Wireless intra-chip computation

In [14], OAC is exploited with the motivation of addressing scaling-out wired interconnects for hyperdimensional computing. In this method, the main goal is a similarity-search task via multiple in-memory computing (IMC) cores, where the input information at each core is the bit-wise MV of the queries from different controllers (i.e., bundling) over a wireless channel as shown in Fig. 6(f). The transmitters at the controllers use BPSK symbols to transmit bit 0 and bit 1 based on their bits. The receivers at the IMC cores receives a slightly different version of the superposed symbols due to the multi-path channel. To ensure that the phases are aligned at the receivers, the authors propose to optimize the phase of transmitted symbols so that the error rate of the bit MV computation at each core is minimized.

G. Wireless communications

1) *Compute-and-forward relaying scheme*: With the compute-and-forward relaying strategy [1], [7], the multiple relay nodes forward the linear functions of the transmitted messages to be decoded at the destination, as illustrated in Fig. 6(d). In [245], compute-and-forward scheme is exploited

to harness the collisions for massive access. It is well-known that when a collision occurs on the channel, non-scheduling based channel access protocols, like the carrier-sensing multiple access with collision avoidance used in Wi-Fi, require the involved devices to access the channel again using a back-off mechanism to reduced the probability of repeated collisions. To address the diminished rate in this case, in [245], collisions are exploited at the pico-stations and the nodes forward a linear combination of the messages to base station along with the corresponding coefficients for decoding.

2) *Physical-layer network coding*: PLNC is one of the well-studied applications of OAC in the area of wireless communications [5]–[7], [163], [164]. A canonical example of PLNC is the communication over a two-way relay channel. In this channel, the devices want to exchange their bits over a relay. A *link-layer* network-coding strategy requires three time slots to accomplish this task: In the first two time slots, the devices send their bits to the relay, sequentially. In the third slot, the relay forwards the XOR of the bits to devices. With *physical-layer* network coding, the same task is accomplished in two time slots by exploiting signal superposition property: The devices transmit simultaneously their signals determined based on the bits. The relay node then forwards either the superposed signal itself (i.e., analog network coding) [5] or the signal after some detection (i.e., digital network coding) [6], [7], [163], [164] to the devices. Since each of the devices knows its own signal, it can obtain the message at the other device.

In [5], the authors exploit the differential-encoding along with minimum-shift keying (MSK) and discuss the practical issues such as synchronization for analog network coding. In [6], it is proposed to use quadrature phase-shift keying (QPSK) symbols at the devices and the relay detects the XOR of bits, results in a corrupted version of the XOR of the transmitted bits. In [163], [164], FSK is utilized with the motivation of reducing strict requirements on power control, phase synchronization, and CFO. The impact of channel on the detector design at the relay for binary FSK [163] and M -ary FSK along with a LDPC code are discussed rigorously. In [7], Bobak shows that the nested-lattice code used in compute-and-forward relaying strategy can also be utilized in two-way relay channel to improve reliability physical layer network coding and an excellent comparison on analog and digital network coding is provided. We also refer the reader to [16] and the references therein for the variants of physical layer network coding.

3) *Overhead reduction*: In [110], the authors use OAC not only for general purpose computations, but also reduce the corresponding CSI overhead. Instead of acquiring the CSI feedback from each ED through orthogonal multiple access, they calculate the optimum receive beamforming vector at the ES by concurrent transmissions. It is shown that the feedback overhead reduction can be reduced 50 times more than the one with conventional training. In [246], the authors propose to determine the power-normalization factor for zero-forcing OAC over-the-air by calculating the minimum function through the queries discussed in Section II-B, instead of estimating the channel of each ED through orthogonal channels.

4) *Cognitive radios*: In [174] and [175], a variant of Goldenbaum's scheme discussed in Section III-B1c is used for a spectrum-sensing application for cognitive radios. In this application, the fusion center desires to detect if the primary user is active or absent by using many sensors. To this end, the symbols that are transmitted from the sensors are either the average signal power or the hard-detection activity results on the primary-user band. The information across the sensors is proposed to be aggregated over-the-air in order to achieve a time-efficient cooperative spectrum sensing. Instead of only using amplitude correction, a weighted sum based on absolute-square of the channels are incorporated to Goldenbaum's scheme to avoid power boost due to the inversion, which effectively corresponds to maximum ratio transmission. In [246], the DFTs of the received signals at the sensors are proposed to be combined over the air for spectrum sensing. The OAC in this study relies on a zero-forcing precoder. In [90], OAC is applied to radio map construction. For this application, Gaussian process regression is considered for a scenario where the nodes are deployed in two-dimensional space and measure the RSSI of a transmitter. It is shown that the proposed approach can speed up the computation time approximately 733x than the one with separation of communication and computation tasks.

H. Security

In [60], OAC is utilized for multiplying Gaussian prime numbers to compute a secret key that can be used in any encryption process or to generate keys with a predetermined key generation functions as illustrated in Fig. 6(i). In this approach, each node has a number and changing the destination node sequentially, all EDs calculate the products. It is argued that this can also provide physical layer security as an eavesdropper cannot directly observe the multiplication. In [247], the authors propose to use OAC for assessing the consensus in a blockchain network. With this approach, each user maps the bits in the hash to the modulation symbols in a constellation and all the users transmit simultaneously. Since the hash should be consistent among the users, the received symbol after superposition should be one of the points in the constellation. By detection, the malicious users with inconsistent hashes are filtering out. In this study, OAC is based on zero forcing.

I. Demonstrations

In the state-of-the-art, early OAC demonstrations are mainly in the areas of WSNs and PLNC. For example, in [165], a statistical OAC is implemented with twenty-one RFID tags to compute the percentages of the activated classes that encode various temperature ranges. A trigger signal is used to achieve time synchronization across the RFIDs. In [103], Goldenbaum and Stańczak's scheme [39] is implemented with three software-defined radios (SDRs) emulating eleven sensor nodes and a fusion center. The arithmetic and geometric mean of the sensor readings are computed over a 5 MHz signal. The time synchronization across the sensor nodes is maintained based on a trigger signal and the proposed method is implemented

in a field-programmable gate array. A calibration procedure is also discussed to ensure amplitude alignment at the fusion center. In [248], the summation is evaluated with a testbed that involves three SDRs as transmitters and an SDR as a receiver. The scheme used in this setup is based on channel inversion and puts limitations on the supported dynamic range to avoid exceeding the maximum transmit power. In [62], six universal software radio peripherals (USRPs) represents the sensor nodes and the experiment is repeated multiple times to emulate the effect of many sensors. The sum operation is implemented by using binary representation of the parameters. For this experiment, AirShare protocol in [249] is utilized to ensure that all transmissions are coherent. In [246], a spectrum sensing example based on OAC is given, but the details related to the protocols for synchronization are omitted. In [250], a real-time implementation of PLNC is demonstrated. To achieve time synchronization, it is proposed to add a sufficiently large time that compensates the transfer time between the computer and SDRs. In this method, the same clock/oscillator is connected to the co-located radios and the transmission time instants are set manually. In [251], by extending [250] into a more general framework, a time-slotted approach is proposed to maintain time-synchronization among the radios. In this method, the radios (i.e., EDs) first align their slot boundaries by compensating the time difference between the first sample of a reference packet transmitted from the relay (or ES) and the first received sample (e.g., noise) marked by the USRP hardware. By exploiting the time-stamp based transmission feature of USRP hardware [251, Section III.B.2], the radios transmit simultaneously at the slot boundaries. In [252], PLNC is implemented by using temperature-compensated oscillators and implementing custom blocks for accurate alignment.

To the best of our knowledge, the demonstrations of OAC schemes for FEEL are limited, but getting more attention in the recent literature. In [182], a custom two-stage protocol that mitigates the TO and CFO is proposed and an OFDM-based OAC with channel inversion is investigated. In [183], a general-purpose time synchronization method that allows a set of SDRs to transmit or receive any in-phase/quadrature data simultaneously while maintaining the baseband processing in the corresponding companion computers (CCs) is proposed. This approach relies on detection of a synchronization waveform and passing a pre-determined number of in-phase/quadrature (IQ) samples to the CC upon its detection. All SDRs wait for a pre-determined duration for CC-based processing and transmit simultaneously the IQ samples in the SDR buffers. By implementing this synchronization method on five SDRs (i.e., Adalm Pluto) along with a control loop that mitigates TO, CFO, and power offset coarsely, the performance of FSK-MV (see Section III-B4a for details) is practically demonstrated for hand-digit recognition task based on MNIST database. The experiment shows that the test accuracy can reach more than 95% for homogeneous and heterogeneous data distributions without using channel state information at the EDs or any method phase synchronization. The experiment is conducted in a small room, where the distance between the EDs and ES are about 5 meters, but the

channel is shown to be frequency-selective. The experiment also shows that the phase rotations in the frequency domain for OFDM is a function of the time synchronization errors at the EDs and ES. In [81], a TCI-based OAC with two USRP N210 SDRs as EDs is used for FEEL. This setup maintains the synchronization through cable connection between the SDRs. In [150], the aforementioned time-stamp based transmission discussed in [250], [251] is adopted to demonstrate the multi-user detection-based computation by using a higher complexity receiver.

For a consensus application, in [247], srsRAN is considered for implementing a channel-inversion based OAC with seven radios. By considering seven users, the authors propose to use user attaching procedures for time synchronization and Long-Term Evolution (LTE) frame structure. However, the details related to the time synchronization among the radios is not provided explicitly.

VI. CONCLUSION

In this section, we summarize main takeaways based on the discussions in the previous sections and highlight several research directions.

A. Takeaways

OAC is a concept that fundamentally disrupts the traditional way of performing communication and computation as separate tasks. The main goal with OAC is to compute a multivariate function in the wireless channel and the arguments of the function are not intended to be obtained at the ES. While function computation requires two sequential steps (i.e., communications and computation) with NOMA or OMA, such separation does not occur for OAC. Hence, the main benefit gained from OAC is the improvement of the computation rate, which otherwise scales down with the number of EDs participating in the computation.

With OAC, a function that structurally matches the underlying operation that multiple-access channel naturally performs can be computed. Due to the signal superposition property of wireless channels, the functions that can be computed are in the space of nomographic functions. By manipulating pre- and post-processing functions of a nomographic function, commonly-used functions such as arithmetic mean, weighted sum, norm, MV, and histogram can be computed. Although the space of nomographic function with continuous pre- and post-processing functions is limited, Kolmogorov's superposition shows that every continuous function can be computed via multiple nomographic functions. Also, some functions such as maximum, minimum, and median can be computed systematically over iterations or based on some approximations.

Achieving reliable OAC under practical wireless channels is a challenging task since the multi-path channel between an ED and ES distorts the transmitted symbols before the signal superposition. Hence, typical equalization methods used for communications cannot be directly utilized for OAC to compensate for the distortion. Hence, most OAC schemes in the state-of-the-art use CSIT along with CSIR to combat the channel. The corresponding precoders are often derived based

on an MSE criterion or an application-specific metric such as training loss for FEEL under certain conditions such as transmit power. To deal with the distortion due to the channel at the expense of more resource consumption, there exist also blind OAC schemes that rely on channel hardening via multiple antennas or non-coherent techniques in the state-of-the-art.

From the encoding perspective, an OAC scheme can directly use continuous-valued parameters along with an analog modulation or utilize the quantized parameters with a digital modulation. In the case of analog encoding, linear or affine transformations are shown to be effective for compression if certain properties, e.g., sparsity, are present in the parameters. For digital schemes, the family of nested-lattice codes is often considered in the literature for reliable computation since the codes in this family can be made to be linear in \mathbb{R} . From the encoding perspective, heavy quantization, e.g., 1-bit quantization for MV computation, is shown to be an effective solution for certain applications such as distributed learning and localization while being compatible with traditional digital communication systems.

The metrics for assessing an OAC scheme differ from the traditional communication metrics such as the data rate, bit-error rate, and block-error rate since OAC aims to compute a function, rather than its arguments. Often, the performance of an OAC scheme is measured with MSE. For a digital OAC scheme, the probability of computing a single function (or a set of functions) incorrectly can also be used as a metric since the image of the function consists of a set of discrete values. The computation rate, i.e., the number of functions calculated per real dimension, is also another metric that can be used for evaluating the efficiency of an OAC scheme. One can also obtain application-specific metrics such as test accuracy and convergence rate for FEEL when it is used with an OAC scheme. Such derivative metrics are beyond the scope of our survey paper.

As a working principle, OAC relies on simultaneous receptions of EDs' signals on the same wireless resources at the ES and shares similar enabling mechanisms for UL-orthogonal frequency division multiple access (OFDMA) and multi-user MIMO. Reliable OAC requires underlying mechanisms such as time-frequency-phase synchronization, power management, and channel estimation or feedback mechanisms to perform well. Depending on the scheme, OAC can impose very stringent requirements. For example, if the computation relies on phase synchronization among the EDs, a sample-level time-synchronization in the network must be maintained and the phase accumulation due to the residual CFOs should be addressed. On the other hand, methods that do not rely on phase synchronization are shown to provide immunity against TO and CFO impairments.

OAC for power management has two folds: transmitter side and receiver side. From the perspective of the transmitter, an OAC scheme should consider not only maximum transmit power limitation but also the ACLR requirements and PA efficiency. From the perspective of the receiver, the power control mechanisms need to be utilized to align the received signal powers at the ES. While aligning the average signal power can

be managed via typical closed-loop power control mechanisms in 4G LTE and 5G NR, a perfect amplitude alignment among the EDs at ES can be challenging as it requires accurate CSIT and/or low-latency feedback in time-varying fading channel conditions, and channel inversion under the transmit power limitations. Cellular architectures for OAC has also a major impact on the computation as it extends the basic single-cell OAC to a higher-complexity computation framework that involves many fusion nodes.

OAC has both negative and positive aspects in terms of security. On the positive side, user privacy is promoted as the transmitted signals cannot be directly observed due to the superposition. On the negative side, potential adversaries can harm the computation, particularly via Byzantine attacks. Similarly, a jammer can interfere with the superposed signals or an eavesdropper can overhear the computation in the wireless channel.

In the state-of-the-art, OAC has been considered for a wide-variety of applications such as localization (e.g., voting-based distributed localization), wireless control systems (e.g., dynamic plants), wireless sensor networks (e.g., environment monitoring and UAV-trajectory optimization), distribution optimization (e.g., FEEL), wireless data center and intra-chip computation (e.g., wireless computation and similarly search), wireless communication systems (e.g., PLNC and spectrum sensing), and security (e.g., key generation). Among these applications, distribution optimization is currently the leading use case of OAC due to the advances in machine learning and artificial intelligence and the desire to use these techniques over wireless networks.

B. Research directions

The results in the state-of-art overall advocate that OAC can address latency issues by improving computation rate. On the other hand, OAC need to be evaluated further along with enabling mechanisms, applications, and corresponding algorithms. To this end, three major research directions that one can pursue are summarized as follows:

Direction 1 - Design the OAC schemes with the consideration of practical limitations: In the literature, OAC primarily is investigated theoretically under certain assumptions. Hence, some of the practical aspects may be omitted. To address this issue, the methods need to be evaluated under more challenging scenarios or designed with the considerations of imperfections and practical limitations. For instance, in practice, imperfect CSI, the residual TO, CFO, and PO, mobility, and PA non-linearity may be inevitable and their impacts on the performance depend on the robustness of the OAC scheme and the corresponding applications to these imperfections. Another way of addressing this issue is to generate convincing results through demonstrations. A plausible demonstration needs not only the implementation of the OAC scheme but also the design of the underlying protocols that maintain signal superposition. Hence, the work in this area often involves developing the corresponding protocols in addition to the OAC scheme itself. Another practical challenge in this direction is that it is often not trivial to configure multiple standard

SDRs for simultaneous transmissions. Even if there are some proof-of-concept OAC demonstrations, there is no widely-accepted multiple-access channel testbed or platform to test different OAC schemes under realistic scenarios in controllable environments.

Direction 2 - Design the algorithms in the applications with the consideration of OAC: Another area that can be improved is the algorithm in the applications. In the literature, the algorithms for many applications are not designed with the consideration of OAC. On the other hand, the algorithm can be designed to facilitate OAC and relax the constraints for enabling mechanisms. For example, distributed training by MV with signSGD, a machine learning concept, is more compatible with digital modulation as compared to the one with SGD and results in various OAC schemes. Similarly, the implementations of plain FL based on stochastic gradients (i.e., FedSGD) or parameter aggregations (FedAve) are mathematically equivalent to each other. However, the corresponding algorithms for FEEL relying on OAC can perform differently as the gradients and parameters have different statistical characteristics that can be exploited for OAC.

Direction 3 - Improve the protocols for OAC with the consideration of standards: To this date, OAC has not been used in any communication standard or a commercial system. In fact, OAC has recently been discussed in AI/ML Technical Interest Group for IEEE 802.11 for distributed learning [253]. In 3GPP meetings, use cases and *potential* requirements for 5G to support machine learning applications under three main categories, i.e., FEEL, SL, and model distribution, are studied [238], [239], which highlights the need for a comprehensive system optimization under communication and computation constraints. Similarly, in International Telecommunication Union (ITU)'s report [228], convergence of communication and computing architecture in International Mobile Telecommunications (IMT) systems towards 2030 is emphasized. Currently, it is not clear if the future wireless networks utilize OAC to facilitate this convergence or if the existing procedures can support an OAC scheme reliably or not. This is because the current wireless standard protocols in the state-of-the-art are designed by assuming that the communication is separated from the computation. Hence, further evaluations of the underlying systems and the enablers for OAC are needed. To achieve a standardized OAC, the procedures for time-frequency synchronization, power control, channel estimation, calibration, re-transmissions, compression, and security aspects along with the architectures need to be re-evaluated. A standardized OAC can insure interoperability among devices from different manufacturers for a large body of applications.

REFERENCES

- [1] B. Nazer and M. Gastpar, "Computation over multiple-access channels," *IEEE Trans. Inf. Theory*, vol. 53, no. 10, pp. 3498–3516, Oct. 2007.
- [2] M. Goldenbaum, H. Boche, and S. Stańczak, "Harnessing interference for analog function computation in wireless sensor networks," *IEEE Trans. Signal Process.*, vol. 61, no. 20, pp. 4893–4906, 2013.
- [3] S.-W. Jeon, C.-Y. Wang, and M. Gastpar, "Computation over Gaussian networks with orthogonal components," *IEEE Transactions on Information Theory*, vol. 60, no. 12, pp. 7841–7861, 2014.

- [4] M. Goldenbaum, H. Boche, and S. Stańczak, "Nomographic functions: Efficient computation in clustered Gaussian sensor networks," *IEEE Trans. Wireless Commun.*, vol. 14, no. 4, pp. 2093–2105, 2015.
- [5] S. Katti, S. Gollakota, and D. Katabi, "Embracing wireless interference: Analog network coding," in *Proceedings of the 2007 Conference on Applications, Technologies, Architectures, and Protocols for Computer Communications*, ser. SIGCOMM '07. New York, NY, USA: Association for Computing Machinery, 2007, pp. 397–408. [Online]. Available: <https://doi.org/10.1145/1282380.1282425>
- [6] S. Zhang, S. C. Liew, and P. P. Lam, "Hot topic: Physical-layer network coding," in *Proceedings of the 12th Annual International Conference on Mobile Computing and Networking*, ser. MobiCom '06. New York, NY, USA: Association for Computing Machinery, 2006, p. 358–365. [Online]. Available: <https://doi.org/10.1145/1161089.1161129>
- [7] B. Nazer and M. Gastpar, "Compute-and-forward: Harnessing interference through structured codes," *IEEE Trans. Inf. Theory*, vol. 57, no. 10, pp. 6463–6486, 2011.
- [8] B. Nazer, A. G. Dimakis, and M. Gastpar, "Local interference can accelerate gossip algorithms," *IEEE Journal of Selected Topics in Signal Processing*, vol. 5, no. 4, pp. 876–887, 2011.
- [9] G. Mergen and L. Tong, "Type based estimation over multiaccess channels," *IEEE Transactions on Signal Processing*, vol. 54, no. 2, pp. 613–626, 2006.
- [10] G. Mergen, V. Naware, and L. Tong, "Asymptotic detection performance of type-based multiple access over multiaccess fading channels," *IEEE Transactions on Signal Processing*, vol. 55, no. 3, pp. 1081–1092, 2007.
- [11] G. Zhu, J. Xu, K. Huang, and S. Cui, "Over-the-air computing for wireless data aggregation in massive IoT," *IEEE Wireless Communications*, vol. 28, no. 4, pp. 57–65, 2021.
- [12] S. Cai and V. K. N. Lau, "Modulation-free M2M communications for mission-critical applications," *IEEE Transactions on Signal and Information Processing over Networks*, vol. 4, no. 2, pp. 248–263, 2018.
- [13] X. Wu, S. Zhang, and A. Özgür, "STAC: Simultaneous transmitting and air computing in wireless data center networks," *IEEE Journal on Selected Areas in Communications*, vol. 34, no. 12, pp. 4024–4034, 2016.
- [14] R. Guirado, A. Rahimi, G. Karunaratne, E. Alarcón, A. Sebastian, and S. Abadal, "Wireless on-chip communications for scalable in-memory hyperdimensional computing," 2022. [Online]. Available: <https://arxiv.org/abs/2205.10889>
- [15] J. B. Predd, S. B. Kulkarni, and H. V. Poor, "Distributed learning in wireless sensor networks," *IEEE Signal Processing Magazine*, vol. 23, no. 4, pp. 56–69, 2006.
- [16] S. C. Liew, S. Zhang, and L. Lu, "Physical-layer network coding: Tutorial, survey, and beyond," *Physical Communication*, vol. 6, pp. 4–42, 2013, network Coding and its Applications to Wireless Communications.
- [17] B. Nazer and M. Gastpar, "Reliable physical layer network coding," *Proceedings of the IEEE*, vol. 99, no. 3, pp. 438–460, 2011.
- [18] J. Park, S. Samarakoon, M. Bennis, and M. Debbah, "Wireless network intelligence at the edge," *Proceedings of the IEEE*, vol. 107, no. 11, pp. 2204–2239, 2019.
- [19] M. Chen, D. Gündüz, K. Huang, W. Saad, M. Bennis, A. V. Feljan, and H. Vincent Poor, "Distributed learning in wireless networks: Recent progress and future challenges," *IEEE J. Sel. Areas Commun.*, pp. 1–26, 2021.
- [20] H. Hellström, J. M. B. da Silva Jr., M. M. Amiri, M. Chen, V. Fodor, H. V. Poor, and C. Fischione, "Wireless for machine learning: A survey," *Foundations and Trends in Signal Processing*, vol. 15, no. 4, pp. 290–399, 2022.
- [21] A. Imteaj, U. Thakker, S. Wang, J. Li, and M. H. Amini, "A survey on federated learning for resource-constrained IoT devices," *IEEE Internet of Things Journal*, vol. 9, no. 1, pp. 1–24, 2022.
- [22] P. Popovski, F. Chiarion, K. Huang, A. E. Kalør, M. Kountouris, N. Pappas, and B. Soret, "A perspective on time towards wireless 6G," *CoRR*, vol. abs/2106.04314, 2021.
- [23] Y. Cui, J. Guo, X. Li, L. Liang, and S. Jin, "Federated edge learning for the wireless physical layer: Opportunities and challenges," *China Communications*, vol. 19, no. 8, pp. 15–30, 2022.
- [24] X. Cao, Z. Lyu, G. Zhu, J. Xu, L. Xu, and S. Cui, "An overview on over-the-air federated edge learning," 2022. [Online]. Available: <https://arxiv.org/abs/2208.05643>
- [25] X. Liu, Y. Deng, A. Nallanathan, and M. Bennis, "Federated and meta learning over non-wireless and wireless networks: A tutorial," 2022. [Online]. Available: <https://arxiv.org/abs/2210.13111>
- [26] B. McMahan, E. Moore, D. Ramage, S. Hampson, and B. A. y. Arcas, "Communication-Efficient Learning of Deep Networks from Decentralized Data," in *Proc. International Conference on Artificial Intelligence and Statistics (AISTATS)*, ser. Proceedings of Machine Learning Research, A. Singh and J. Zhu, Eds., vol. 54. PMLR, 20–22 Apr 2017, pp. 1273–1282.
- [27] D. Gündüz, Z. Qin, I. E. Aguerri, H. S. Dhillon, Z. Yang, A. Yener, K. K. Wong, and C.-B. Chae, "Beyond transmitting bits: Context, semantics, and task-oriented communications," 2022. [Online]. Available: <https://arxiv.org/abs/2207.09353>
- [28] G. Zhu, Z. Lyu, X. Jiao, P. Liu, M. Chen, J. Xu, S. Cui, and P. Zhang, "Pushing AI to wireless network edge: An overview on integrated sensing, communication, and computation towards 6G," 2022. [Online]. Available: <https://arxiv.org/abs/2211.02574>
- [29] X. Li, Y. Gong, K. Huang, and Z. Niu, "Over-the-air integrated sensing, communication, and computation in IoT networks," 2022. [Online]. Available: <https://arxiv.org/abs/2211.03345>
- [30] H. Lee, B. Lee, H. Yang, J. Kim, S. Kim, W. Shin, B. Shim, and H. V. Poor, "Towards 6G hyper-connectivity: Vision, challenges, and key enabling technologies," 2023. [Online]. Available: <https://arxiv.org/abs/2301.11111>
- [31] U. Altun, G. Karabulut Kurt, and E. Ozdemir, "The magic of superposition: A survey on simultaneous transmission based wireless systems," *IEEE Access*, vol. 10, pp. 79 760–79 794, 2022.
- [32] B. Yamansavascilar, A. Ozgovde, and C. Ersoy, "Air computing: A survey on a new generation computation paradigm in 6G wireless networks," 2022. [Online]. Available: <https://arxiv.org/abs/2209.04640>
- [33] Z. Wang, Y. Zhao, Y. Zhou, Y. Shi, C. Jiang, and K. B. Letaief, "Over-the-air computation: Foundations, technologies, and applications," 2022. [Online]. Available: <https://arxiv.org/abs/2210.10524>
- [34] M. Goldenbaum, H. Boche, and S. Stańczak, "Analog computation via wireless multiple-access channels: Universality and robustness," in *Proc. IEEE International Conference on Acoustics, Speech and Signal Processing (ICASSP)*, 2012, pp. 2921–2924.
- [35] —, "Analyzing the space of functions analog-computable via wireless multiple-access channels," in *Proc. International Symposium on Wireless Communication Systems (ISWCS)*, 2011, pp. 779–783.
- [36] —, "On analog computation of vector-valued functions in clustered wireless sensor networks," in *Proc. IEEE Annual Conference on Information Sciences and Systems (CISS)*, 2012, pp. 1–6.
- [37] M. Goldenbaum, S. Stanczak, and M. Kaliszan, "On function computation via wireless sensor multiple-access channels," in *Proc. IEEE Wireless Communications and Networking Conference (WCNC)*, 2009, pp. 1–6.
- [38] M. Goldenbaum and S. Stańczak, "Computing the geometric mean over multiple-access channels: Error analysis and comparisons," in *IEEE Asilomar Conference on Signals, Systems and Computers*, 2010, pp. 2172–2178.
- [39] M. Goldenbaum and S. Stanczak, "Robust analog function computation via wireless multiple-access channels," *IEEE Trans. Commun.*, vol. 61, no. 9, pp. 3863–3877, 2013.
- [40] D. A. Sprecher, "A representation theorem for continuous functions of several variables," *Proceedings of the American Mathematical Society*, vol. 16, no. 2, pp. 200–203, 1965.
- [41] R. Buck, "Approximate complexity and functional representation," *Journal of Mathematical Analysis and Applications*, vol. 70, no. 1, pp. 280–298, 1979.
- [42] M. Frey, "Distributed function approximation over noisy channels," Ph.D. dissertation, Technische Universität Berlin, 2023.
- [43] R. C. Buck, "Nomographic functions are nowhere dense," *Proceedings of the American Mathematical Society*, vol. 85, no. 2, pp. 195–199, 1982.
- [44] V. I. Arnol'd, "On the representation of functions of two variables in the form $\chi[\phi(x) + \psi(y)]$," *Uspekhi Mat. Nauk*, vol. 12, pp. 119–121, 1957.
- [45] A. K. Kolmogorov, "On the representation of continuous functions of several variables by superposition of continuous functions of one variable and addition," *Doklady Akademii Nauk SSSR*, vol. 114, pp. 953–956, 1957.
- [46] Y. Sternfeld, "Dimension, superposition of functions and separation of points, in compact metric spaces," *Proceedings of the American Mathematical Society*, vol. 50, no. 1, pp. 13–53, 1965.
- [47] D. Hilbert, "Mathematical problems," *Bulletin of the American Mathematical Society*, vol. 8, no. 10, pp. 437–479, 1902.
- [48] D. A. Sprecher, "On the structure of continuous functions of several variables," *Transactions of the American Mathematical Society*, vol. 115, pp. 340–355, 1965.

- [49] J. Braun and M. Griebel, "On a constructive proof of kolmogorov's superposition theorem," *Constructive Approximation*, vol. 30, no. 3, pp. 653–675, 2009.
- [50] J. Braun, "An application of Kolmogorov's superposition theorem to function reconstruction in higher dimensions," Ph.D. dissertation, Rheinische Friedrich-Wilhelms-Universität Bonn, 2009.
- [51] F. Girosi and T. Poggio, "Representation properties of networks: Kolmogorov's theorem is irrelevant," *Neural Computation*, vol. 1, no. 4, pp. 465–469, 1989.
- [52] V. Kurkova, "Kolmogorov's Theorem Is Relevant," *Neural Computation*, vol. 3, no. 4, pp. 617–622, 12 1991.
- [53] J. Schmidt-Hieber, "The Kolmogorov–Arnold representation theorem revisited," *Neural Networks*, vol. 137, pp. 119–126, 2021.
- [54] M. Frey, I. Bjelaković, and S. Stańczak, "Over-the-air computation in correlated channels," *IEEE Transactions on Signal Processing*, vol. 69, pp. 5739–5755, 2021.
- [55] S. Y. Khavinson, *Best approximation by linear superpositions (approximate nomography)*, ser. Translations of mathematical monographs. American Mathematical Society, 1996.
- [56] S. Limmer, J. Mohammadi, and S. Stańczak, "A simple algorithm for approximation by nomographic functions," in *IEEE Annual Allerton Conference on Communication, Control, and Computing (Allerton)*, 2015, pp. 453–458.
- [57] I. Bjelaković, M. Frey, and S. Stańczak, "Distributed approximation of functions over fast fading channels with applications to distributed learning and the max-consensus problem," in *Proc IEEE Annual Allerton Conference on Communication, Control, and Computing (Allerton)*, 2019, pp. 1146–1153.
- [58] A. Giridhar and P. Kumar, "Computing and communicating functions over sensor networks," *IEEE Journal on Selected Areas in Communications*, vol. 23, no. 4, pp. 755–764, 2005.
- [59] —, "Toward a theory of in-network computation in wireless sensor networks," *IEEE Communications Magazine*, vol. 44, no. 4, pp. 98–107, 2006.
- [60] U. Altun, S. T. Basaran, G. K. Kurt, and E. Ozdemir, "Scalable secret key generation for wireless sensor networks," *IEEE Systems Journal*, pp. 1–11, 2022.
- [61] S. Huang, Y. Zhou, T. Wang, and Y. Shi, "Byzantine-resilient federated machine learning via over-the-air computation," in *Proc. IEEE International Conference on Communications Workshops (ICC Workshops)*, 2021, pp. 1–6.
- [62] O. Abari, H. Rahul, and D. Katabi, "Over-the-air function computation in sensor networks," 2016. [Online]. Available: <https://arxiv.org/abs/1612.02307>
- [63] L. Chen, N. Zhao, Y. Chen, F. R. Yu, and G. Wei, "Over-the-air computation for IoT networks: Computing multiple functions with antenna arrays," *IEEE Internet of Things Journal*, vol. 5, no. 6, pp. 5296–5306, 2018.
- [64] N. Agrawal, M. Frey, and S. Stańczak, "A scalable max-consensus protocol for noisy ultra-dense networks," in *Proc. IEEE International Workshop on Signal Processing Advances in Wireless Communications (SPAWC)*, 2019, pp. 1–5.
- [65] S.-W. Jeon and B. C. Jung, "Adaptive analog function computation via fading multiple-access channels," *IEEE Commun. Lett.*, vol. 22, no. 1, pp. 213–216, 2018.
- [66] L. Chen, X. Qin, and G. Wei, "A uniform-forcing transceiver design for over-the-air function computation," *IEEE Wireless Commun. Lett.*, vol. 7, no. 6, pp. 942–945, 2018.
- [67] W. Liu, X. Zang, Y. Li, and B. Vucetic, "Over-the-air computation systems: Optimization, analysis and scaling laws," *IEEE Trans. Wireless Commun.*, vol. 19, no. 8, pp. 5488–5502, 2020.
- [68] S.-W. Jeon and B. C. Jung, "Opportunistic function computation for wireless sensor networks," *IEEE Trans. Wireless Commun.*, vol. 15, no. 6, pp. 4045–4059, 2016.
- [69] Proakis, *Digital Communications 5th Edition*. McGraw Hill, 2007.
- [70] S.-C. Chang and E. Weldon, "Coding for t-user multiple-access channels," *IEEE Trans. Inf. Theory*, vol. 25, no. 6, pp. 684–691, 1979.
- [71] D. Tse and P. Viswanath, *Fundamentals of Wireless Communication*. USA: Cambridge University Press, 2005.
- [72] F. Wu, L. Chen, N. Zhao, Y. Chen, F. R. Yu, and G. Wei, "Computation over wide-band multi-access channels: Achievable rates through sub-function allocation," *IEEE Transactions on Wireless Communications*, vol. 18, no. 7, pp. 3713–3725, 2019.
- [73] N. Zhang, M. Tao, J. Wang, and S. Shao, "Coded over-the-air computation for model aggregation in federated learning," *IEEE Communications Letters*, pp. 1–5, 2022.
- [74] L. Chen, N. Zhao, Y. Chen, F. R. Yu, and G. Wei, "Communicating or computing over the MAC: Function-centric wireless networks," *IEEE Transactions on Communications*, vol. 67, no. 9, pp. 6127–6138, 2019.
- [75] G. Zhu, Y. Wang, and K. Huang, "Broadband analog aggregation for low-latency federated edge learning," *IEEE Trans. Wireless Commun.*, vol. 19, no. 1, pp. 491–506, Jan. 2020.
- [76] M. M. Amiri and D. Gündüz, "Federated learning over wireless fading channels," *IEEE Trans. Wireless Commun.*, vol. 19, no. 5, pp. 3546–3557, Feb. 2020.
- [77] G. Zhu, Y. Du, D. Gündüz, and K. Huang, "One-bit over-the-air aggregation for communication-efficient federated edge learning: Design and convergence analysis," *IEEE Trans. Wireless Commun.*, vol. 20, no. 3, pp. 2120–2135, Nov. 2021.
- [78] M. M. Amiri, D. Gündüz, S. R. Kulkarni, and H. Vincent Poor, "Convergence of federated learning over a noisy downlink," *IEEE Trans. Wireless Commun.*, pp. 1–1, 2021.
- [79] S. Park and W. Choi, "Byzantine fault tolerant distributed stochastic gradient descent based on over-the-air computation," *IEEE Trans. Commun.*, pp. 1–15, 2022.
- [80] H. Sifaou and G. Y. Li, "Over-the-air federated learning under byzantine attacks," 2022. [Online]. Available: <https://arxiv.org/abs/2205.02949>
- [81] L. Li, C. Huang, D. Shi, H. Wang, X. Zhou, M. Shu, and M. Pan, "Energy and spectrum efficient federated learning via high-precision over-the-air computation," *arXiv preprint arXiv:2208.07237*, 2022.
- [82] Z. Zhang, G. Zhu, R. Wang, V. K. N. Lau, and K. Huang, "Turning channel noise into an accelerator for over-the-air principal component analysis," *IEEE Transactions on Wireless Communications*, pp. 1–1, 2022.
- [83] M. Krouka, A. Elgabri, C. B. Issaid, and M. Bennis, "Communication-efficient federated learning: A second order newton-type method with analog over-the-air aggregation," *IEEE Transactions on Green Communications and Networking*, vol. 6, no. 3, pp. 1862–1874, 2022.
- [84] W. Fang, Z. Yu, Y. Jiang, Y. Shi, C. N. Jones, and Y. Zhou, "Communication-efficient stochastic zeroth-order optimization for federated learning," 2022. [Online]. Available: <https://arxiv.org/abs/2201.09531>
- [85] W. Guo, R. Li, C. Huang, X. Qin, K. Shen, and W. Zhang, "Joint device selection and power control for wireless federated learning," *IEEE Journal on Selected Areas in Communications*, vol. 40, no. 8, pp. 2395–2410, 2022.
- [86] L. Qiao and Y. Zhou, "Timely status update for wireless data aggregation via over-the-air computation," in *Proc. IEEE Global Communications Conference*, Dec. 2022, pp. 1–6.
- [87] N. A. Mitsiou, P. S. Bouzinis, P. D. Diamantoulakis, R. Schober, and G. K. Karagiannis, "Accelerating distributed optimization via over-the-air computing," 2022. [Online]. Available: <https://arxiv.org/abs/2212.14003>
- [88] M. Fu, Y. Zhou, Y. Shi, C. Jiang, and W. Zhang, "UAV-assisted multi-cluster over-the-air computation," 2022. [Online]. Available: <https://arxiv.org/abs/2210.10963>
- [89] S. Razavikia, J. A. Peris, J. M. B. da Silva Jr, and C. Fischione, "Blind asynchronous over-the-air federated edge learning," in *Proc. IEEE Global Communications Conference Workshops (GLOBECOM WRKSH) - Edge Learning over 5G Mobile Networks and Beyond*, Dec. 2022, pp. 1–6.
- [90] K. Sato, "Over-the-air Gaussian process regression based on product of experts," in *Proc. IEEE Global Communications Conference Workshops (GLOBECOM WRKSH) - Edge Learning over 5G Mobile Networks and Beyond*, Dec. 2022, pp. 1–7.
- [91] N. Mital and D. Gündüz, "Bandwidth expansion for over-the-air computation with one-sided csi," in *Proc. IEEE International Symposium on Information Theory (ISIT)*, 2022, pp. 1271–1276.
- [92] T. Sery and K. Cohen, "On analog gradient descent learning over multiple access fading channels," *IEEE Trans. Signal Process.*, vol. 68, pp. 2897–2911, 2020.
- [93] M. Seif, R. Tandon, and M. Li, "Wireless federated learning with local differential privacy," in *Proc. IEEE International Symposium on Information Theory (ISIT)*, 2020, pp. 2604–2609.
- [94] X. Zhong, X. Yuan, H. Yang, and C. Zhong, "UAV-assisted hierarchical aggregation for over-the-air federated learning," in *Proc. IEEE Global Communications Conference*, Dec. 2022, pp. 1–6.
- [95] C. Feres, B. Levy, and Z. Ding, "Over-the-air collaborative learning in joint decision making," in *Proc. IEEE Global Communications Conference (GLOBECOM)*, 2022, pp. 1–6.
- [96] W.-T. Chang, M. S. Eldin Mohamed, and R. Tandon, "On the necessity of aligning gradients for wireless federated learning," in *Proc. IEEE*

- International Workshop on Signal Processing Advances in Wireless Communications (SPAWC)*, 2021, pp. 226–230.
- [97] R. Paul, Y. Friedman, and K. Cohen, “Accelerated gradient descent learning over multiple access fading channels,” *IEEE Journal on Selected Areas in Communications*, vol. 40, no. 2, pp. 532–547, 2022.
 - [98] R. Jiang and S. Zhou, “Cluster-based cooperative digital over-the-air aggregation for wireless federated edge learning,” in *IEEE/CIC International Conference on Communications in China (ICCC)*, 2020, pp. 887–892.
 - [99] J. Lee, Y. Jang, H. Kim, S.-L. Kim, and S.-W. Ko, “Over-the-air consensus for distributed vehicle platooning control (extended version),” 2022. [Online]. Available: <https://arxiv.org/abs/2211.06225>
 - [100] M. Goldenbaum and S. Stańczak, “Computing functions via SIMO multiple-access channels: How much channel knowledge is needed?” in *Proc. IEEE International Conference on Acoustics, Speech and Signal Processing (ICASSP)*, 2010, pp. 3394–3397.
 - [101] M. Goldenbaum and S. Stanczak, “On the channel estimation effort for analog computation over wireless multiple-access channels,” *IEEE Wireless Commun. Lett.*, vol. 3, no. 3, pp. 261–264, 2014.
 - [102] S.-W. Wu, A. Şahin, Z.-M. Huang, and C.-Y. Chen, “Z-complementary code sets with flexible lengths from generalized boolean functions,” *IEEE Access*, vol. 9, pp. 4642–4652, 2021.
 - [103] A. Kortke, M. Goldenbaum, and S. Stańczak, “Analog computation over the wireless channel: A proof of concept,” in *Proc. IEEE Sensors*, 2014, pp. 1224–1227.
 - [104] T. Lo, “Maximum ratio transmission,” *IEEE Trans. Commun.*, vol. 47, no. 10, pp. 1458–1461, 1999.
 - [105] L. Su and V. K. N. Lau, “Hierarchical federated learning for hybrid data partitioning across multitype sensors,” *IEEE Internet of Things Journal*, vol. 8, no. 13, pp. 10922–10939, Jan. 2021.
 - [106] J. Joung, “Space-time line code,” *IEEE Access*, vol. 6, pp. 1023–1041, 2018.
 - [107] M. A. Abdul Careem and A. Dutta, “Real-time prediction of non-stationary wireless channels,” *IEEE Trans. Wireless Commun.*, vol. 19, no. 12, pp. 7836–7850, 2020.
 - [108] H. Jung and S.-W. Ko, “Performance analysis of UAV-enabled over-the-air computation under imperfect channel estimation,” *IEEE Wireless Commun. Lett.*, pp. 1–1, Nov. 2021.
 - [109] H. U. Sami and B. Güler, “Over-the-air personalized federated learning,” in *Proc. IEEE International Conference on Acoustics, Speech and Signal Processing (ICASSP)*, 2022, pp. 8777–8781.
 - [110] G. Zhu and K. Huang, “MIMO over-the-air computation for high-mobility multimodal sensing,” *IEEE Internet of Things Journal*, vol. 6, no. 4, pp. 6089–6103, 2019.
 - [111] K. Yang, T. Jiang, Y. Shi, and Z. Ding, “Federated learning via over-the-air computation,” *IEEE Trans. Wireless Commun.*, vol. 19, no. 3, pp. 2022–2035, 2020.
 - [112] M. A. Sedaghat, A. Bereyhi, S. Asaad, and R. R. Mueller, “How to coordinate edge devices for over-the-air federated learning?” 2022. [Online]. Available: <https://arxiv.org/abs/2211.03449>
 - [113] X. Cao, G. Zhu, J. Xu, and K. Huang, “Optimized power control for over-the-air computation in fading channels,” *IEEE Trans. Wireless Commun.*, vol. 19, no. 11, pp. 7498–7513, 2020.
 - [114] F. Ang, L. Chen, N. Zhao, Y. Chen, and F. R. Yu, “Robust design for massive CSI acquisition in analog function computation networks,” *IEEE Transactions on Vehicular Technology*, vol. 68, no. 3, pp. 2361–2373, 2019.
 - [115] N. Evgenidis, V. Papanikolaou, P. D. Diamantoulakis, and G. K. Karagiannis, “Optimization of Adaptive Channel Estimation in Over-the-Air Computing Systems,” “1” “2023”. [Online]. Available: https://www.techrxiv.org/articles/preprint/Optimization_of_Adaptive_Channel_Estimation_in_Over-the-Air_Computing_Systems/21936300
 - [116] P. Park, H. Shin, and P. Di Marco, “Mimo over-the-air computation for distributed estimation,” *Applied Sciences*, vol. 13, no. 3, 2023.
 - [117] S. Wang, Y. Hong, R. Wang, Q. Hao, Y.-C. Wu, and D. W. K. Ng, “Edge federated learning via unit-modulus over-the-air computation,” *IEEE Trans. Commun.*, pp. 1–16, 2022.
 - [118] H. Zhang, L. Chen, N. Zhao, Y. Chen, and F. Richard Yu, “Interference management of analog function computation in multi-cluster networks,” *IEEE Transactions on Communications*, pp. 1–17, 2022.
 - [119] Y.-S. Lee, K.-H. Lee, and B. C. Jung, “Beamforming techniques for over-the-air computation in MIMO IoT networks,” *Sensors*, vol. 20, no. 22, 2020.
 - [120] M. Jiang, Y. Li, G. Zhang, and M. Cui, “Joint beamforming optimization in multi-relay assisted MIMO over-the-air computation for multi-modal sensing data aggregation,” *IEEE Commun. Lett.*, vol. 25, no. 12, pp. 3937–3941, 2021.
 - [121] J. Huang, Q. Zhang, Q. Li, and J. Qin, “Robust parallel analog function computation via wireless multiple-access mimo channels,” *IEEE Signal Processing Letters*, vol. 22, no. 9, pp. 1297–1301, 2015.
 - [122] Z. Lin, Y. Gong, and K. Huang, “Distributed over-the-air computing for fast distributed optimization: Beamforming design and convergence analysis,” 2022. [Online]. Available: <https://arxiv.org/abs/2204.06876>
 - [123] A. Bereyhi, A. Vagollari, S. Asaad, R. R. Müller, W. Gerstacker, and H. V. Poor, “Matching pursuit based scheduling for over-the-air federated learning,” 2022. [Online]. Available: <https://arxiv.org/abs/2206.06679>
 - [124] G. Shi, S. Guo, J. Ye, N. Saeed, and S. Dang, “Multiple parallel federated learning via over-the-air computation,” *IEEE Open Journal of the Communications Society*, vol. 3, pp. 1252–1264, 2022.
 - [125] A. Nakai-Kasai and T. Wadayama, “Precoder design for correlated data aggregation via over-the-air computation in sensor networks,” in *Proc. IEEE Global Communications Conference Workshops (GLOBECOM WRKSH) - Workshop on Wireless Communications for Distributed Intelligence*, Dec. 2022, pp. 1–6.
 - [126] X. Liu, W. Ni, H. Tian, and Y. Wu, “Simultaneous federated learning and information transmission over time-varying MIMO channels,” in *Proc. IEEE Global Communications Conference Workshops (GLOBECOM WRKSH) - Edge Learning over 5G Mobile Networks and Beyond*, Dec. 2022, pp. 1–6.
 - [127] T. Qin, W. Liu, B. Vucetic, and Y. Li, “Over-the-air computation via broadband channels,” *IEEE Wireless Commun. Lett.*, vol. 10, no. 10, pp. 2150–2154, 2021.
 - [128] Z. Chen and Y. Malitsky, “Over-the-air computation with multiple receivers: A space-time approach,” 2022. [Online]. Available: <https://arxiv.org/abs/2208.11751>
 - [129] S. Tang, P. Popovski, C. Zhang, and S. Obana, “Multi-slot over-the-air computation in fading channels,” 2021. [Online]. Available: <https://arxiv.org/abs/2010.13559>
 - [130] J. Joung and J. Fan, “Over-the-air computation strategy using space-time line code for data collection by multiple unmanned aerial vehicles,” *IEEE Access*, vol. 9, pp. 105 230–105 241, 2021.
 - [131] Y. Saifullah, Y. He, A. Boag, G.-M. Yang, and F. Xu, “Recent progress in reconfigurable and intelligent metasurfaces: A comprehensive review of tuning mechanisms, hardware designs, and applications,” *Advanced Science*, vol. n/a, no. n/a, p. 2203747, 2022.
 - [132] W. Fang, Y. Jiang, Y. Shi, Y. Zhou, W. Chen, and K. B. Letaief, “Over-the-air computation via reconfigurable intelligent surface,” *IEEE Transactions on Communications*, vol. 69, no. 12, pp. 8612–8626, 2021.
 - [133] H. Liu, X. Yuan, and Y.-J. A. Zhang, “Reconfigurable intelligent surface enabled federated learning: A unified communication-learning design approach,” *IEEE Transactions on Wireless Communications*, vol. 20, no. 11, pp. 7595–7609, 2021.
 - [134] —, “CSIT-free model aggregation for federated edge learning via reconfigurable intelligent surface,” *IEEE Wireless Communications Letters*, vol. 10, no. 11, pp. 2440–2444, 2021.
 - [135] F. Zhu, Y. Zhao, W. Xu, and X. You, “Csit-free model aggregation for multi-RIS-assisted over-the-air computation,” in *Proc. IEEE International Symposium on Wireless Communication Systems (ISWCS)*, 2022, pp. 1–5.
 - [136] W. Zhang, J. Xu, W. Xu, X. You, and W. Fu, “Worst-case design for ris-aided over-the-air computation with imperfect csi,” *IEEE Communications Letters*, vol. 26, no. 9, pp. 2136–2140, 2022.
 - [137] J. Zheng, H. Tian, W. Ni, W. Ni, and P. Zhang, “Balancing accuracy and integrity for reconfigurable intelligent surface-aided over-the-air federated learning,” *IEEE Transactions on Wireless Communications*, pp. 1–1, 2022.
 - [138] H. Li, R. Wang, W. Zhang, and J. Wu, “One bit aggregation for federated edge learning with reconfigurable intelligent surface: Analysis and optimization,” *IEEE Transactions on Wireless Communications*, vol. 18, no. 9, pp. 1–17, 2022.
 - [139] P. S. Bouzinis, N. A. Mitsiou, P. D. Diamantoulakis, D. Tyrovolas, and G. K. Karagiannis, “Intelligent over-the-air computing environment,” *IEEE Wireless Communications Letters*, pp. 1–4, 2022.
 - [140] S. G. Sanchez, G. Reus-Muns, C. Bocanegra, Y. Li, U. Muncuk, Y. Naderi, Y. Wang, S. Ioannidis, and K. R. Chowdhury, “AirNN: Over-the-air computation for neural networks via reconfigurable intelligent surfaces,” *IEEE/ACM Transactions on Networking*, pp. 1–14, 2022.
 - [141] Z. Wang, Y. Zhou, Y. Zou, Q. An, Y. Shi, and M. Bennis, “A graph neural network learning approach to optimize ris-assisted federated

- learning,” *IEEE Transactions on Wireless Communications*, pp. 1–16, 2023.
- [142] W. Ni, Y. Liu, Z. Yang, H. Tian, and X. Shen, “Integrating over-the-air federated learning and non-orthogonal multiple access: What role can ris play?” *IEEE Transactions on Wireless Communications*, pp. 1–1, 2022.
- [143] M. M. Amiri, T. M. Duman, D. Gündüz, S. R. Kulkarni, and H. V. Poor, “Blind federated edge learning,” *IEEE Trans. Wireless Commun.*, vol. 20, no. 8, pp. 5129–5143, 2021.
- [144] X. Wei, C. Shen, H. J. Yang, and H. V. Poor, “Random orthogonalization for federated learning in massive MIMO systems,” in *Proc. IEEE International Conference on Communications (ICC)*, Apr. 2022, pp. 1–6.
- [145] O. Aygün, M. Kazemi, D. Gündüz, and T. Duman, “Hierarchical over-the-air federated edge learning,” in *Proc. IEEE International Conference on Communications (ICC)*, May 2022, pp. 1–6.
- [146] O. Aygün, M. Kazemi, D. Gündüz, and T. M. Duman, “Over-the-air federated edge learning with hierarchical clustering,” 2022. [Online]. Available: <https://arxiv.org/abs/2207.09232>
- [147] —, “Over-the-air federated learning with energy harvesting devices,” in *Proc. IEEE Global Communications Conference (GLOBECOM)*, 2022, pp. 1–6.
- [148] B. Tegin and T. M. Duman, “Federated learning with over-the-air aggregation over time-varying channels,” *IEEE Trans. Wireless Commun.*, pp. 1–14, 2023.
- [149] X. Zhao, L. You, R. Cao, Y. Shao, and L. Fo, “Broadband digital over-the-air computation for asynchronous federated edge learning,” in *Proc. IEEE International Conference on Communications (ICC)*, May 2022, pp. 1–6.
- [150] L. You, X. Zhao, R. Cao, Y. Shao, and L. Fu, “Broadband digital over-the-air computation for wireless federated edge learning,” 2022. [Online]. Available: <https://arxiv.org/abs/2212.06596>
- [151] L. You, Z. Tang, P. Wang, Z. Wang, H. Dai, and L. Fu, “Quick and reliable lora physical-layer data aggregation through multi-packet reception,” 2022. [Online]. Available: <https://arxiv.org/abs/2212.06582>
- [152] E. Becirovic, Z. Chen, and E. G. Larsson, “Optimal MIMO combining for blind federated edge learning with gradient sparsification,” in *Proc. IEEE International Workshop on Signal Processing Advances in Wireless Communication (SPAWC)*, 2022, pp. 1–5.
- [153] A. Şahin, B. Everette, and S. Hoque, “Distributed learning over a wireless network with FSK-based majority vote,” in *Proc. IEEE International Conference on Advanced Communication Technologies and Networking (CommNet)*, Dec. 2021, pp. 1–9.
- [154] —, “Over-the-air computation with DFT-spread OFDM for federated edge learning,” in *Proc. IEEE Wireless Communications and Networking Conference (WCNC)*, Apr. 2022, pp. 1–6.
- [155] S. Hoque, M. H. Adeli, and A. Şahin, “Chirp-based over-the-air computation for long-range federated edge learning,” in *Proc. IEEE International Symposium on Personal, Indoor and Mobile Radio Communications (PIMRC)*, Sep. 2022, pp. 1–7.
- [156] M. H. Adeli and A. Şahin, “Multi-cell non-coherent over-the-air computation for federated edge learning,” in *Proc. IEEE International Conference on Communications (ICC)*, Apr. 2022, pp. 1–6.
- [157] J. Bernstein, Y.-X. Wang, K. Azizadenesheli, and A. Anandkumar, “signSGD: Compressed optimisation for non-convex problems,” in *Proc. International Conference on Machine Learning (ICML)*. PMLR, 2018, pp. 560–569.
- [158] A. Şahin, “Distributed learning over a wireless network with non-coherent majority vote computation,” 2022. [Online]. Available: <https://arxiv.org/abs/2209.04692>
- [159] S. Hoque and A. Şahin, “Chirp-based over-the-air computation for privacy-preserving distributed localization,” in *Proc. IEEE INFOCOM Workshops Wireless-Sec: 5G and Beyond Wireless Security*, May 2023, pp. 1–6.
- [160] A. Gadre, F. Yi, A. Rowe, B. Iannucci, and S. Kumar, “Quick (and dirty) aggregate queries on low-power WANs,” in *Proc. ACM/IEEE International Conference on Information Processing in Sensor Networks (IPSN)*, 2020, pp. 277–288.
- [161] A. Sahin, “Over-the-air computation based on balanced number systems for federated edge learning,” 2022. [Online]. Available: <https://arxiv.org/abs/2210.07012>
- [162] A. Şahin and R. Yang, “Over-the-air computation over balanced numerals,” in *Proc. IEEE Global Communications Conference Workshops (GLOBECOM WRKSHP) - Workshop on Wireless Communications for Distributed Intelligence*, Dec. 2022, pp. 1–6.
- [163] M. C. Valenti, D. Torrieri, and T. Ferrett, “Noncoherent physical-layer network coding with FSK modulation: Relay receiver design issues,” *IEEE Transactions on Communications*, vol. 59, no. 9, pp. 2595–2604, 2011.
- [164] T. Ferrett and M. C. Valenti, “Noncoherent LDPC-coded physical-layer network coding using multitone FSK,” *IEEE Transactions on Communications*, vol. 66, no. 6, pp. 2384–2395, 2018.
- [165] P. Jakimovski, F. Becker, S. Sigg, H. R. Schmidtke, and M. Beigl, “Collective communication for dense sensing environments,” in *Proc. IEEE Intelligent Environments*, 2011, pp. 157–164.
- [166] M. Zhu, C. Feng, C. Guo, Z. Liu, N. Jiang, and O. Simeone, “Semantics-aware remote estimation via information bottleneck-inspired type based multiple access,” 2022. [Online]. Available: <https://arxiv.org/abs/2212.09337>
- [167] F. Molinari, N. Agrawal, S. Stańczak, and J. Rausch, “Max-consensus over fading wireless channels,” *IEEE Transactions on Control of Network Systems*, vol. 8, no. 2, pp. 791–802, 2021.
- [168] —, “Over-the-air max-consensus in clustered networks adopting half-duplex communication technology,” *IEEE Transactions on Control of Network Systems*, pp. 1–10, 2022.
- [169] J. Choi, “Communication-efficient distributed sgd using random access for over-the-air computation,” *IEEE Journal on Selected Areas in Information Theory*, pp. 1–1, 2022.
- [170] J. Dong, Y. Shi, and Z. Ding, “Blind over-the-air computation and data fusion via provable wirtinger flow,” *IEEE Trans. Signal Process.*, vol. 68, pp. 1136–1151, 2020.
- [171] S. K. Jha, P. Mayekar, and H. Tyagi, “Fundamental limits of over-the-air optimization: Are analog schemes optimal?” in *Proc. IEEE Global Communications Conference (GLOBECOM)*, 2021, pp. 1–6.
- [172] M. M. Amiri and D. Gündüz, “Machine learning at the wireless edge: Distributed stochastic gradient descent over-the-air,” *IEEE Trans. Signal Process.*, vol. 68, pp. 2155–2169, 2020.
- [173] H. Ma, X. Yuan, Z. Ding, D. Fan, and J. Fang, “Over-the-air federated multi-task learning via model sparsification and turbo compressed sensing,” 2022. [Online]. Available: <https://arxiv.org/abs/2205.03810>
- [174] M. Zheng, C. Xu, W. Liang, H. Yu, and L. Chen, “Time-efficient cooperative spectrum sensing via analog computation over multiple-access channel,” *Computer Networks*, vol. 112, pp. 84–94, 2017. [Online]. Available: <https://www.sciencedirect.com/science/article/pii/S1389128616303632>
- [175] M. Zheng, L. Chen, W. Liang, H. Yu, and J. Wu, “Energy-efficiency maximization for cooperative spectrum sensing in cognitive sensor networks,” *IEEE Transactions on Green Communications and Networking*, vol. 1, no. 1, pp. 29–39, 2017.
- [176] Y. Shao, D. Gündüz, and S. C. Liew, “Federated edge learning with misaligned over-the-air computation,” *IEEE Trans. Wireless Commun.*, pp. 1–16, 2021.
- [177] C. Zhong, H. Yang, and X. Yuan, “Over-the-air federated multi-task learning over mimo multiple access channels,” 2021.
- [178] M. Goldenbaum, H. Boche, and S. Stańczak, “Reliable computation of nomographic functions over gaussian multiple-access channels,” in *IEEE International Conference on Acoustics, Speech and Signal Processing*, 2013, pp. 4814–4818.
- [179] M. Tang, S. Cai, and V. K. N. Lau, “Radix-partition-based over-the-air aggregation and low-complexity state estimation for IoT systems over wireless fading channels,” *IEEE Transactions on Signal Processing*, pp. 1–14, 2022.
- [180] N. Michelusi, “Decentralized federated learning via non-coherent over-the-air consensus,” 2022. [Online]. Available: <https://arxiv.org/abs/2210.15806>
- [181] D. Tse and P. Viswanath, *Fundamentals of Wireless Communication*. USA: Cambridge University Press, 2005.
- [182] H. Guo, Y. Zhu, H. Ma, V. K. N. Lau, K. Huang, X. Li, H. Nong, and M. Zhou, “Over-the-air aggregation for federated learning: Waveform superposition and prototype validation,” *Journal of Communications and Information Networks*, vol. 6, no. 4, pp. 429–442, 2021.
- [183] A. Şahin, “A demonstration of over-the-air-computation for FEEL,” in *Proc. IEEE Global Communications Conference Workshops (GLOBECOM WRKSHP) - Edge Learning over 5G Mobile Networks and Beyond*, Dec. 2022, pp. 1–7.
- [184] Y. Shao, D. Gündüz, and S. C. Liew, “Federated edge learning with misaligned over-the-air computation,” in *Proc. IEEE International Workshop on Signal Processing Advances in Wireless Communications (SPAWC)*, 2021, pp. 236–240.
- [185] Y. Shao, D. Gunduz, and S. C. Liew, “Bayesian over-the-air computation,” 2021. [Online]. Available: <https://arxiv.org/abs/2109.03780>

- [186] H. Hellström, V. Fodor, and C. Fischione, "Over-the-air federated learning with retransmissions," in *2021 IEEE 22nd International Workshop on Signal Processing Advances in Wireless Communications (SPAWC)*, 2021, pp. 291–295.
- [187] —, "Over-the-air federated learning with retransmissions (extended version)," *arXiv preprint arXiv:2111.10267*, 2021.
- [188] —, "Unbiased over-the-air computation via retransmissions," in *Proc. IEEE Global Communications Conference*, Dec. 2022, pp. 1–6.
- [189] X. Xie, C. Hua, and J. Hong, "Joint power control for over-the-air computation in multicarrier wireless system," in *Proc. IEEE Global Communications Conference*, Dec. 2022, pp. 1–6.
- [190] X. Fan, Y. Wang, Y. Huo, and Z. Tian, "BEV-SGD: Best effort voting SGD against byzantine attacks for analog aggregation based federated learning over the air," *IEEE Internet of Things Journal*, pp. 1–14, 2022.
- [191] W. Guo, C. Huang, X. Qin, L. Yang, and W. Zhang, "Dynamic clustering and power control for two-tier wireless federated learning," 2022. [Online]. Available: <https://arxiv.org/abs/2205.09316>
- [192] J. Mao, H. Yang, P. Qiu, J. Liu, and A. Yener, "CHARLES: Channel-quality-adaptive over-the-air federated learning over wireless networks," in *Proc. IEEE International Workshop on Signal Processing Advances in Wireless Communication (SPAWC)*, 2022, pp. 1–5.
- [193] X. Cao, G. Zhu, J. Xu, and K. Huang, "Cooperative interference management for over-the-air computation networks," *IEEE Trans. Wireless Commun.*, vol. 20, no. 4, pp. 2634–2651, 2021.
- [194] F. Li, Q. Ye, E. T. Fapi, W. Sun, and Y. Jiang, "Utility optimization for over-the-air computation systems with spectrum sharing," in *Proc. IEEE International Conference on Communications (ICC)*, May 2022, pp. 1–6.
- [195] Z. Wang, Y. Zhou, Y. Shi, and W. Zhuang, "Interference management for over-the-air federated learning in multi-cell wireless networks," *IEEE Journal on Selected Areas in Communications*, vol. 40, no. 8, pp. 2361–2377, 2022.
- [196] Z. Wang, W. Liu, Y. Li, and B. Vucetic, "Over-the-air computation systems: Optimal design with sum-power constraint," *IEEE Wireless Communications Letters*, vol. 9, no. 9, pp. 1524–1528, 2020.
- [197] Y. Xue, L. Su, and V. K. N. Lau, "FedOComp: Two-timescale online gradient compression for over-the-air federated learning," *IEEE Internet of Things Journal*, vol. 9, no. 19, pp. 19330–19345, 2022.
- [198] Y. Wang, C. Zou, D. Wen, and Y. Shi, "Federated learning over LEO satellite," in *Proc. IEEE Global Communications Conference Workshops (GLOBECOM WORKSHOPS) - Edge Learning over 5G Mobile Networks and Beyond*, Dec. 2022, pp. 1–6.
- [199] C. Vahapoglu, M. Mortaheb, and S. Ulukus, "Hierarchical over-the-air fedgradnorm," 2022. [Online]. Available: <https://arxiv.org/abs/2212.07414>
- [200] A. Madhan-Sohini, D. Dominic, N. Shah, and R. Prasad, "Over-the-air clustered wireless federated learning," 2022. [Online]. Available: <https://arxiv.org/abs/2211.03363>
- [201] S. M. Azimi-Abarghouy and V. Fodor, "Multi-server over-the-air federated learning," 2022. [Online]. Available: <https://arxiv.org/abs/2211.16162>
- [202] E. Ozfatura, S. Rini, and D. Gündüz, "Decentralized SGD with over-the-air computation," in *Proc. IEEE Global Communications Conference*, 2020, pp. 1–6.
- [203] M. Lee, G. Yu, and H. Dai, "Privacy-preserving decentralized inference with graph neural networks in wireless networks," 2022. [Online]. Available: <https://arxiv.org/abs/2208.06963>
- [204] Y. Lu, Z. Yu, and N. Suri, "Privacy-preserving decentralized federated learning over time-varying communication graph," 2022. [Online]. Available: <https://arxiv.org/abs/2210.00325>
- [205] Y. Chen, G. Zhu, and J. Xu, "Over-the-air computation with imperfect channel state information," in *Proc. IEEE International Workshop on Signal Processing Advances in Wireless Communication (SPAWC)*, 2022, pp. 1–5.
- [206] Q. Qi and X. Chen, "Robust design of federated learning for edge-intelligent networks," 2022. [Online]. Available: <https://arxiv.org/abs/2205.06955>
- [207] X. Wei, C. Shen, J. Yang, and H. V. Poor, "Random orthogonalization for federated learning in massive mimo systems," 2022. [Online]. Available: <https://arxiv.org/abs/2210.09881>
- [208] R. Jin, J. Hu, G. Min, and H. Lin, "Byzantine-robust and efficient federated learning for the internet of things," *IEEE Internet of Things Magazine*, vol. 5, no. 1, pp. 114–118, 2022.
- [209] C. Dwork and A. Roth, "The algorithmic foundations of differential privacy," *Foundations and Trends® in Theoretical Computer Science*, vol. 9, no. 3–4, pp. 211–407, 2014.
- [210] Y. Zhang, D. Liu, and O. Simeone, "Leveraging channel noise for sampling and privacy via quantized federated Langevin Monte Carlo," in *Proc. IEEE International Workshop on Signal Processing Advances in Wireless Communication (SPAWC)*, 2022, pp. 1–5.
- [211] J. Liao, Z. Chen, and E. G. Larsson, "Over-the-air federated learning with privacy protection via correlated additive perturbations," 2022. [Online]. Available: <https://arxiv.org/abs/2210.02235>
- [212] M. S. E. Mohamed, W.-T. Chang, and R. Tandon, "Privacy amplification for federated learning via user sampling and wireless aggregation," *IEEE Journal on Selected Areas in Communications*, vol. 39, no. 12, pp. 3821–3835, 2021.
- [213] D. Liu and O. Simeone, "Privacy for free: Wireless federated learning via uncoded transmission with adaptive power control," *IEEE Journal on Selected Areas in Communications*, vol. 39, no. 1, pp. 170–185, 2021.
- [214] J. Jiang, K. Han, Y. Du, G. Zhu, Z. Wang, and S. Cui, "Optimized power control for over-the-air federated averaging with data privacy guarantee," *IEEE Transactions on Vehicular Technology*, pp. 1–6, 2022.
- [215] N. Yan, K. Wang, C. Pan, and K. K. Chai, "Device scheduling for over-the-air federated learning with differential privacy," 2022. [Online]. Available: <https://arxiv.org/abs/2210.17181>
- [216] J. Zhang, J. Zhang, D. W. K. Ng, and B. Ai, "Federated learning-based cell-free massive mimo system for privacy-preserving," 2022. [Online]. Available: <https://arxiv.org/abs/2211.16945>
- [217] H. Jeon, D. Hwang, J. Choi, H. Lee, and J. Ha, "Secure type-based multiple access," *IEEE Transactions on Information Forensics and Security*, vol. 6, no. 3, pp. 763–774, 2011.
- [218] N. Yan, K. Wang, K. Zhi, C. Pan, K. K. Chai, and H. V. Poor, "Toward secure and private over-the-air federated learning," 2022. [Online]. Available: <https://arxiv.org/abs/2210.07669>
- [219] M. Frey, I. Bjelaković, and S. Stańczak, "Towards secure over-the-air computation," in *Proc. IEEE International Symposium on Information Theory (ISIT)*, 2021, pp. 700–705.
- [220] C. Hu, Q. Li, Q. Zhang, and J. Qin, "Secure transceiver design and power control for over-the-air computation networks," *IEEE Communications Letters*, vol. 26, no. 7, pp. 1509–1513, 2022.
- [221] L. Maňny and A. Wachter-Zeh, "Secure over-the-air computation using zero-forced artificial noise," 2022. [Online]. Available: <https://arxiv.org/abs/2212.04288>
- [222] G. Zhu, Y. Wang, and K. Huang, "Broadband analog aggregation for low-latency federated edge learning (extended version)," *arXiv preprint arXiv:1812.11494*, 2019.
- [223] D. Liu, P. Ning, and W. K. Du, "Attack-resistant location estimation in sensor networks," in *Proc. IEEE International Symposium on Information Processing in Sensor Networks (IPSN)*, 2005, pp. 99–106.
- [224] M. Tang, S. Cai, and V. K. N. Lau, "Over-the-air aggregation with multiple shared channels and graph-based state estimation for industrial IoT systems," *IEEE Internet of Things Journal*, vol. 8, no. 19, pp. 14 638–14 657, 2021.
- [225] —, "Remote state estimation with asynchronous mission-critical IoT sensors," *IEEE Journal on Selected Areas in Communications*, vol. 39, no. 3, pp. 835–850, 2021.
- [226] P. Park, P. Di Marco, and C. Fischione, "Optimized over-the-air computation for wireless control systems," *IEEE Commun. Lett.*, vol. 26, no. 2, pp. 1–5, 2022.
- [227] X. Zeng, X. Zhang, and F. Wang, "Optimized UAV trajectory and transceiver design for over-the-air computation systems," *IEEE Open Journal of the Computer Society*, pp. 1–9, 2022.
- [228] ITU. (2022, Nov.) Future technology trends of terrestrial International Mobile Telecommunications systems towards 2030 and beyond . [Online]. Available: https://www.itu.int/dms_pub/itu-r/opb/rep/R-REP-M.2516-2022-PDF-E.pdf
- [229] N. Zhang and M. Tao, "Gradient statistics aware power control for over-the-air federated learning," *IEEE Trans. Wireless Commun.*, vol. 20, no. 8, pp. 5115–5128, 2021.
- [230] K. Liang, H. Zhong, H. Chen, and Y. Wu, "Wyner-ziv gradient compression for federated learning," *arXiv preprint arXiv:2111.08277*, 2021.
- [231] O. Gupta and R. Raskar, "Distributed learning of deep neural network over multiple agents," *Journal of Network and Computer Applications*, vol. 116, pp. 1–8, 2018.
- [232] A. Singh, P. Vepakomma, O. Gupta, and R. Raskar, "Detailed comparison of communication efficiency of split learning and federated learning," 2019. [Online]. Available: <https://arxiv.org/abs/1909.09145>
- [233] P. Vepakomma, O. Gupta, A. Dubey, and R. Raskar, "Reducing leakage in distributed deep learning for sensitive health data," *arXiv preprint arXiv:1812.00564*, 2019.

- [234] C. Thapa, M. A. P. Chamikara, and S. Camtepe, "Splitfed: When federated learning meets split learning," *arXiv preprint arXiv:2004.12088*, 2020.
- [235] P. Vepakomma, O. Gupta, T. Swedish, and R. Raskar, "Split learning for health: Distributed deep learning without sharing raw patient data," *arXiv preprint arXiv:1812.00564*, 2018.
- [236] K. Wei, J. Li, C. Ma, M. Ding, S. Wei, F. Wu, G. Chen, and T. Ranbaduge, "Vertical federated learning: Challenges, methodologies and experiments," 2022. [Online]. Available: <https://arxiv.org/abs/2202.04309>
- [237] Z. Zhang, G. Zhu, and S. Cui, "Low-latency cooperative spectrum sensing via truncated vertical federated learning," 2022. [Online]. Available: <https://arxiv.org/abs/2208.03694>
- [238] 3GPP. (2022, Sep.) TR 22.876 V0.1.0 - Study on AI/ML Model Transfer-Phase 2. [Online]. Available: https://ftp.3gpp.org/Specs/archive/22_series/22.876/22876-010.zip
- [239] ——. (2021, Dec.) TR 22.876 V18.2.0 - Study on traffic characteristics and performance requirements for AI/ML model transfer in 5GS (Release 18). [Online]. Available: https://www.3gpp.org/ftp/Specs/archive/22_series/22.874/22874-i20.zip
- [240] M. Krouka, A. Elgabli, C. b. Issaid, and M. Bennis, "Communication-efficient split learning based on analog communication and over the air aggregation," in *Proc. IEEE Global Communications Conference (GLOBECOM)*, 2021, pp. 1–6.
- [241] Y. Yang, Z. Zhang, and Z. Yang, "Over-the-air split learning with MIMO-based neural network and constellation-based activation," in *IEEE International Workshop on Machine Learning for Signal Processing*, 2022, pp. 1–7.
- [242] Y. Yang, Z. Zhang, Y. Tian, Z. Yang, C. Huang, C. Zhong, and K.-K. Wong, "Over-the-air split machine learning in wireless mimo networks," 2022. [Online]. Available: <https://arxiv.org/abs/2210.04742>
- [243] Y. Gu, C. She, Z. Quan, C. Qiu, and X. Xu, "Distributed graph neural networks for optimizing wireless networks: Message passing over-the-air," 2022. [Online]. Available: <https://arxiv.org/abs/2207.08498>
- [244] F. Molinari and J. Raisch, "Exploiting wireless interference for distributively solving linear equations," *IFAC-PapersOnLine*, vol. 53, no. 2, pp. 2999–3006, 2020, 21st IFAC World Congress.
- [245] M. Goldenbaum, P. Jung, M. Raceala-Motoc, J. Schreck, S. Stańczak, and C. Zhou, "Harnessing channel collisions for efficient massive access in 5G networks: A step forward to practical implementation," in *Proc. IEEE International Symposium on Turbo Codes and Iterative Information Processing (ISTC)*, 2016, pp. 335–339.
- [246] L. Chen, N. Zhao, Y. Chen, F. R. Yu, and G. Wei, "Over-the-air computation for cooperative wideband spectrum sensing and performance analysis," *IEEE Transactions on Vehicular Technology*, vol. 67, no. 11, pp. 10 603–10 614, 2018.
- [247] X. Xie, C. Hua, P. Gu, and W. Xu, "Aircon: Over-the-air consensus for wireless blockchain networks," 2022. [Online]. Available: <https://arxiv.org/abs/2211.16700>
- [248] U. Altun, S. T. Başaran, H. Alakoca, and G. K. Kurt, "A testbed based verification of joint communication and computation systems," in *Proc. IEEE Telecommunication Forum (TELFOR)*, 2017, pp. 1–4.
- [249] O. Abari, H. Rahul, D. Katabi, and M. Pant, "Airshare: Distributed coherent transmission made seamless," in *Proc. IEEE Conference on Computer Communications (INFOCOM)*, 2015, pp. 1742–1750.
- [250] L. Lu, L. You, Q. Yang, T. Wang, M. Zhang, S. Zhang, and S. C. Liew, "Real-time implementation of physical-layer network coding," in *Proc. ACM Software Radio Implementation Forum (SRIF)*, 2013, pp. 71–76.
- [251] L. You, S. C. Liew, and L. Lu, "Reliable physical-layer network coding supporting real applications," *IEEE Transactions on Mobile Computing*, vol. 16, no. 8, pp. 2334–2350, 2017.
- [252] Y. Tan, S. C. Liew, and T. Huang, "Mobile lattice-coded physical-layer network coding with practical channel alignment," *IEEE Transactions on Mobile Computing*, vol. 17, no. 8, pp. 1908–1923, 2018.
- [253] A. Şahin. (2022, Sep.) Wireless for ML - Over-the-air computation. [Online]. Available: <https://mentor.ieee.org/802.11/dcn/22/11-22-1483-01-aiml-wireless-for-ml-over-the-air-computation.pptx>